NAVAL POSTGRADUATE SCHOOL

MONTEREY, CALIFORNIA

THESIS

ADDITIVE MANUFACTURING OF SILICON CARBIDE (SiC) CERAMIC ROCKET NOZZLES

by

Kenneth N. Wooten

June 2020

Thesis Advisor: Ibrahim E. Gunduz
Second Reader: Claudia C. Luhrs

THIS PAGE INTENTIONALLY LEFT BLANK

REPORT DOCUMENTATION PAGE	*Form Approved OMB No. 0704-0188*

1. AGENCY USE ONLY *(Leave blank)*	**2. REPORT DATE** June 2020	**3. REPORT TYPE AND DATES COVERED** Master's thesis

4. TITLE AND SUBTITLE ADDITIVE MANUFACTURING OF SILICON CARBIDE (SiC) CERAMIC ROCKET NOZZLES	**5. FUNDING NUMBERS**
6. AUTHOR(S) Kenneth N. Wooten	
7. PERFORMING ORGANIZATION NAME(S) AND ADDRESS(ES) Naval Postgraduate School Monterey, CA 93943-5000	**8. PERFORMING ORGANIZATION REPORT NUMBER**
9. SPONSORING / MONITORING AGENCY NAME(S) AND ADDRESS(ES) N/A	**10. SPONSORING / MONITORING AGENCY REPORT NUMBER**

11. SUPPLEMENTARY NOTES The views expressed in this thesis are those of the author and do not reflect the official policy or position of the Department of Defense or the U.S. Government.

12a. DISTRIBUTION / AVAILABILITY STATEMENT Approved for public release. Distribution is unlimited.	**12b. DISTRIBUTION CODE** A

13. ABSTRACT (maximum 200 words)

Rocket motor nozzles are typically made of materials such as graphite and fiber-reinforced phenolics or epoxies with low erosion rates, relatively low manufacturing costs, and/or reduced weight. Additive manufacturing (AM) methods enable unique control of geometry and composition and can improve the weight and thermal performance of rocket nozzles. A newly developed AM process called vibration assisted printing (VAP) can process a unique combination of ceramic-forming polymer binders with a large amount of solid particles at very high solid loadings and viscosities. This research investigated the formulation, pre-processing and post-processing of these materials, determined their final microstructure and phase composition, and compared them to some of the materials utilized in rockets today. Some of the parameters investigated included mixture ratio, curing temperature, and sintering temperature of silicon carbide (SiC)-ceramic forming polymer particles. These mixtures were used for 3D printing of SiC-ceramic matrix/SiC composite parts. The results of the study will help improve the performance of modern-day rockets and other applications within the aerospace industry.

14. SUBJECT TERMS additive manufacturing, rocket nozzle, ceramic forming polymers, vibration assisted printing, VAP, composites, silicon carbide, SiC	**15. NUMBER OF PAGES** 119
	16. PRICE CODE

17. SECURITY CLASSIFICATION OF REPORT	**18. SECURITY CLASSIFICATION OF THIS PAGE**	**19. SECURITY CLASSIFICATION OF ABSTRACT**	**20. LIMITATION OF ABSTRACT**
Unclassified	Unclassified	Unclassified	UU

NSN 7540-01-280-5500 Standard Form 298 (Rev. 2-89) Prescribed by ANSI Std. 239-18

THIS PAGE INTENTIONALLY LEFT BLANK

Approved for public release. Distribution is unlimited.

ADDITIVE MANUFACTURING OF SILICON CARBIDE (SiC) CERAMIC ROCKET NOZZLES

Kenneth N. Wooten
Lieutenant, United States Navy
BS, Virginia Commonwealth University, 2013
MS, American Military University, 2018

Submitted in partial fulfillment of the
requirements for the degree of

MASTER OF SCIENCE IN SPACE SYSTEMS OPERATIONS

from the

NAVAL POSTGRADUATE SCHOOL
June 2020

Approved by: Ibrahim E. Gunduz
Advisor

Claudia C. Luhrs
Second Reader

James H. Newman
Chair, Space Systems Academic Group

THIS PAGE INTENTIONALLY LEFT BLANK

ABSTRACT

Rocket motor nozzles are typically made of materials such as graphite and fiber-reinforced phenolics or epoxies with low erosion rates, relatively low manufacturing costs, and/or reduced weight. Additive manufacturing (AM) methods enable unique control of geometry and composition and can improve the weight and thermal performance of rocket nozzles. A newly developed AM process called vibration assisted printing (VAP) can process a unique combination of ceramic-forming polymer binders with a large amount of solid particles at very high solid loadings and viscosities. This research investigated the formulation, pre-processing and post-processing of these materials, determined their final microstructure and phase composition, and compared them to some of the materials utilized in rockets today. Some of the parameters investigated included mixture ratio, curing temperature, and sintering temperature of silicon carbide (SiC)-ceramic forming polymer particles. These mixtures were used for 3D printing of SiC-ceramic matrix/SiC composite parts. The results of the study will help improve the performance of modern-day rockets and other applications within the aerospace industry.

THIS PAGE INTENTIONALLY LEFT BLANK

TABLE OF CONTENTS

THIS PAGE INTENTIONALLY LEFT BLANK

LIST OF FIGURES

LIST OF TABLES

THIS PAGE INTENTIONALLY LEFT BLANK

LIST OF ACRONYMS AND ABBREVIATIONS

AM	Additive Manufacturing
ASTM	American Society for Testing and Materials
C/C	Carbon-Carbon (bond)
C/SiC	Carbon-Silicon Carbon (bond)
CMCs	Ceramic Matrix Composites
CO_2	Carbon Dioxide
CT	X-Ray Computed Tomography
°C	Degrees Celsius (SI Unit for Temperature)
DSC	Differential Scanning Calorimetry
EDS	Energy Dispersive X-Ray Spectroscopy
°F	Degrees Fahrenheit (Imperial Unit for Temperature)
Hg	Mercury (Periodic Table Element)
K	Kelvin - Base Unit for Temperature (SI Unit)
MPa	Mega Pascals (SI Unit for Pressure)
N	Newtons (SI Unit for Force)
NASA	National Aeronautics and Space Administration
PCS	Polycarbosilanes
PDCs	Polymer-Derived Ceramics
PDXL	XRD X-Ray Analysis Software
PIP	Polymer Infiltration and Pyrolysis
PLA	Plastic Filament for 3D Printing-Polylactic Acid
PVA	Plastic Filament Polyvinyl Alcohol for 3D Printing
Psi	Pound Force per square inch (Imperial Unit for Pressure)
RPM	Rotations per Minute
RTM	Resin Transfer Molding
SEM	Scanning Electron Microscope
SiC	Silicon Carbide (Carbon)
SiC-B-C-N	Silicon Boride/Carbide/Nitride
SiC/SiC	Silicon Carbide-Silicon Carbide (bond)
SiOC	Silicon Oxycarbide

SMP	Silicon Carbide Matrix Precursor
STL	Stereolithography CAD File
TG-DTA/DSC	Thermogravimetry-Differential Temperature Analysis/Differential Scanning
TGA	Thermal Gravimetric Analysis/Analyzer
TPES	Total Primary Energy Supply
TVAC	Thermal Vacuum Oven
UHTCs	Ultra High Temperature Ceramics
VAP	Vibration Assisted Printer/Printing
wt.	weight
XRD	X-Ray Powder Diffraction

ACKNOWLEDGMENTS

I would like to thank numerous parties that helped me along my path toward completing this thesis. First, Professor Emre Gunduz has my sincerest appreciation and gratitude for the countless hours he spent guiding me in the lab, the research, and the process toward a respectable publication. Without his extraordinary tutelage, his deep insight, expertise, and persistent guidance, the research and thesis would not have come to fruition. He has really been an amazing instructor, professor, mentor, and friend.

I would like to thank Professors Claudia Luhrs and Troy Ansell for their assistance in learning instruments and conducting research and analysis. Without their knowledge and support throughout the testing and analysis, it would have taken a toll on the amount of meaningful data. Not being in the MAE department made this hard for me, but they provided great support in addition to Professor Gunduz.

Another thanks goes out to the faculty and staff of the Space Systems Academic Group. Without the oversight and support of Professor James Newman, I would not have been able to pursue and complete such a rewarding degree at NPS. With the help of CDR William Crane, Professors Stephen Tackett, Dan Bursch, Charles Racoosin, and Wenschel Lan, I was able to maximize my learning capacity while acquiring an even greater love for space.

Outside of my curriculum support, I would not have been able to make the most of my time here without CAPT Christopher Bone. Thank you for the mentorship you brought and the assistance with a variety of aspects involving my future career in the USN. Having support from you meant a lot.

Beyond the professors and distinguished individuals above, I must thank my curriculum cohort for their support making my time here memorable and fun. A special thanks goes out to Maj. Kelly Raisch for the help in and out of the lab. Having you by my side in the lab as we both worked on our theses as we tested, failed, and succeeded together made it much more enjoyable. You and your family have been awesome and a pleasure to know and spend time with.

A thanks also goes out to LT. Daniel Reuter. Having you as a roommate continued our fun times from Whidbey, WA, to here and made sure I did more than just career-guided work. You got me out to explore and enjoy almost all of what Monterey and California had to offer.

Also, thank you to every person at NPS who I interacted with and got to spend some time with, either in or out of the classroom. Your interaction contributed to my enjoyment of everything NPS had to offer.

Lastly, I must thank the individuals in my life who have been there through thick and thin and have heavily influenced my life: my parents, Steven and Nikolitsa Wooten. Without them, I would not have been as goal-driven, determined, and successful as I am today. Thank you for everything you both have done and continue to do. I will continue to make you two proud and show you both just how much you are loved.

I. INTRODUCTION

A. MOTIVATION

Throughout the past decade, additive manufacturing (AM) has undergone drastic changes in terms of available capabilities and fabrication technologies. As the AM technology has matured, opportunities for its implementations in military and civilian applications ranging from aerospace to consumer products has also expanded tremendously. AM, which is also known as 3D printing, involves constructing parts layer by layer and providing greater, advantageous capabilities previously unavailable through conventional manufacturing methods. With AM materials becoming more and more sophisticated, a greater emphasis has been placed on creating advanced thermo-structural composites such as carbon/carbon (C/C), carbon/silicon carbide (C/SiC), and SiC/SiC, "due to their high-temperature strength, thermal shock resistance, low thermal expansion coefficient, good thermal conductivity, hardness, abrasion resistance, and low density" [1]. In the aerospace industry, materials are often continuously tested to extreme temperatures to compensate for strenuous operating environments. The advancement of these composites provides a promising future.

For the focus of the aerospace industry, rocket nozzles are one of the many application areas that could be influenced by the development of additively manufactured composites. The ability to manipulate carbon fibers or other fillers into specific orientations creates the opportunity for controlling both, mechanical and thermal properties, in a 3D-printed part [2]. For applicability in rocket nozzles, additively manufactured composites will need to withstand temperatures as high as 3315°C [3].

A newer AM approach termed VAP provides a potential for creating such composites at high resolution and with very low porosity. This approach or direct-write method resonates the nozzle to generate large vibration amplitudes, which inertially reduces the effective friction at the nozzle exit, allowing extremely viscous materials to be 3D-printed with lower porosity [4] (Figure 1). With the ability to drastically reduce the friction, VAP allows different higher-performance materials to be used that could not be

previously processed due to their viscosity, while allowing better dimensional control of the part being printed.

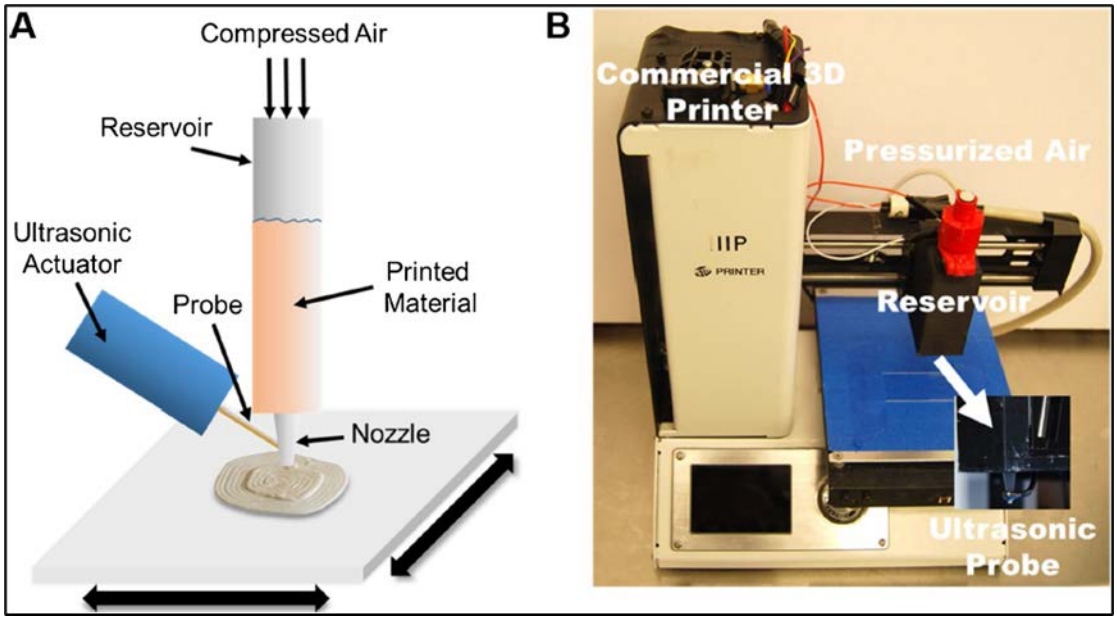

Figure 1. (A) Nozzle Configuration Used to Deposit Material as the Build Plate and Nozzle are Moved. (B) The 3D System. Source: [5].

Due to the extreme temperatures and pressures at which rocket engine nozzles operate, the materials that are used typically are complex and expensive to develop. 3D printing can allow a greater ability to potentially counteract the significant erosion undergone by composites such as graphite and C-C at high temperature-operating conditions by manipulation of the composite design prior to printing.[6].

One of the major contributing factors for pursuing AM of composites is due to the interest of the U.S. Department of Defense (DoD) to utilize AM much more widely. Progress within the DoD is steadily being made through AM implementation plans, funding, research, and successful AM efforts with a focus on improving defense systems [7]. The military has even implemented plans on how it wants to proceed forward within AM and have made them into instructions for military officials, leaders, and individuals to follow. Going forward, the potential for AM within military applications will continue to

expand and improve as it becomes better integrated for use. This research aims to positively impact and support these goals.

Within the aerospace industry and with rocket nozzles specifically, there is a continual effort to improve the current methods and components of platforms, whether they are spacecraft, rockets to lift those payloads, or aircraft. Incorporating AM within these areas of focus has improved the potential for future advancements to be much more capable then their previous predecessors. “With the ability to additively produce materials that are lightweight, have high strength, have inner structures with void and honeycomb-sandwich structures that help achieve maximum specific strength and stiffness”, 3D printing was able to develop an Airbus engine that achieved a 65% reduction of weight components [3]. For flight and structure, the platform needs to be able to withstand high speeds and temperatures while also being able to lift mass. If the mass of the components is lower, it allows for additional weight to be put in other critical or important systems/components. Hence, that is why the researching AM is important within the aerospace industry.

For rockets, the research is nascent and ongoing. 3D printing on metal materials represents an innovative platform for research into alloys that can operate in high-temperature conditions such as rocket engines. In this rocket engine-operational environment, the materials required would need to be able to endure higher environmental temperatures up to 3315°C and be 700 times more resistant to high temperature corrosion [3]. Through improvements in thermal resistance and the ability to reduce costs by making material not only lighter but more durable, NASA and other private companies are striving to research better alternatives in AM processing to produce the most cost-effective and durable components for market. Regulations and practices will still be kept in place for testing and making sure that the materials and components produced still operate within the safe and appropriate conditions for manned and unmanned operations.

Besides the inclusion of AM within the aerospace industry, optimization of the performance is the primary driving factor for many of the rockets or space launchers. In most cases, “the dry mass of the vehicle has to ideally be as low as possible along with all subsystems and equipment” being able to meet their highest efficiency requirements [8]. With all the different components of a spacecraft system, the rocket or propulsion system

is normally the most critical part since their efficiency and ability to lift large payloads into orbit plays an important part in whether a mission can be carried out effectively.

Even though there are different shapes for rocket nozzles, the biggest consideration that is evaluated during the manufacturing is the ability of the flow to be separated. That is why designing a rocket nozzle to decrease performance losses through minimizing over-expansion of flow "during low-altitude operation with pressures higher than nozzle exit pressure or under-expansion during high-altitude operation with pressures lower than nozzle exit pressure" are critical and continually looked at from a design perspective [9]. Within rocket nozzle manufacturing, there continues to be improvements and developments that could drastically improve the current capabilities. Along with AM, the possibilities for improvements encompass a wider variety of options due to different chemicals potentially being used for material composition. With different chemicals being used, this could make certain nozzle shapes operate better due to the chemical, thermal, and mechanical properties of the components. Further exploration into these areas of study is needed to discover what provides the greatest capabilities and growth of understanding of AM within the aerospace industry. Ultimately, the biggest motivation for pursuing potential AM techniques within the aerospace industry is to create or develop higher-performance ceramics that have much higher and superior properties for aerospace applications.

B. BACKGROUND

This research is focused on the AM of SiC rocket nozzles using a new AM approach called VAP, which enables extrusion and deposition of highly solids-loaded, viscous, heterogeneous materials. With this approach, a unique material system will be employed, where mixtures of ceramic-forming polymers and powders of SiC will be mixed and 3D printed to produce parts with very low porosity and at near net-shape, or very close to its final shape, prior to the pyrolysis of the polymer binder that forms a SiC matrix. The following sections provide the relevant background for AM, ceramic-forming polymers, rocket nozzles, and the relevant characterization methods that will be used to evaluate the properties and performance of the processed materials.

1. Additive Manufacturing

Additive manufacturing, also known as 3D printing, is an emerging technology and continuously developing approach that involves the building of parts usually layer by layer. The parts can be printed using liquid, solid, or powder-based processes. The biggest advantage of AM is its ability to assist the development and manufacturing of complex and intricate components at a "substantial reduction in manufacturing time, costs, and material wastage" through computer software and a 3D printer [10]. The beneficial aspect of using AM within the commercial and military industries is its ability to customize a lot of the product design while also being able to influence features, geometries, consolidating parts, and weight. Additionally, through AM, CO_2 emissions and total primary energy supply (TPES) can be decreased exponentially compared to the current methods of production [10].

With all materials that undergo AM, primary areas of focus that need to be examined upon completion include but are not limited to, the final part stability, thermal/ heat/moisture resistance, and overall strength. As with any other manufacturing process, some key consideration defects are porosity, shrinkage, oxidation, and susceptibility to corrosion [11]. Due to the fact that 3D printing is able to take less time to develop some of these components, continual improvements can be made on a smaller scale to greatly enhance the deficits of materials before a greater extent of the part is created. A great example of this is NASA's Marshall Space Flight Center developing and improving current AM techniques for nozzle fabrication such as Laser Wire Direct Closeout (LWDC) allowing for the manufacturing of less-expensive nozzles in significantly less time" [12]. Regardless of the AM technique or approach used, multiple alternatives exist, each providing differing methods on making the components cheaper, stronger, and overall, more capable.

With the potential for materials to undergo reactions during processing, it is important that these AM methods are able to mitigate these unwanted reactions. One of the primary unwanted reactions is oxidation, and its prevention increases the ability of the parts to sustain higher temperatures and provide a greater resistance to deformations or changes of the microstructure [13]. By having materials such as phenolics or epoxies being utilized

within the rocket nozzles, the elimination of the oxygen chains improves the materials' ability to help with the resistance of the composites to higher degrees of temperature, while reducing the current extensive methods of manufacturing such materials [2]. AM provides a greater capability and improvement to many of the existing fabrication methods currently in place. For example, through its unique "ability to deposit carbon fibers into specific orientations", it brings about unique possibilities to control mechanical and thermal properties of any additively manufactured part for ablative purposes [2]. By implementing these newer AM approaches, there exists a wider range and vast realm of design and performance possibilities on improving current applications and products.

One of the specific improvements of AM is the potential to augment the ability to process materials for rocket nozzles composed of ceramic composites. For most AM processes focused on ceramics, the biggest concern is creating parts that have little to no porosity upon post-processing with little shrinkage and distortion. Most AM processes use ceramic-forming polymers or polymer-particle mixtures with low solids fractions (<30 vol.%). These 3D-printed, ceramic precursors show significant volume shrinkage after sintering due to removal of pores and densification. Although the overall size change can be accounted for by making models larger, the shrinkage is typically non-uniform for many asymmetric designs. For extrusion-based approaches, the number/quantity of solids fractions are limited as the mixtures can get clogged within the nozzle of the 3D printer. The viscosity of the material mixture plays an influential part on whether it is more susceptible for clogging or not.

The newly developed VAP AM system at NPS and Purdue University can process very high solids-loaded, (>76 vol.%) extremely viscous, powder-polymer mixtures at high resolutions and speeds [2]. This capability enables unique approaches. For example, the ability to print mixtures consisting mostly of SiC powders with small amounts of SiC-forming polymers, can result in sintered products coming out near net-shape with unique geometric features like cooling channels and potentially better thermal and mechanical properties. A similar approach has been recently demonstrated for a mixture of silicon oxycarbide-forming polymer mixed with short, graphite fibers using VAP (Figure 2). Because VAP AM can print more highly viscous materials and a greater range of materials,

the mixing methods and formulation optimization prior to 3D printing needs to be experimented on by varying weight percentages of components and processing conditions.

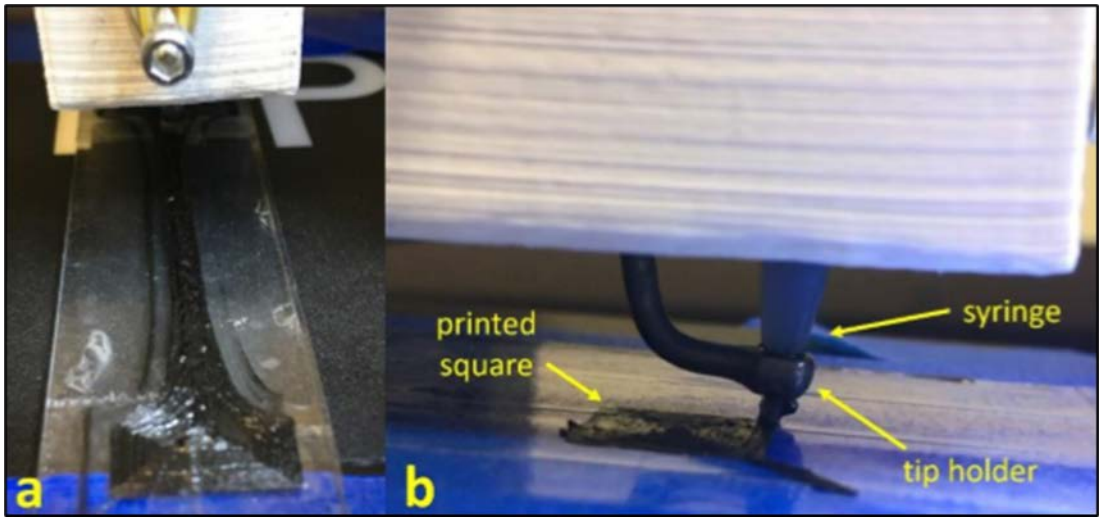

The width of microscope slide is 25 mm, and the width of square is approx. 20 mm. The mixture appeared to retain its shape and geometry as more layers were deposited and extruded consistently.

Figure 2. Examples of 3D Printing a Dog Bone (a) and a Square (b) Using a Mixture of Short-Fiber, Graphite Powders with Silicon Oxycarbide-Forming Polymer. Source:[14].

2. Ceramic-Forming Polymers

Ceramic-forming polymers have been used over the past few decades in developing polymer-derived ceramics (PDCs). The idea behind their application is to formulate polymers that can be easily cured into desired shapes, which can then be decomposed in a controlled way to yield a useful ceramic material such as SiC (Figure 3). Most preceramic polymers are processed by using polymer infiltration pyrolysis (PIP), injection molding, coatings using solvents, extrusion, or resin transfer molding (RTM) [13]. When making some of these polymers, a greater focus is given to creating polymers with high molecular weight so that when they are pyrolyzed or undergo heat treatment, the resultant product still has a stable and supportive molecular structure for physical properties. Considering the process of pyrolysis, preceramic polymers can include these polymeric fillers to act as "sacrificial fillers" or a way to decrease the possibility of porosity and unwanted "carbon-

containing moieties in the material" [13]. It is crucial during the preceramic polymer forming process that the materials created have the desired characteristics in the final product, such as a greater temperature stability, creep resistance, oxidation resistance, and overall stronger structures.

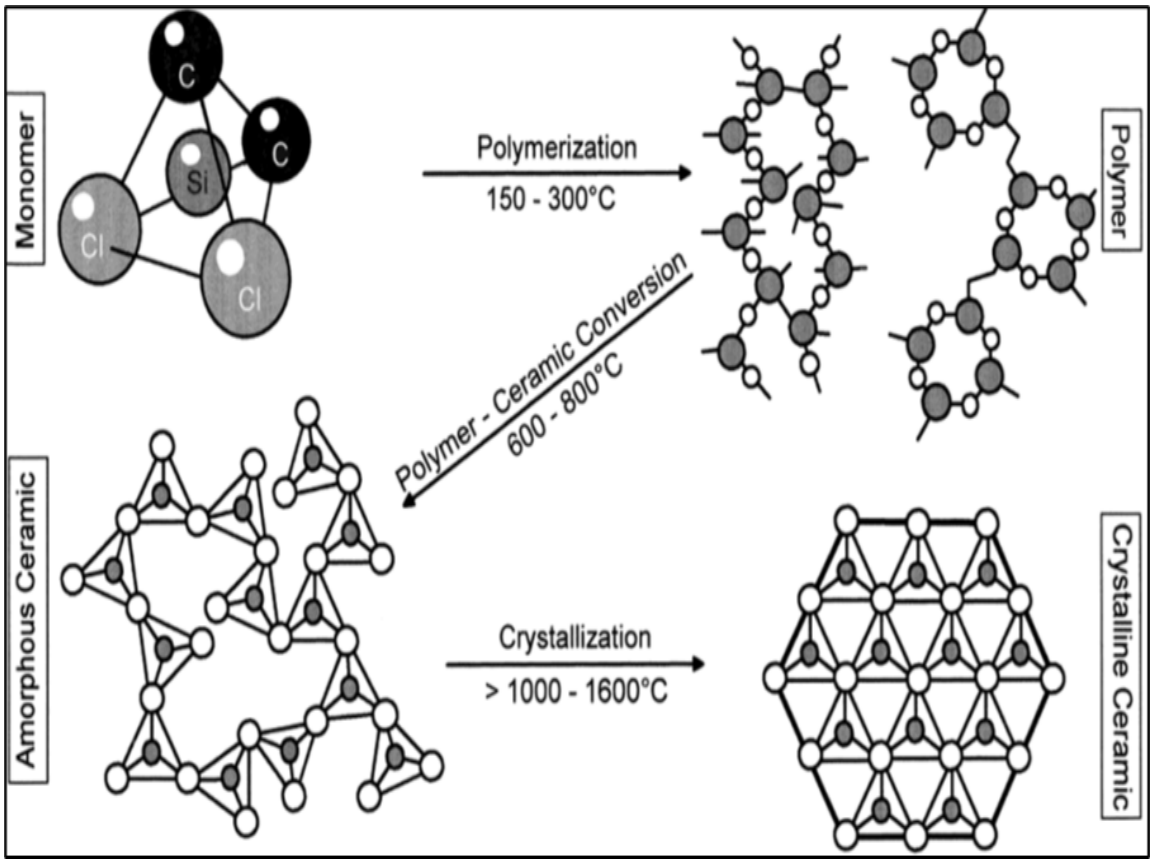

Figure 3. Scheme of Molecular and Microstructural Transitions during Ceramic Manufacturing from Preceramic Polymers. Source: [15].

Once ceramic composites or polymer-derived ceramics are formulated, the properties are determined by the temperatures at which they were pyrolyzed. Higher temperatures being able to decompose oxygen-containing molecules or eliminate oxygen from the material will allow the final ceramics to typically exhibit weight loss and strength improvement. That is why the removal of unwanted carbon atoms within the ceramic is vital for maintaining a strong, crystalline, interconnected structure with improved weight percentages. Another note to consider is that oxygen can easily contaminate the processing

of the ceramics, hence why fillers are sometimes important to consider during this processing. Sacrificial fillers can help remove the oxygen within processing which can strengthen the overall micro-structure bonds. With the processing of polymers during the preceramic to ceramic stages, shrinkage, porosity and cracks are bound to happen with the drying of the materials from a higher temperature. That is why during the early stages of processing PDCs, understanding the different characteristics that could arise from different stages and materials are important in order to make desirable and more improved products.

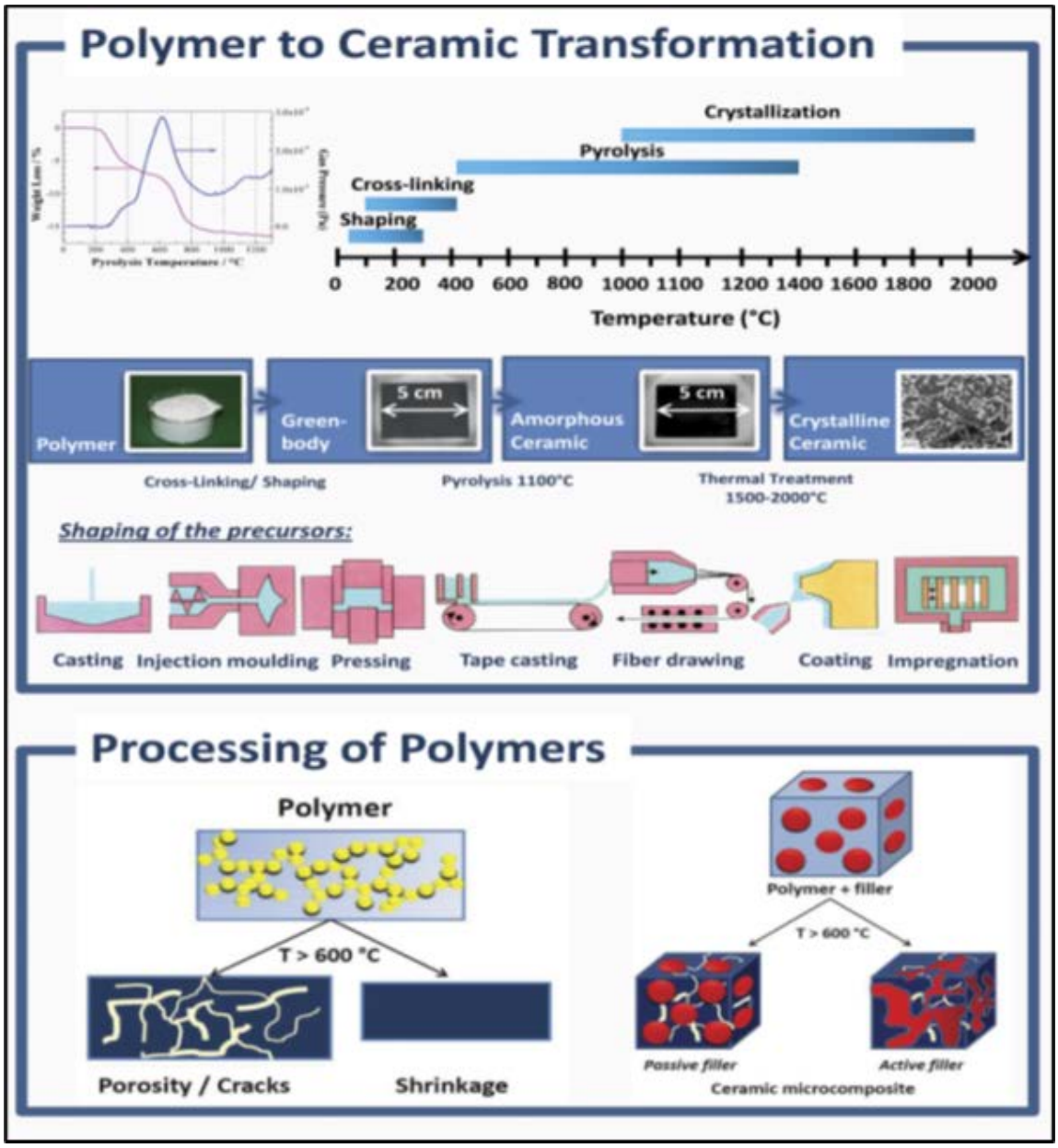

Figure 4. (Top) Depiction Is of Polymer to Ceramic Transformation with Emphasis on Pyrolysis Temperature and How It Becomes More Structured. (Bottom) Depiction Is a Simple View of What Happens During Processing Polymers. Source: [16].

When discussing materials or PDCs that could provide the potential for improvements within aeronautics and astronautics, SiC fibers/powders seem to be promising. The mechanical properties of "porous SiC ceramics can be improved depending on their porosity, pore size, microstructure, and compositions of the bonding phase and

additives," which is why the initial stages of processing these preceramic polymers are important to make SiC much more favorable [17]. Additionally, combining carbon with SiC enables a much more desirable, oxidation-resistant matrix, a more robust/tough cured composite, and improved tensile strength [17], [18]. Whether combining additional SiC or carbon to the preceramic mixture, manipulating its geometry and porosity within the fabrication will determine whether the material is stronger and more efficient than its singular properties.

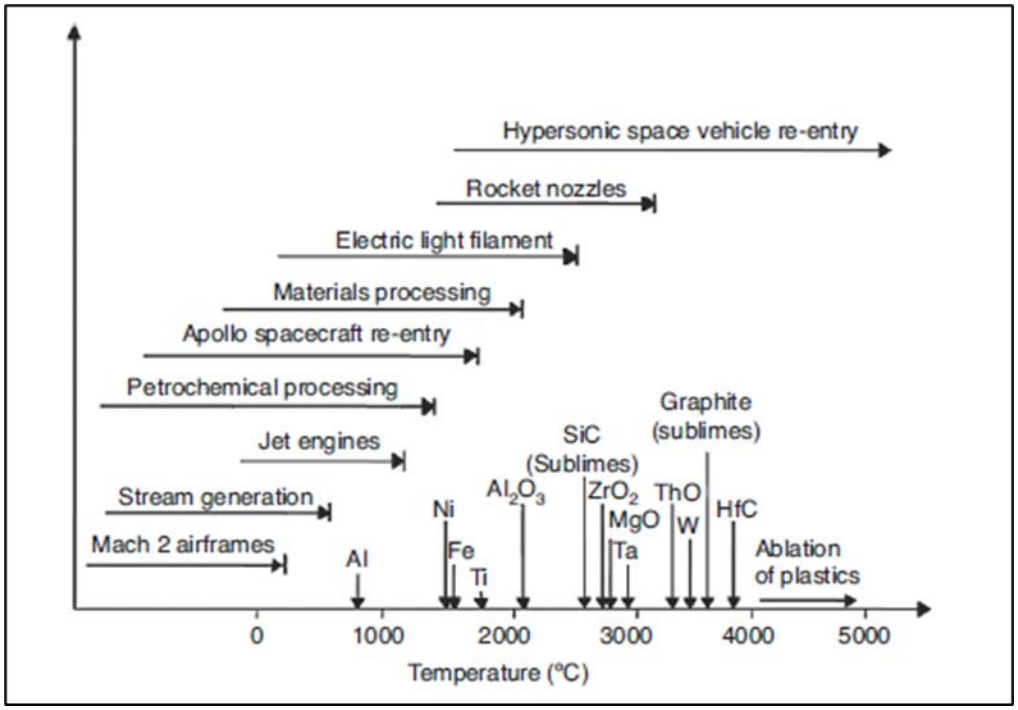

SiC has potential to improve based on the ability to remove/reduce porosity and increase thermal and mechanical properties.

Figure 5. Typical Operating Temperatures in High-Temperature Environments. Source: [19].

Fabricating these high-temperature, structural composites with reduced cost and processing steps is an important driving factor for all ceramic-forming polymer development. Therefore, starting with a polymer matrix allows for the shape to be formed whereas pyrolysis helps to obtain desired ceramic thermal and mechanical properties [20]. Since SiC can be synthesized from polysiloxane (Si-O-C or silicon oxycarbide) through

heating to remove oxygen, further pre-manipulation through mixing and carbothermal reduction earlier on can help acquire greater mass quantities of SiC to improve chemical properties [21]. As the material requirements for platforms and designs become more sophisticated and complex, a greater emphasis and desire will be placed on developing even more advanced ceramic-forming polymers and, in the end, better PDCs.

Within AM, ceramic-forming polymers have been utilized more for commercial and military applications. Some of the preceramic polymers utilized include oxygen-rich SiC, silicon nitride, silicon oxycarbide (SiOC), and silicon oxynitride [18]. With each polymer containing different chemical properties, each has been used differently depending on the purpose needed within commercial and military applications. The mixing of these preceramic polymers in a variety of combinations enables the manufacturer to improve properties such as corrosion, wear, thermal conductivity, and heat resistance [1]. Material engineers along with chemists have continually experimented with manipulation of these polymers to determine which combinations and processes yield the most desirable product for its intended purpose. Making components or mixtures from SiC is useful and has been used in AM due to its ability to withstand high heat and pressure while also being able to manufacture it into hard, lightweight, and thermally resistant ceramics.

Besides the ability to manipulate the properties of each preceramic polymer through curing and mixing, the ceramic-forming polymers during pyrolysis greatly depend on the oxygen present. Within AM, less porosity will result in a greater structure with potentially greater mechanical and chemical properties. Oxygen containing ceramic polymers are limited to temperatures below 1200°C whereas those that are oxygen poor, such as Si-B-C-N systems tend to offer the potential for significantly higher temperature applications [22]. With applications for thermal-barrier coatings, ablatives, and/or newer materials to be utilized within the aerospace industry and specifically rocket nozzles, the use of low-oxygen, ceramic-forming polymers is preferred over those with greater concentrations of oxygen.

AM of ceramics within the commercial industry produces parts with diverse and improved properties in size, shape, complexity, composition, and detail, while also presenting the opportunity to decrease costs. With improved ceramics, these newer AM

ceramics are also able to undergo sintering or application of heat to cause natural polymers to form much more defined, intricate, and newer products.

For preceramic polymers being able to be easily converted or changed between different phases, such as solid to liquid or a paste, the physical properties are easily malleable and can help in the creation of ceramic materials or PDCs [13]. That is why many commercial industries are continually experimenting with the limitless possibilities for developing ceramic compositions with improved properties and characteristics.

Fillers being used during the AM of parts often are incorporated to help produce further ceramic phases that can meet alternate outcomes, if desired, such as a reactor with decomposition products of any potential polymer-forming carbides or a reactor to inert gases during pyrolysis instead of with the main ceramic. With improvements in AM and preceramic polymers, convenient technical solutions and process improvements could be implemented that would enable manufacturers to overcome problems intrinsic to AM in general [23]. Some of those problems include, but are not limited to, structural support to prevent creep or sagging during printing and layer support as each is printed on top of each other.

3. Rocket Nozzles/Aerospace Industry

Rocket nozzles used for spacecraft experience extremely high temperatures due to the combustion of the fuel with oxidizers and high pressures. The ablative materials required to protect some of the launch systems must be lightweight but still capable of withstanding rapid erosion and extreme temperatures. Likewise, “system components need to be protected from extreme flow temperatures of 1,000 to 4,000°C and highly abrasive particles at velocities” up to potentially 2,000 m/s [24]. PDCs and ceramic matrix composites (CMCs) provide a measure on improving protective ablative materials. Through lower density and a higher-temperature stability, these allow for weight reduction within not only space launch vehicles, but also military aircraft/engines and less cooling needed for engine performance.

For most space launch vehicles, the rocket nozzles or exhaust flow can be different depending on the type of nozzle. With varying nozzle sizes, wall thicknesses, and flow

patterns (just to list a few parameters), the composition of these nozzles could influence and contribute to the overall performance. Differing material composition could provide for an optimized strength-to-weight ratio, varying levels of thermal shock and erosion resistance, and resistance to shear force/stress [25]. Additionally, nozzles experience changes in pressures and temperatures with varying altitudes as they exhaust fumes. These changes influence their overall effectiveness.

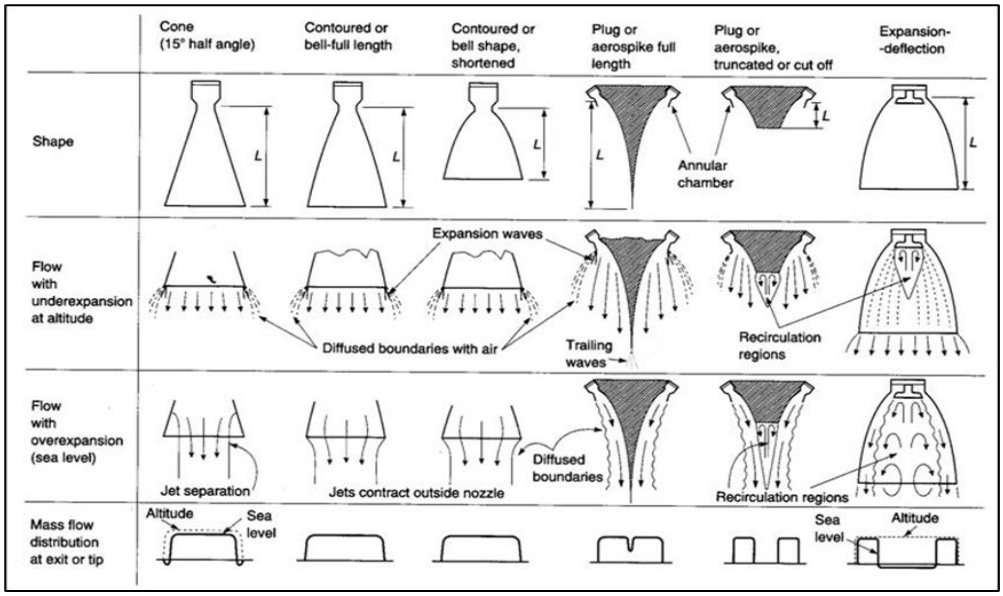

Simplified diagram of several different nozzle configurations and their flow effects.

Figure 6. Nozzle Exhaust Flow Patterns. Source: [26].

When designing nozzles, several parameters are considered to ensure that they suffer minimal degradation. Among those considerations include “aerodynamic inside contour, thermal design for the thickness of the nozzle lining material, and the overall design” structure so that it can withstand the motor-firing produced mechanical loads [27]. Since the inside of the nozzle experiences extreme temperatures and a harsh environment due to the pressure and particles being exhausted when solid propellants are used, ablative high-temperature composites of graphite are used. Ablative composites containing graphite usually possess a high heat of ablation, high enthalpy of phase change, sufficient strength with a mean value of about 45 MPa, high specific heat, high thermal shock resistance, and

crack propagation resistance of 1.7 MPa [28]. These characteristics show why they are used as the standard material composition for nozzles, specifically for space launch vehicles. The protection from the ablative materials is helpful especially because the melting temperature of the rocket nozzle is lower than the temperature of the gaseous products exiting from the nozzle.

During the construction or development of rocket nozzles, another factor that also goes into play for whether the ablatives will work depends on if the rocket will be liquid-fueled or solid-fueled. For most of the cases where the ablatives would work better for rocket nozzles, those were primarily referring to the solid-fueled rocket engines. Those ablatives or composites would just need to be able to withstand higher temperatures of the gases exiting the nozzle. In liquid-fueled rockets, the nozzle and the combustion chamber would need to be cooled, so the ablatives would still work but additionally act as an ablative-cooling mechanism for the nozzle [26]. The primary difference between the two is that in a liquid-fueled rocket engine, fuel flow can be controlled and is more efficient compared to a solid-fueled rocket. Furthering development within AM of composites has allowed ablatives to be used for improving air flow while decreasing the overall degradation of the nozzle over time. Maximum heat transfer and flow also is usually reached near the nozzle throat and mainly in the outward radial direction [29]. That is where ablatives are normally more prominent for the rocket nozzles. Since rockets are becoming more reusable within the commercial industry, such as with SpaceX, improving the coating material in the nozzles would greatly reduce overall costs and improve overall efficiency, enabling greater payloads and propellants to be used.

4. Characterization of Additively Manufactured Products

Most additively manufactured products need to be characterized to understand their mechanical and thermal properties in relation to their structures. These properties help to identify characteristics of the components that were used and the performance of the final products. Depending on the stages of development, the materials undergo several steps before arriving to the desired product, and each step has an importance on the properties discovered through these tests.

The relevant testing methods include, but are not limited to, mechanical (tensile and compression) testing, microscopic imaging using a scanning electron microscope (SEM) and/or an optical microscope, energy-dispersive x-ray spectroscopy (EDS), x-ray powder diffraction (XRD), x-ray computed tomography (CT) and thermal testing. Under the American Society for Testing and Materials (ASTM) standards, mechanical testing measures the force required to break a part in a specific geometry under tension or compression to evaluate its elastic modulus, yield strength, and ultimate tensile strength or crush strength (when compression is applied). SEM/EDS and/or optical microscopy help to determine microstructure, porosity and composition of the materials that can influence their mechanical and thermal properties. X-ray CT scanning can generate the 3D geometry of a part non-destructively and can reveal pores and irregularities within. Thermal testing helps to determine the thermal conductivity of the material [30]. These are just a few of the primary tests conducted on materials to determine some of their physical properties and whether they are sufficient for a desired objective or mission.

a. Scanning Electron Microscopy (SEM)

Following the mechanical testing, the SEM and/or optical microscope can help examine to see how much porosity is within the component or material. When it comes to whether the material is durable and/or capable of preventing erosion or corrosion due to pores being available for other ions to accumulate in, having a smaller porosity amount is much more desirable for additively manufactured materials, let alone, any materials manufactured for use. For the SEM, it utilizes electrons that are fired through lenses and apertures that eventually hit the sample where secondary electrons are bounced off the sample to form a 3D image up to magnifications of more than 30,000x compared to a typical magnification of light microscopes at ~1,000x [31]. The optical microscope would be able to assist with images of the material at lower magnifications and would be able to provide light to the materials whereas the SEM would be in black and white. Through both forms of visual observation, materials can be analyzed, and valuable insight can be derived about whether the material is non-uniform in places along with how much porosity and density a material may have at certain parts of its geometry.

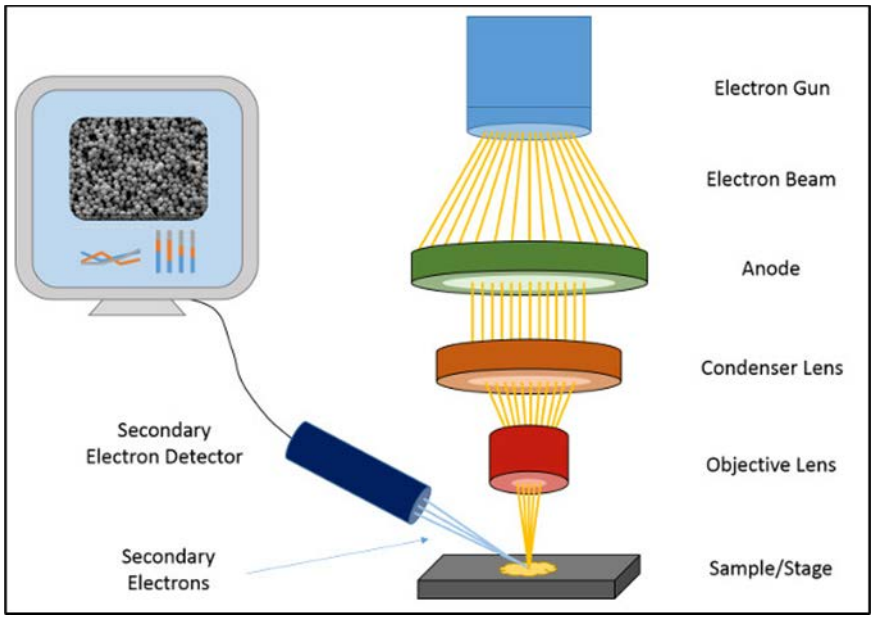

Figure 7. Schematic of the SEM. Source: [31].

b. X-Ray Computed Tomography (CT)

Next, x-ray CT primarily uses x-rays to develop a 3D image of the material and determine the distribution of its crystalline structure along with identifying features associated with the morphology of the material. For this process, it involves directing x-rays at the material being examined from multiple orientations and analyzing drops or decreases in the "intensity along series of linear paths" [32]. From those decreases in intensities, calculations are conducted from an algorithm to figure out just how much of the x-ray was attenuated during the beaming of x-rays. Just like SEM or optical microscopy, this is another method of analyzing the geometry and physical properties of the manufactured material to determine the expected reliability and performance.

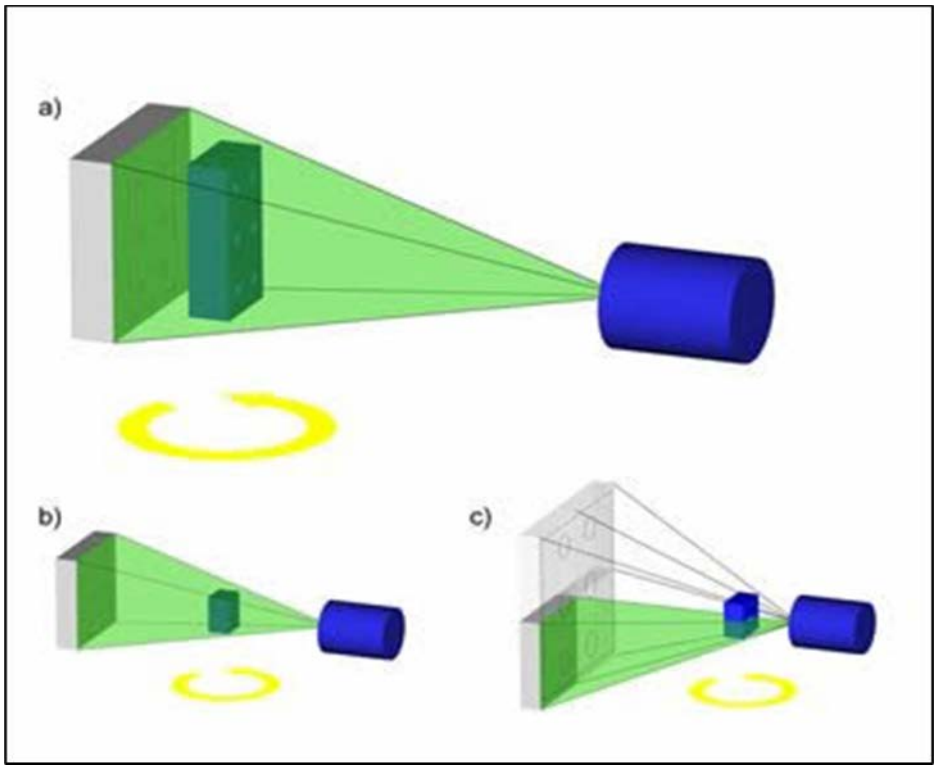

"a) Basic principle: Similar to a pinhole camera, the radiation emitted by a point X-ray source travels through the measured object to a flat sensor - images are taken for various rotated positions; b) Magnification adjustment: movement of the measured object relative to the sensor and to the radiation source; c) Raster tomography; images from various positions are stitched" [33].

Figure 8. X-Ray Tomography. Source: [33].

c. Electron Dispersive Spectroscopy (EDS)

Another test that can be done, usually in complement to SEM, is that of EDS. EDS is an analytical tool that helps to break down the elemental composition or characterization of the sample within the instrument. Normally, a specific area of interest is identified that had secondary electron and backscatter come off the material, where an x-ray is then emitted when the electrons have returned to a ground state [34]. The detector then picks up the x-rays which help to essentially give elemental composition of the material.

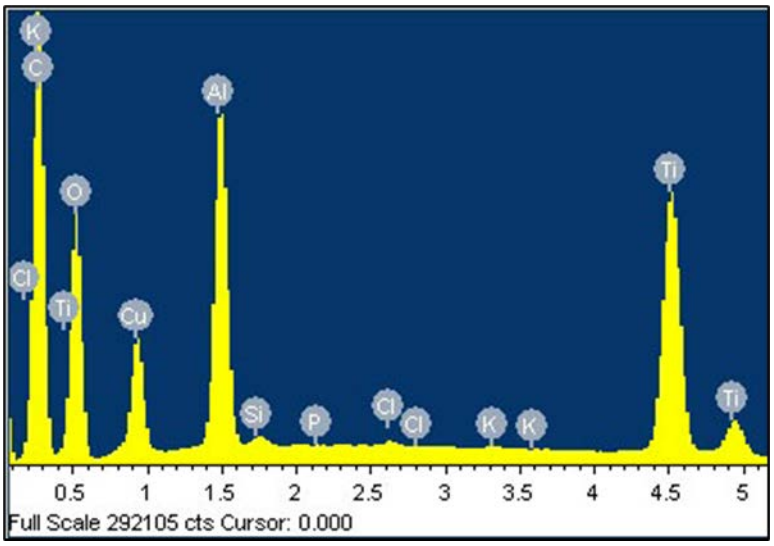

Figure 9. Example of EDS Analysis That Gives Elemental Composition Depiction for a Material. Source: [35].

d. X-Ray Powder Diffraction (XRD)

Along with EDS and x-ray CT, x-ray powder diffraction (XRD) can also be conducted which also helps to analyze the composition of the material. Specifically, through XRD, it is a rapid analytical technique that helps to identify phase identification of the material. To do this, "x-rays are generated in a cathode ray tube by heating a filament to produce electrons," which are then accelerated toward a target through the application of voltage where it bombards the material with electrons [36]. With the sample additionally rotating, the x-ray spectra and count rate produced from the material are used to help identify, not only the geometry, but also the phase it is in. In most cases, this helps to make sure that the material is known and does not have any unknown components or mismatch between films or layers. Once again, this instrument is another valuable insight technique used to help further classify the material being tested.

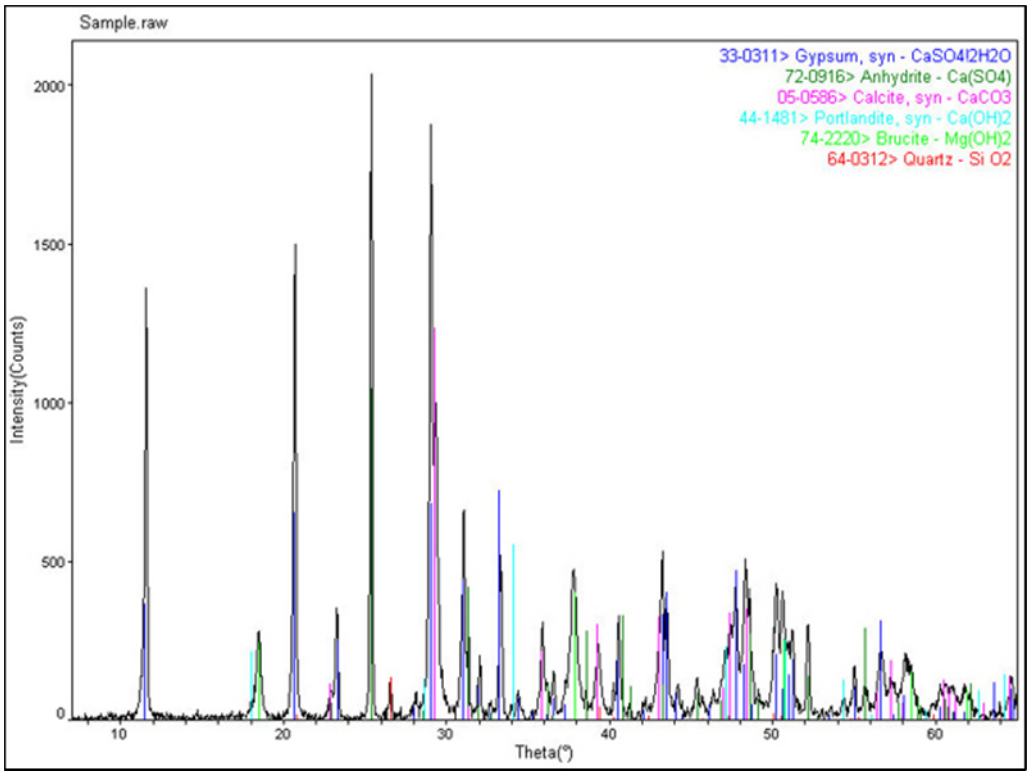

Raw sample where peaks represent intensity of the wavelength, and theta represents the angle of the x-ray beam in respect to the direction into planes of the material.

Figure 10. Example of XRD Analysis Source: [37].

Lastly, for thermal testing, it is based upon whether the analysis needs to be destructive or non-destructive. If the testing needs to be non-destructive, there are various approaches that can be taken that end up measuring the amount of excitable energy within the material from an outside thermal source. As for destructive testing, this can include, but not limited to, the scorching or actual testing of the material's ability to withstand varying degrees of temperature or thermal energy. Thermal testing will be dictated by the purposes and overall focus of data needing to be obtained from the research.

C. OBJECTIVES

The objective of this thesis is to additively manufacture SiC rocket nozzles using SiC powder blends with SiC-forming polymers using a VAP AM system. The effort includes the use of 3D-printed molds with a regular fused filament fabrication system to compare the printed part quality and properties to some of the materials utilized in rockets

today. Specifically, the mixture ratio and processing settings of the SiC ceramic-forming polymer mixtures will be investigated to improve mechanical and thermal properties that would be advantageous for the overall efficiency of ablatives or protective coatings used in a rocket nozzle's performance. Through 3D printing the ceramic matrix of SiC composites, the focus would be to demonstrate potential geometric features that could improve the overall performance of modern-day rockets. The objectives could be further broken down into steps that are trying to be accomplished during the thesis:

1. The mixing, curing, sintering, mechanical and thermal testing of the mixed (blended with a mixer) samples without printing followed by characterization of their microstructures.
2. Investigate the curing, sintering, mechanical and thermal testing of the mixed samples with 3D VAP followed by characterization of their microstructures.
3. Investigate the differences in dimensions, porosity, density, and adhesion of non-printed (filled in molds) SiC powder with SiC polymer and then printed SiC powder with SiC polymer.
4. Test the nozzles through thermal testing available such as torching them through an applied heat source or rocket lab.

THIS PAGE INTENTIONALLY LEFT BLANK

II. EXPERIMENTAL METHODS

A. MATERIALS

The preceramic polymer material used in this study is SiC Matrix Precursor 10 (SMP-10), acquired from Starfire Systems, Glenville, NY. SMP-10 is a polycarbosilane and forms SiC upon pyrolysis. From the technical data sheet, it has a reported density of 0.998 g/cm^3. It is the only liquid precursor to SiC ceramics at room temperature and can produce a silicon to carbon atomic ratio of 1:1 meaning the yields are near stoichiometric [38]. With the properties of this precursor, it is possible to produce highly, pure ceramics (Figures 11 & 12). The recommended curing temperature for SMP-10 is 250°C. SMP-10 can be pyrolyzed, forming amorphous SiC at approximately 800°C and forms crystalline SiC beyond 1000°C. Powders of 99.5% purity SiC with a mesh size of -400 were used from Sigma-Aldrich for the blend. The powder has a green-grey to bluish-black tint within its powdered and crystalline forms, when it is of high purity [39]. In this study, the 3D-printed formulations investigated contain 80–85 wt.% SiC in powder form and SMP-10 for the remaining amount.

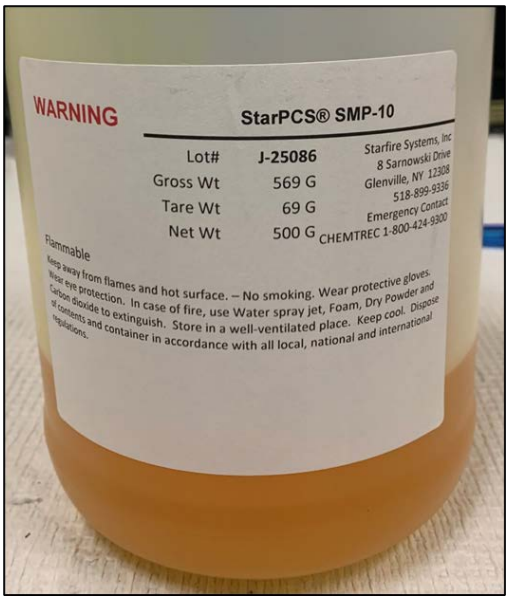

Figure 11. SMP-10 Precursor Polymer.

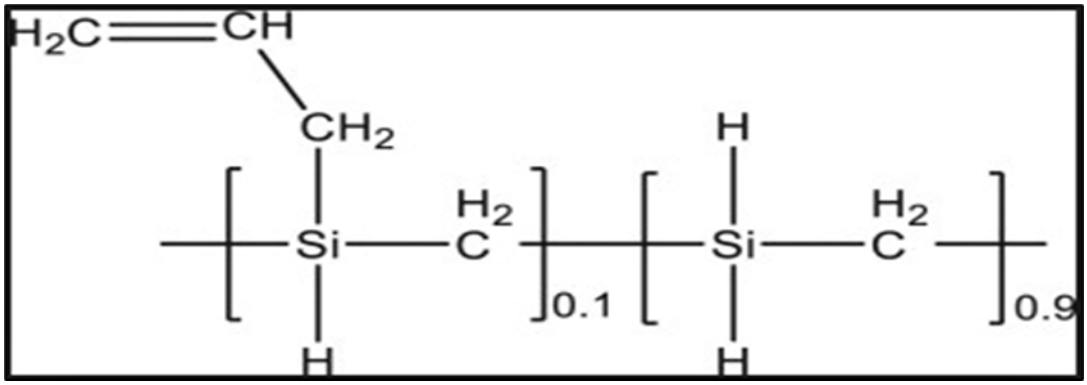

Figure 12. Reported Structure of SMP-10. Source: [40].

B. SAMPLE PREPARATION

1. Precursor Processing

For the initial stages of the precursor processing, the SMP-10 was left out for up to 7 days in air to remove the most volatile species. This was done to minimize mass loss in later stages which reduces porosity. The SMP-10 losses were minimal, around 1–2% by mass, after this treatment. Prior reports suggest using vacuum and heating to drive out these volatiles around the same amount [41]. The viscosity of the material at these elevated temperatures allows for the low molecular-weight oligomers to become volatilized but not rapidly cured [42]. However, initial testing suggested that this was not necessary and that just room temperature exposure generated similar amounts of mass loss.

After measuring the mass loss, the polymer was kept in a closed container until sample preparation. The samples were mixed at the appropriate mass ratios and kept sealed until further processing.

Throughout this research, the primary SMP-10 polymer underwent several approaches on trying to remove the volatiles from the material. Each approach focused on allowing the polymer to be exposed to varying levels of either heat or air to remove any unwanted components in the compound. The approaches conducted through the preparation of the SMP-10 are highlighted below:

Approach #1: The SMP-10 was aired out for 24 hours. Mass loss was then measured at the end of the 24-hour period.

Approach #2: The SMP-10 was placed into a beaker on a hot plate set to have a surface temperature that ranged through multiple trials from 90℃ to 130℃. It was then heated for 4 hours and measured for mass loss (Figure 13).

Approach #3: The SMP-10 was placed into a beaker on a hot plate with a surface temperature around 90℃ and had a magnetic stirrer spinning during the duration of the 4 hours it was heated. Mass loss was then measured.

Approach #4: The SMP-10 was placed into a container and then placed into a thermovac for 24 hours under vacuum (-760mmHg) at 90℃. Mass loss was then measured at the end of the 24-hour period.

Approach #5: The SMP-10 was placed into a container and then placed into a thermovac for 18 hours under vacuum (-760 mmHg) at 70℃.

Figure 13. Hot Plate Used for Heating SiC Precursor for Mass Loss.

These approaches were conducted to identify the most advantageous, mass-loss method. After proceeding through some of the approaches, it was then determined that the SMP-10 was aged over time since mass percentages varied. Hence, the last approach was the most appropriate for the already partially cured state of the aging SMP-10. Upon completion of curing the SMP-10 (Figure 14) for removing the most volatiles, the next step

was to mix it with the SiC powders to produce varying levels of viscosity for printing within the VAP.

Figure 14. SMP-10 Post-Curing.

a. Mixing

Most of the mass loss was observed during the curing of the SMP-10, showing an approximate 10 wt.% mass loss during the heat treatment in the curing process due to volatilization of low molecular-weight oligomers [40]. However, due to the aging of the SMP-10 and the different approaches, lower levels of mass loss were obtained. After the mixing, the SiC formed a thick-paste adequate to print through VAP with a focus on more viscous material. The SiC powders used were Sigma-Aldrich (coarse (-200-450 mesh particle size-Lot # MKBJ8589V) and fine (-400 mesh particle size-Lot # MKBN2849V)) powders (Figure 15). Ratios of powder varied from 75–84 wt.% and SiC precursor (post-mass loss) varied from 16–25 wt.%. Mixing of fine-to-coarse powder ratios were also tested with ranges between 40% fine and 60% coarse up to 100% of fine powder.

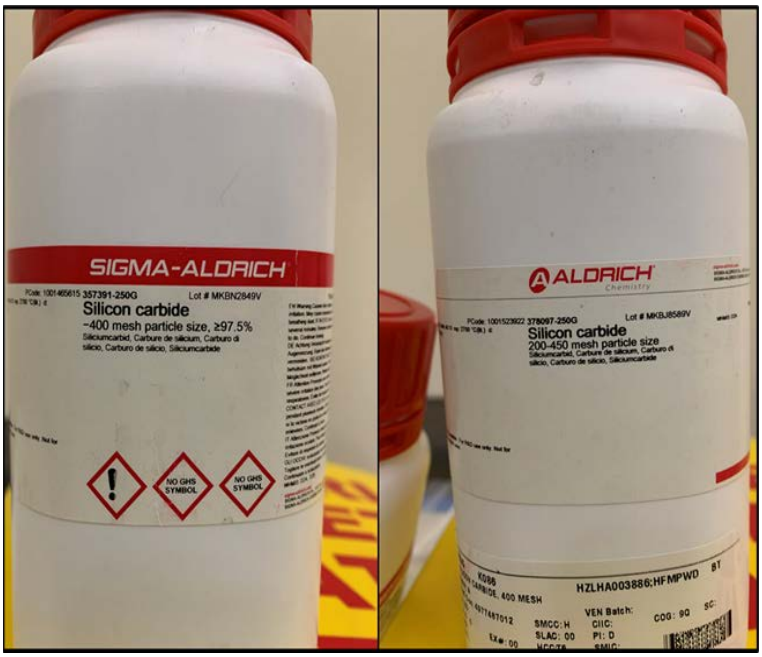

Figure 15. SiC Fine (~400 Mesh Particle Size) and Coarse (200-400 Mesh Particle Size) Powders.

Each approach was focused on varying levels of powders to SiC precursor to maximize the solids loading and to ensure a greater, viscous-printed end-result compared to conventional 3D printers. Prior to putting the material into the mixer, the powder and precursor were mixed with a spatula. The mixer used next was the FlackTek, Inc. Speedmixer (Model #DAC 150.1 FVZ-K). The approaches taken for mixing the SiC precursor and SiC powders are shown below (Figures 16-18).

Approach #1: Mixed at 1200 RPM for 1 min (x2)

Mixed at 3000 RPM for 15 secs (x2)

Mixed at 1200 RPM for 2 mins

Mixed at 3000 RPM for 15 secs (x2)

Mixed at 1200 RPM for 2 mins

Approach #2: Mixed at 1200 RPM for 1 min (x2)

Mixed at 3000 RPM for 15 secs under vacuum (x2)

Mixed at 1200 RPM for 2 mins under vacuum

Approach #3: Mixed at 1200 RPM for 1 min under vacuum (x2)

Mixed at 3000 RPM for 5 secs under vacuum followed w/ immediate. fan cool

*Repeated for one more cycle all under vacuum

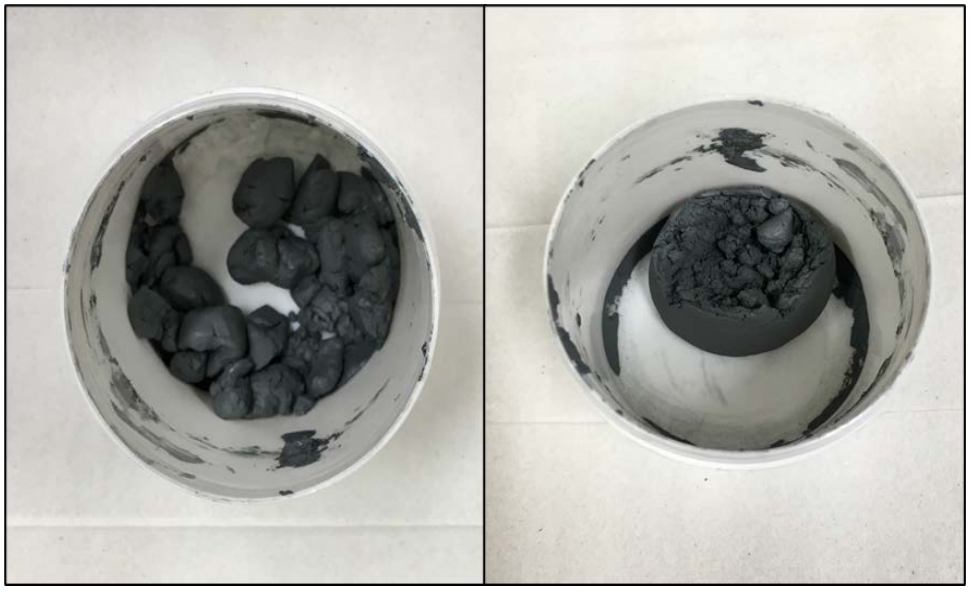

Figure 16. SiC Powder + SMP-10 Mixture (Left-After Mixing at 1200 RPM, Right-After Mixing at 3000 RPM).

Figure 17. Vacuum-Sealed Holder for SiC + SMP-10 Mixture to be Mixed in.

Figure 18. FlackTek, Inc. Speedmixer

Upon completion of mixing, visual observation using a spatula was conducted to see if the material was adequate to be put through VAP. Stiffness and viscosity were key components observed after mixing. The mixing was adjusted due to the possibility of curing while mixing especially at 3000 RPM (timing adjusted from 15 secs to 5 secs). Vacuum mixing was also conducted with a specialized container to help remove potential air and further the mixing of the precursor and the powders. The last approach was decided upon for maximum efficacy based off powder/precursor mixture ratio.

b. Curing

The next step in processing the SiC polymer and the SiC powder into a ceramic is curing. In curing, the polymer chains of SiC are crosslinked bringing about enough hardening of the material and meshing of components. To do this, the materials were exposed to heat and the corresponding reactions can be denoted by the appropriate equations below signaling the two equations they would respectively undergo during curing (Eq. 5 and Eq. 6) [42].

$$\equiv Si{-}CH2{-}CH{=}CH2 + \equiv Si{-}H \rightarrow \equiv Si{-}CH2{-}CH2{-}CH2{-}Si\equiv \quad (5)$$

$$\equiv Si{-}H + H{-}Si \rightarrow \equiv Si{-}Si\equiv + H2 \quad (6)$$

Samples of predetermined precursor to powder ratios outlined previously were placed in the Accutemp-09 Series (248.8℃) Vacuum Drying Oven (S/N: 2018110133) a.k.a. thermovac or thermo-vacuum (Figure 19).

Figure 19. Accutemp-09 Series (248.8℃) Thermovac.

Samples were either filled into (1 cm^3) silicon-molded cubes and placed into the thermovac or printed through VAP in (1 cm^3) cubes and placed into the thermovac. Throughout the research, the curing approaches changed only slightly since the focus was to eliminate any air gaps within the material and to help improve the crosslinking of SiC chains. Approaches for the thermovac that were conducted are highlighted below [41]: (All were based off Potticary Thesis work)

Approach #1: SiC samples were placed into thermovac under vacuum (-760 mmHg) at 100℃ for 10 hours followed by max temperature of furnace (248.8℃) for 3 hours.

Approach #2: SiC samples were placed into thermovac for 4 hours at each: 80℃ for 4 hours, 100℃ for 4 hours, and then 248.8℃ for 4 hours.

Approach #3: SiC samples were placed into thermovac under vacuum at 80℃ for 4 hours, 100℃ for 4 hours, and then 248.8℃ for 4 hours.

Thermovac temperature and curing duration times were varied due to the uneven curing and sample expansion throughout the earlier tests. Removing the air pockets in the samples was key so during pyrolysis, there would be less sample fragmentation. Fragmentation mostly arose due to a sudden build-up of air pressure from the production of gases in a confined space. Upon completion of the last stage of curing at 248.8℃ for the designated time, the samples were then ready to undergo pyrolysis.

c. Pyrolysis

Pyrolysis involves the thermally induced breakdown of cured polymers within a nonreactive atmosphere (such as a vacuum or nitrogen gas). For this pyrolysis, a high-temperature furnace was used (Lindberg/Blue M (M/N: CC59256PCOMC-1)-Control Module/Controls and (M/N: STF54434C)-Tube Furnace) (Figure 20), under an nitrogen atmosphere with a gas mass flow rate of (100 ml/s) on the SiC prepared samples.

Figure 20. Gas Tanks Pictured in Top Left (Connected to Nitrogen-Green Tank), Control Module in Top Right, and Tube Furnace in Bottom Center with Partial Endcaps on Tube (Denoted Black).

Prior to running the furnace, the pre-programmed parameters were as followed:

- Temperature heating rate of 10°C/min until it reached 1600°C and then hold for 1 hour followed by a ramp down to approximately 25°C.

The parameters above were then adjusted due to issues concerning heat building up and cracking the alumina tube the samples were placed in (stated below):

- Temperature heating rate of 5°C/min until it reached 1600°C and then hold for 1 hour followed by a ramp down to approximately 25°C.

The idea was that the rapid heating, cold gas flow, and the differential between the middle and the ends going outside the furnace caused the alumina tube to crack. Max temperature for pyrolysis was followed from research on polycarbosilanes [41]. After the program conditions were set into the control box, the samples were placed into rectangular

crucibles which were then placed into the middle of the furnace tube. The ends were then sealed with caps that had a tube allowing nitrogen gas to flow in through the entrance and then out of the end. Prior to starting the program, the connections were checked for leaks. The system was then started with the pre-programmed, set-up parameters. At the end of the runs, the system was cooled back down to approximately 25°C and samples were removed. Examination of the post-pyrolysis samples was then conducted.

2. Analysis During Sample Preparation

a. Scanning Electron Microscope (SEM)

Throughout the experimentation and testing, SEM was conducted on a Zeiss Neon 40 FESEM (S/N: 6227118257) (Figure 21). SEM was specifically utilized to characterize pore formation in the samples and determine the extent of the porosity and cracking. Samples were examined pre-curing, post-curing, and post-pyrolysis. The samples were examined at different stages of the sample preparation to determine microstructure and to see whether oxides were present and when crystallization occurred. Throughout the analysis, samples were examined under an accelerating voltage range of 5–20 kV, a working distance of 5mm, and an aperture range between 30–60 µm. Magnifications were conducted at 200x, 500x, 1,000x, and 2,000x for more specific analysis at areas of interest through each sample's surface. SEM analysis was able to provide context on whether certain mixes and approaches to preparing SiC were adequate along with if further adjustments of the ratio of the precursor and powders were needed. The overall purposes of the SEM were to ensure that preparation was reducing porosity, and to be able to compare the differences between a 3D-printed material and a molded sample.

Figure 21. Zeiss Neon 40 FESEM Scanning Electron Microscope (SEM).

b. Energy-Dispersive X-Ray Spectroscopy (EDS)

Immediately following the SEM imaging process, EDAX Pegasus EDS could be conducted from the same device on samples depending on whether material composition was needed. This was done to provide further context on whether impurities or any volatiles were still present within the material. As each stage was analyzed for the sample, determination on when oxides were eliminated could be revealed along with if any contamination or other chemicals could have been created during a stage of sample preparation. When testing the samples of SiC, identifying what percentage of each element was present helped to further provide additional context on possible properties. The TEAM software interface was what produced the resulting spectra of the image frozen on the SEM capture screen. Specifications for EDS for each sample of SiC were generally at a beam current of 15 mA, 15 kV, a 60 µm aperture, and 1,000x magnification. Stoichiometric ratio results were pulled as each sample underwent EDS.

c. X-Ray Powder Diffraction (XRD)

Prior to conducting any mixing for sample preparation, XRD was conducted on the SiC powders to determine if it was in the appropriate crystalline phase prior to subjecting it to temperature changes and mixes. Samples were grinded down to a small powder prior to putting it into the XRD. XRD was done using the Rigaku Corporation MiniFlex 600 W (C/N: 2005L101) (Figure 22). The measurement conditions for each sample started at a Theta scan range of 10 degrees and stopped at 90 degrees with a step size of 0.01 and 10 deg/min. Each run lasted approximately 8 minutes. XRD was also conducted on samples that were cured and some samples that went through VAP. Throughout this analysis, XRD helped determine the phase transformation for the samples as a function of solids loading and processing temperature to help determine which phases of SiC were forming based off temperature and mass loss. The results could produce amorphous (1 peak rounded) or crystalline (3 sharp peaks) phases depending on the state of the SiC. Identification of the crystalline phases were pulled from the Rigaku PDXL Crystallography Software and the Joint Committee on Powder Diffraction Standards (ICPDS) Database.

Figure 22. Rigaku XRD Analyzer.

d. Particle Distribution Analyzer

After some testing of potential mix ratios to be utilized between the precursor and powders, the particulate distribution analyzer by Horiba (Partica Model #LA-950S2) was

used (Figure 23). The purpose of this instrument was to determine the particle sizes of the SiC powders used since that would influence the mixing and printer viability. Specifically, the coarse powders contained larger particles that were considered unsuitable for VAP with the syringe nozzle size. With different variables being altered throughout the sample preparation, the powders were examined to provide further characterization of the starting powders before any fundamental changes occurred during curing, mixing, and/or pyrolysis since the particulate distribution analyzer could analyze particles ranging in size from 10 nm – 3 mm [43].

For this instrument, three runs were performed on each, the SiC fine and SiC coarse powders. Because the material was analyzed in acetone, the refractive index had to be corrected for the characterizing material and the dispersing liquid to be analyzed. Prior to each test being completed, the vials were filled with acetone and then had a magnetic plunger placed into them. Next, the vial was placed into a wet test holder for calibration. After calibration, the vial was removed from the analyzer cell and then had 10 micrometers of SiC placed into the vial for the first test and reinstalled back into the wet test holder. From then, the analysis was initiated and took roughly a few minutes before a graph with a distribution curve was generated showing measurements of the particles contained in the sample. The test was then repeated for a 15 micrometer SiC sample followed by a 20 micrometer SiC sample for the third and final test. With the results, a more delineated approach was taken for the SiC polymer-to-powder mixing.

Figure 23. Horiba Partica (Model #LA-950S2) Particulate Distribution Analyzer.

e. Thermal Gravimetric Analysis (TGA)

The TGA utilized to examine SiC samples was the NETZSCH Simultaneous TG-DTA/DSC Apparatus (Model # STA 449 F3 Jupiter) (Figure 24). The purpose of TGA was to determine the change of the mass of the samples with respect to temperature. TGA helped to determine how the polymer samples changed in mass during the chemical reactions involved for curing, pyrolysis, and thermal testing. With TGA specifically, the ceramic yield of a preceramic polymer can be deduced [41]. During TGA, the gas evolution or the gases that form as intermediaries could also be monitored. Through DSC, determination on when SiC underwent certain exothermic or endothermic reactions were depicted.

The NETZSCH TGA was used on two separate SiC post-cured samples in addition with the Proteus and Aeolos Software for mass spectra analysis and TGA scanning. Prior to inputting samples into the TGA, a correction test was done with an empty crucible to simulate the conditions without a sample. After a calibration test, it would be able to

provide more accurate changes when the actual heating/test of SiC was done. For the two runs conducted with SiC, the first one was used to provide a clear depiction of the overall mass changes that the SiC sample underwent from 30℃ up to 1400℃. For the second sample, it was stopped right before the major drop in energy (endothermic) so that XRD analysis could be done using the two examined samples for further clarification on the phases they were in. The samples had an average mass of 20 mg and were placed in a crucible and heated up to no more than 1400 K at a heating rate of 2 K/min. The mass and the released gases were simultaneously monitored. Argon gas was utilized as the inert gas being inputted into the system during testing to prevent any unwanted reactions with the samples.

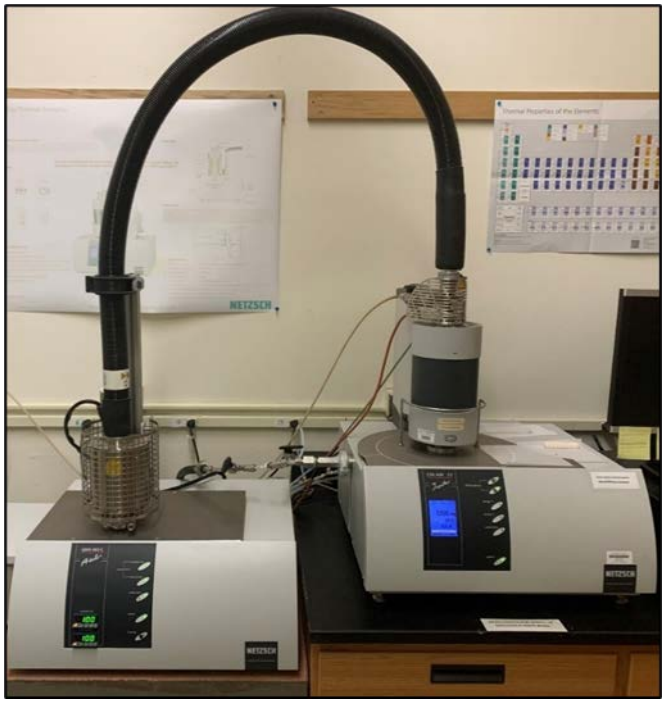

Figure 24. NETZSCH Thermal Gravimetric Analyzer.

f. Vibration-Assisted Printing (VAP 3D Printing)

Throughout the initial trials of printing, various methods were approached for VAP (Figure 25). Printing was adjusted for pressure applied to the nozzle to help with the SiC material being pushed through. Speed was factored in and adjusted as well for how fast the

nozzle moved for extruding the material in a desired configuration. Adjustments were made to the base of the printer that also changed desired temperatures such as having a heated base from a hotplate to help with the material build, layer upon layer, after it printed. Frequencies were also manipulated to adjust for the ultrasonic vibrations allowing for the heavier, solids-loaded SiC material to be pushed through the nozzle. The syringes used were packed withapproximately 5–8 grams of mixed material with the pressure varying from 10–110 psi depending on viscosities. Models were exported as STL files, then processed for slicing to GCODE files.

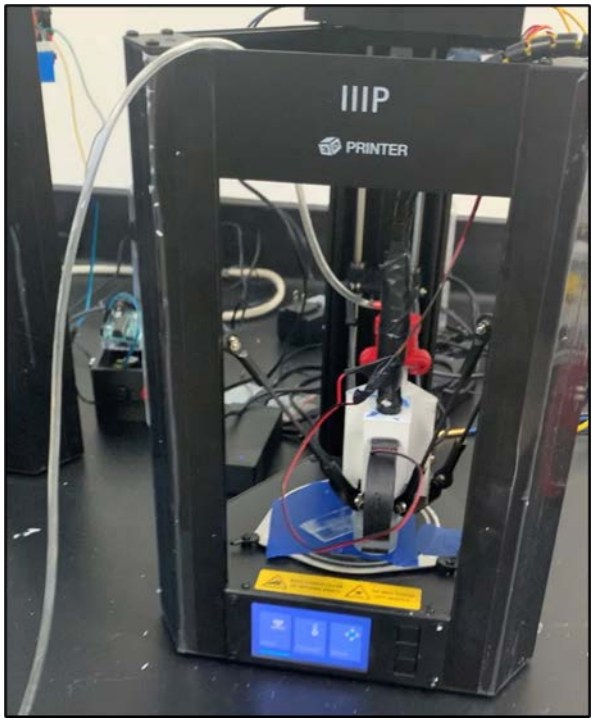

Figure 25. Vibration-Assisted Printer (VAP).

3. Rocket Nozzle Preparation and Analysis Procedures

Upon figuring out the correct mixture ratio and the additional steps required to create a SiC material capable of higher solids loading and one with a greater viscosity using the procedures described in the prior sections, the focus was shifted to the preparation of the rocket nozzle through AM. For the rocket nozzle, a 25 mm outer diameter

stereolithography (STL) model provided by NASA was used as a basis. This model has been used in the past for comparison of various AM methods. The rocket nozzle had a height of 24.45 mm. The length of the bottom of the nozzle was approximately 20 mm. During initial VAP, test-cube prints, the material printed tended to flatten and sag at the bottom as layers stacked higher. Since the SiC, ceramic-forming mixture would not be able to hold its shape for the rocket nozzle height, it was decided to hand-fill a mold for material processing and characterization. The negative of the nozzle model was created using Siemens NX computer software for the molds. The models were sliced using Simplify3D software for 3D printing. A custom python script was used to postprocess the GCODE files for VAP. The initial prints used a single-head, VAP system, whereas subsequent work was started using a dual-head, FDM-VAP system to simultaneously print a thermoplastic polymer and the ceramic-forming mixtures layer by layer. After successful modeling, a nozzle was then printed with PLA to make sure the STL model did not have any structural issues (Figure 26).

Figure 26. 3D Model of the Rocket Nozzle from Left to Right and a 3D-Printed PLA Sample.

The SiC material for the hand-molded, rocket nozzles (Figure 27) would be compacted into the mold after the mixing process in which it would then undergo curing and then pyrolysis. During the final stage of curing at 248.8℃, the PLA can be expected to melt off leaving the SiC nozzle since PLA melts above 170℃ [44]. Upon completion of curing, the SiC nozzle samples underwent pyrolysis as described previously.

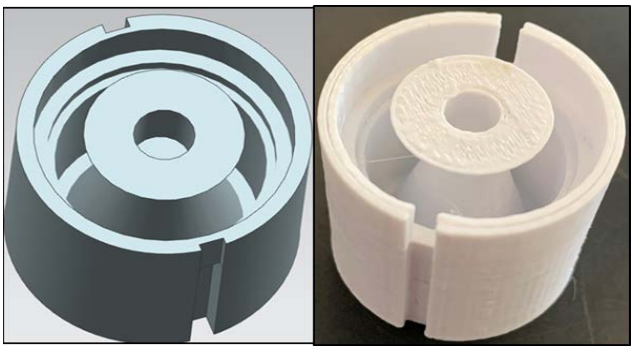

Figure 27. (Left) 3D Model of the Negative Mold of Rocket Nozzle. (Right) PLA Printed Negative Mold of Rocket Nozzle.

Prior to pyrolysis, SEM/EDS was conducted on the rocket nozzle to analyze the microstructure along with determine the porosity and if volatiles were present either from the PLA or other compounds. After pyrolysis, further SEM/EDS was conducted to then determine the micro-structure, porosity, and composition.

THIS PAGE INTENTIONALLY LEFT BLANK

III. RESULTS AND DISCUSSION

A. SILICON CARBIDE MIXTURE PREPARATION

1. SMP-10 Pre-Curing

Throughout the duration of the processing trials, SMP-10 pre-curing was investigated for 7 months. The work to adjust the temperature and the approach, along with time of heating the SMP-10, was decided upon after testing samples at various masses and durations under heating. At the beginning of the testing, a hot-plate approach with a magnetic stirrer was used to try to induce some mass loss. A magnetic stirrer and a sample batch size of 20 grams were used to allow the magnetic stirrer to mix and prevent the development of a film on the top of the SMP-10. Hot plate temperatures ranged between 45°C-105°C with approximate heating durations around 4 hours. One sample was tested at room temperature for 24 hours airing out to determine if the precursor lost any mass with just exposure to the atmosphere. Based on the results utilizing the hot plate and the airing out, mass-loss percentages ranged between 0.882%-2.941% with an outlier at 8.247%, although this might be due to a measurement error. The outlier was a smaller sample mass at 0.692 g whereas the other samples yielding most of the mass-loss percentages were larger sample sizes at approximately 19–20 grams of SMP-10 (Table 1).

Table 1. SMP-10 Mass-Loss Samples not Using Thermo-Vacuum

Method	SMP-10 (g) (Initial)	Temperature (°C)	Heated for time (hrs)	SMP-10 (g) (Final)	Mass Loss (g)	Mass Loss (%)
Hot Plate	0.692	75	3.5	0.635	0.057	8.237
Hot Plate w/ Vacuum + Magnetic Stirrer	20.054	45	4	19.877	0.177	0.882
Hot Plate + Magnetic Stirrer	20.066	75	4.5	19.665	0.401	1.997
Hot Plate w/ Vacuum + Magnetic Stirrer	19.665	75	4	19.270	0.395	2.008

Method	SMP-10 (g) (Initial)	Temperature (°C)	Heated for time (hrs)	SMP-10 (g) (Final)	Mass Loss (g)	Mass Loss (%)
Hot Plate w/ Magnetic Stirrer	20.102	77	4	19.511	0.591	2.941
Hot Plate w/ Magnetic Stirrer	19.511	105	4	18.987	0.524	2.685
Airing at Room Temp	3.021	Room Temp	24	2.983	0.039	1.274

Over a period of 7 months, SMP-10 pre-curing was conducted utilizing the thermo-vacuum at low vacuum. The temperature that most of the samples underwent was at approximately 90°C. Time heated ranged from 1–48 hours. Sample sizes were nominally 1 and 10 grams (Refer to Tables 2 and 3). Mass-loss percentages varied based off the time heated and the sample size. The smaller, gram batches had an inconsistent but greater amount of mass loss than the larger batches.

Table 2. SMP-10 Mass-Loss Samples under 10g Placed in Thermo-Vacuum.

THERMO-VACUUM (-760 MMHG) SMALL (< 10 GRAM) SAMPLES					
SMP-10 (g) (Initial)	Temperature (°C)	Heated for time (hrs)	SMP-10 (g) (Final)	Mass Loss (g)	Mass Loss (%)
1.046	90	1.2	0.998	0.048	4.578
1.014	90	1	0.941	0.073	7.173
1.040	90	2	0.932	0.108	10.422
1.016	90	3	0.896	0.120	11.832
1.132	90	4	1.001	0.131	11.572
1.134	90	4	0.999	0.135	11.905
1.174	90	6	1.028	0.147	12.486
1.167	90	6	1.025	0.142	12.129
1.023	90	8	0.919	0.104	10.129
1.109	90	8	1.002	0.107	9.640
1.096	90	8	0.991	0.105	9.538
1.05	90	24	0.9	0.15	14.285
1.02	90	48	0.852	0.168	16.471 (Gelled)
5.072	70	24	4.732	0.34	6.703

Table 3. SMP-10 Mass-Loss Samples at Approximately 10 g Placed in Thermo-Vacuum.

THERMO-VACUUM (LOW VACUUM) SMALL (> 10 GRAM) SAMPLES					
SMP-10 (g) (Initial)	**Temperature (°C)**	**Heated for time (hrs)**	**SMP-10 (g) (Final)**	**Mass Loss (g)**	**Mass Loss (%)**
10.022	90	24	9.24	0.782	7.803
10.018	90	24	9.261	0.757	7.556
10.003	90	24	9.163	0.840	8.399
10.014	90	24	9.179	0.835	8.336
10.028	90	24	9.232	0.797	7.943
10.044	90	24	9.230	0.814	8.107
10.031	85	24	9.139	0.892	8.892
11.539	70	12	11.019	0.52	4.506
11.019	70	6.25	10.895	0.124	1.125
10.601	70	18	9.976	0.625	5.896

Once 10-gram batches were used for samples for about 24 hours, the mass-loss percentages remained much more consistent. One sample was consecutively heated for varying times to determine if mass loss would change per increment of time heated (shown in Table 4). Mass loss remained consistent with consecutively heated, timed treatments.

Table 4. SMP-10 Mass-Loss Consecutive Sample Placed in Thermo-Vacuum.

THERMO-VACUUM (LOW VACUUM) CONSECUTIVELY HEATED SAMPLE					
SMP-10 (g) (Initial)	**Temperature (°C)**	**Heated for time (hrs)**	**SMP-10 (g) (Final)**	**Mass Loss (g)**	**Mass Loss (%)**
9.388	90	1	9.314	0.073	0.781
9.314	90	2	9.209	0.105	1.127
9.209	90	2	9.128	0.081	0.880
9.128	90	1	9.069	0.059	0.646
9.069	90	2	8.987	0.082	0.904
8.987	90	2	8.920	0.067	0.745

THERMO-VACUUM (LOW VACUUM) CONSECUTIVELY HEATED SAMPLE					
SMP-10 (g) (Initial)	**Temperature (°C)**	**Heated for time (hrs)**	**SMP-10 (g) (Final)**	**Mass Loss (g)**	**Mass Loss (%)**
9	90	3	8.893	0.027	0.300
8.893	90	2.5	8.845	0.048	0.540

SMP-10 has a recommended shelf life of 1 year. However, gelling and thickening was observed after six months of opening the container, which was especially drastic between the 5th and 6th months of testing. This might be due to thermal conditions of the laboratory, which might have seen increased temperatures that accelerated this aging process. The curing of this sample with previous settings of 90°C resulted in hardening of the polymer. Therefore, the final approach to conducting mass loss for SMP-10 was heating it at 70°C for 18 hours with a size of about 10 grams per sample under low vacuum. The mass-loss percentages were then approximately between 6–7%. If the temperature, size of sample (in mass), or time under heat was changed, then mass loss would also change (Refer to Figure 28 for all samples).

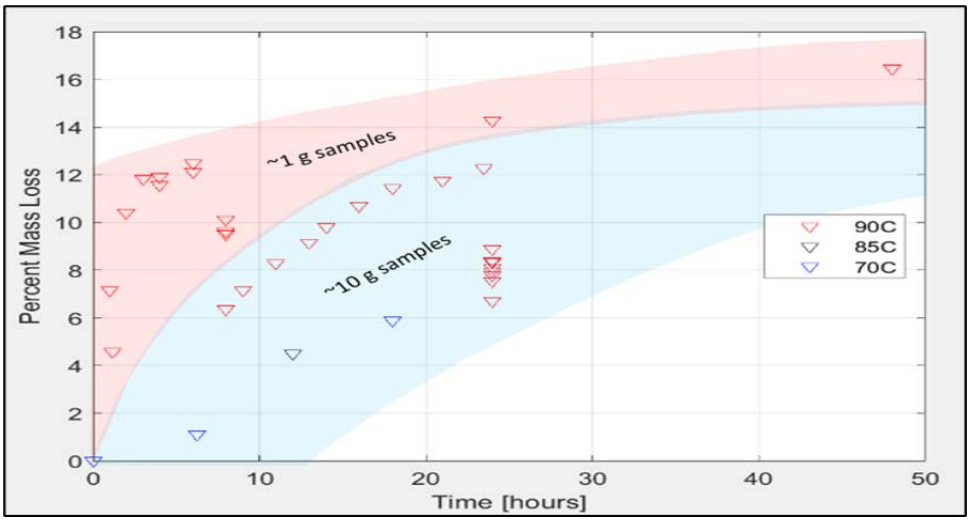

Description: ~10-gram samples provided a consistent amount of mass loss for 24 hours under heat at around 8 wt.%. After discovery of SMP-10 aging and having a shelf life, temperature was adjusted to 70°C and heated still for 18 hours with 10-gram samples. Resulting mass-loss percentages still ranged at approximately 6 wt.%.

Figure 28. SMP-10 Pre-Curing Mass Loss of all Samples.

SMP-10 pre-curing was important as a foundational step for the SiC mixing to help reduce mass loss occurring during the curing and pyrolysis of the actual mixed material to minimize shrinkage. Additionally, partially curing the SMP-10 allowed for the viscosity to increase, which overall, helped with printed-material consistency.

2. Mixing of SMP-10 and SiC Powders

Throughout the mixing of SMP-10, the materials were taken primarily from the 10-gram batches. At the beginning, most of the samples contained approximately 1 gram of SMP-10 mixed with a range of 3–4.5 grams of coarse SiC powder (ratios of 75–82 wt.% powder and 18–25 wt.% cured SMP-10) (Refer to Table 5). The viscosity of these mixtures continually varied with solids fraction.

Table 5. Coarse Powder Only Sample Mixtures.

Powder (g)	**SMP-10 (g)**	**Mix Ratio (Powd/SMP)**	**Mix Regimen**	**Notes**
4.035	1.008	80/20	Hand Mixed	Aired 72 hrs: 1.1% mass loss
4.003	0.757	84/16	Hand Mixed	Aired 24 hrs: 0.3% mass loss
4.104	0.951	82/18	2 min @ 2,510 RPM	
3.327	0.826	80/20	1 min @ 1,200 RPM (x2)	
3.595	0.896	80/20	1 min @ 1,200 RPM (x2)	
2.842	0.932	75/25	1 min @ 1,200 RPM (x2)	
3.313	0.932	78/22	1 min @ 1,200 RPM (x2)	0.471g powder added to previous batch
4.425	1.001	80/20	1 min @ 1,200 RPM (x2)	Too runny
4.562	0.999	82/18	1 min @ 1,200 RPM (x2)	Too gritty
4.113	1.028	80/20	1 min @ 1,200 RPM (x2) 15 sec @ 3,000 RPM (x2)	
3.645	1.025	78/22	1 min @ 1,200 RPM (x2) 15 sec @ 3,000 RPM (x2)	
3.454	0.919	79/21	1 min @ 1,200 RPM (x2) 15 sec @ 3,000 RPM (x2)	
3.819	1.014	79/21	1 min @ 1,200 RPM (x2) 15 sec @ 3,000 RPM (x2)	
3.874	1.024	79/21	1 min @ 1,200 RPM (x2) 15 sec @ 3,000 RPM (x2)	

Testing for a smoother consistency and an adequate viscosity was the focus of varying the ratios and determining the appropriate ratio between cured SMP-10 and the SiC powders. Fine SiC powder was then mixed into the coarse powder to increase solids loading and improve consistency during VAP of the mixtures. Ratios for cured SMP-10 to powder ranged primarily between 80–84% SiC powder and 16–20% cured SMP-10 with a powder mixture of 40–60% coarse and 40–60% fine (Refer to Table 6). During ceramics fabrication process, utilizing fine powders can help improve overall microstructure, remove more porosity, and induce a better flow of mixture [41]. Fine-tuning the powdered mixture to cured SMP-10 mixture was useful in allowing the precursor and the powder to sufficiently adhere to each other along with increasing the maximum amounts of the solids loading through improved packing.

Table 6. Introduction of Fine SiC Powder to Mixtures.

Powder (g)	**SMP-10 (g)**	**Mix Ratio (Powd/SMP)**	**Mix Regimen**	**Notes**
4.007	0.88	82/18	Two cycles of: 1 min @ 1,200 RPM (x2) 15 sec @ 3,000 RPM (x2) 2 min @ 1,200 RPM	60% Coarse/40% Fine
4.096	0.898	82/18	Two cycles of: 1 min @ 1,200 RPM (x2) 15 sec @ 3,000 RPM (x2) 2 min @ 1,200 RPM	50% Coarse/50% Fine
4.107	0.912	82/18	Two cycles of: 1 min @ 1,200 RPM (x2) 15 sec @ 3,000 RPM (x2) 2 min @ 1,200 RPM	40% Coarse/ 60% Fine
4.721	0.912	84/16	1 min @ 1,200 RPM (x2) 15 sec @ 3,000 RPM (x2) 2 min @ 1,200 RPM	Fine powder added to previous mixture
4.018	1.051	80/20	Two cycles of: 1 min @ 1,200 RPM (x2) 15 sec @ 3,000 RPM (x2) 2 min @ 1,200 RPM	100% Fine powder
16.034	4.006	80/20	1 min @ 1,200 RPM (x2) 15 sec @ 3,000 RPM w/vacuum (x2)	100% Fine powder

Powder (g)	**SMP-10 (g)**	**Mix Ratio (Powd/SMP)**	**Mix Regimen**	**Notes**
			2 min @ 1,200 RPM w/vacuum	
20.25	4.75	81/79	1 min @ 1,200 RPM (x2) 15 sec @ 3,000 RPM w/vacuum (x2) 2 min @ 1,200 RPM w/vacuum	100% Fine powder Mixture broke up in nozzle during VAP
20.25	4.993	80/20	1 min @ 1,200 RPM (x2) 15 sec @ 3,000 RPM w/vacuum (x2) 2 min @ 1,200 RPM w/vacuum	100% Fine powder Pre-processed SMP-10 added to previous mixture
21.291	5.000	81/19	1 min @ 1,200 RPM (x2) 15 sec @ 3,000 RPM w/vacuum (x2) 2 min @ 1,200 RPM w/vacuum	100% Fine powder
21.535	5.000	82/18	1 min @ 1,200 RPM (x2) 15 sec @ 3,000 RPM w/vacuum (x2) 2 min @ 1,200 RPM w/vacuum	100% Fine powder Fine powder added to previous mixture
22.008	5.000	84/16	1 min @ 1,200 RPM (x2) 15 sec @ 3,000 RPM w/vacuum (x2) 2 min @ 1,200 RPM w/vacuum	100% Fine powder Fine powder added to previous mixture
22.008	5.231	83/17	1 min @ 1,200 RPM (x2) 15 sec @ 3,000 RPM w/vacuum (x2) 2 min @ 1,200 RPM w/vacuum	100% Fine powder Pre-processed SMP-10 added to previous mixture
24.560	5.03	83/17	1 min @ 1,200 RPM (x2) 15 sec @ 3,000 RPM w/vacuum (x2) 2 min @ 1,200 RPM w/vacuum 15 sec @ 3,000 RPM	100% Fine powder
24.560	5.197	82.5/17.5	1 min @ 1,200 RPM (x2) 15 sec @ 3,000 RPM w/vacuum (x2) 2 min @ 1,200 RPM w/vacuum	100% Fine powder Pre-processed SMP-10 added to previous mixture;

Powder (g)	SMP-10 (g)	Mix Ratio (Powd/SMP)	Mix Regimen	Notes
				mixture began to harden
23.166	4.999	82.25/17.75	1 min @ 1,200 RPM (x2) 15 sec @ 3,000 RPM w/vacuum (x2) 2 min @ 1,200 RPM w/vacuum 15 sec @ 3,000 RPM	100% Fine powder
21.647	4.752	82/18	1 min @ 1,200 RPM (x2) 15 sec @ 3,000 RPM w/vacuum (x2) 2 min @ 1,200 RPM w/vacuum 15 sec @ 3,000 RPM	100% Fine powder
21.647	5.080	81/19	1 min @ 1,200 RPM (x2) 15 sec @ 3,000 RPM w/vacuum (x2) 2 min @ 1,200 RPM w/vacuum 15 sec @ 3,000 RPM	100% Fine powder

The optimal solids loading for VAP was determined to be at the 80–84 wt.% range. However, as will be shown in the following section, the coarse powders were discovered to contain many large particles beyond their specification that tended to restrict and clog flow during printing. As such, the formulations were switched to using only fine powders.

The mixing procedure for the SMP-10 and the powder yielded different consistencies as well depending on the approaches taken in the Flacktek Mixer. Raising the rotational speed to 1200 RPM for a minute each for two rounds allowed for the material to become more compact and well mixed. This was then followed by 3000 RPM for 15 seconds to allow for a greater shear mixing of the SMP-10 and powders. However, it was observed that this caused the material to partially cure and harden the mixture during mixing. This is due to the excessive heating of these extremely viscous materials under significant shear deformations in this kind of centrifugal mixing process. The duration of this high shear stage was reduced to 5 seconds. Initially, the material was mixed without a vacuum and then changed to utilizing a vacuum as it was observed that some air was being

entrapped in the mixture which caused expansion during curing. After the ratio of powder-to-SMP-10 was finalized at 80:20 wt.% and of 100% fine powder, the mixing procedure started with two 1-minute cycles of 1200 RPM with 1 minute of cooling for initial mixing followed by 3000 RPM for 5 seconds under vacuum with fan cooling afterwards to ensure the most adequate amount of mixing.

a. VAP Printing of Mixture

After each mixture was prepared, the materials were tested through single-head VAP extrusion and 3D printing of 6mm cubes with a nozzle size of 0.5 mm, layer heights of 0.2, 0.3, and 0.5 mm, a print rate of 10 mm/s, and a back pressure in the range of 20-100 psi depending on the material composition. The print rate was primarily limited by the printed track that dragged the rest of the sample at high speeds.

The earlier samples using just coarse powder and a designated ratio of SMP-10, resulted in clumpy and non-uniform prints. The bottom of the cubes tended to deform as more layers were printed due to the nozzle pushing on the sample as it squished the extruded material from a diameter of 0.5 mm down to the layer height of 0.2 mm (Refer to Figure 29). This is typically not a problem with polymer printers as the bottom layer is already solidified but it becomes an issue when the printed material is not hardened. Increasing the layer height to 0.3 mm and above helped this issue.

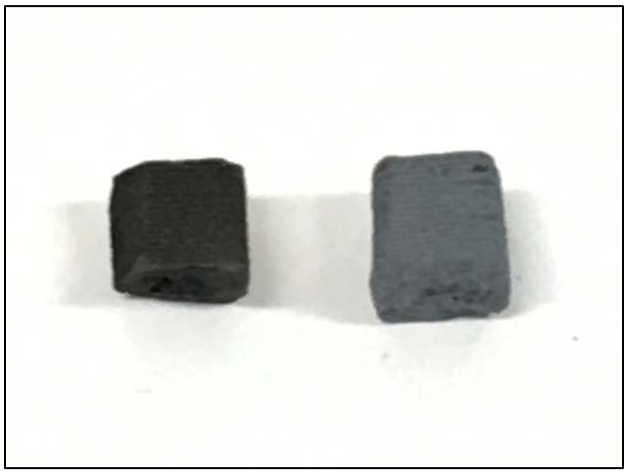

Figure 29. VAP Printed Samples.

Following these results, adjustments were made to the formulations as described previously incorporating fine powders into the coarse powder. This was intended to reduce the amount of deformation and creep that occurred as the specific powder area for the same volume would increase interparticle friction and stiffen the mixture, while also improving the consistency. The interparticle friction and steady mixture allowed the material that came out of the nozzle to be more continuous rather than separated clumps. Still, the printed material tended to have substantial creep at the base. Upon discovering the results of the particle size distribution analyzer for the coarse powder, 100% of fine powder was used and the ratios of SMP-10-to-powder were maintained around 80:20 wt.%. Printing consistency remained adequate and sustainable at this ratio including the type of powder used. After developing the appropriate mixture, mixing procedures, and testing of the mixture through VAP, it was then carried over to dual-extrusion VAP. This was specifically utilized for rocket nozzle applications by using two separate heads to print polymer on one side for support and viscous mixtures on the other side.

3. Curing and Pyrolysis of Mixture

After completing the printing of the materials and molding, the samples were then put into the thermo-vacuum for curing. The curing was done in three stages to have a slow-and-steady curing rather than having the material heat up and expand quickly due to gases that are expunged. Additionally, only some of the stages were performed under vacuum to help prevent any potential foaming and expansion in the not-yet hardened mixtures so that the SMP-10 would partially cure prior to completing its full cure at approximately 250°C based on its properties [41]. During curing, the SMP-10 precursor and the powders are meant to sufficiently crosslink to form a solid polymer. For pyrolysis, the purpose is to change the preceramic polymer into a ceramic. The curing duration was selected depending on the sample size with thicker samples requiring longer times. Using some leftover samples for testing, it appeared that each 6.35 mm depth required approximately 4 hours. For example, a cube with an edge length of 12.7 mm would require 4 hours of curing time for each temperature step. The three stages of curing at 80°C for 4 hours, 100°C for 4 hours and then 248.8°C for 4 hours helped to fully cure SMP-10. The molded-cube samples were placed into the thermo-vacuum in a silicon tray and the printed samples were placed on

glass slides. Then they underwent each phase slowly. Upon completion of the curing, the samples from both, the printed and non-printed parts, were hardened through crosslinking. For the initial curing stages, the process helped to remove lower, molecular-weight PCS so that the resulting products had less impurities and a much stronger micro-structure [45]. Samples came out roughly in cube-sized samples as highlighted in the figure below.

Figure 30. Molded SiC Post-Curing with 50:50 Coarse-to-Fine Powder and 82% Powder and 18% SMP-10 (All 3).

After completion of curing, pyrolysis was performed using the Thermo-Scientific High-Temperature Furnace (Figure 31) up to a temperature of 1600°C. The inert gas was nitrogen and after the first few trials, the alumina tubes shown in the figure cracked and the tubes were replaced for housing the samples. Additionally, most, if not all the initial samples, fragmented leaving miniature pieces of SiC remaining. This could have been due to trapped air, which prompted a switch to vacuum mixing of the samples or the rate of temperature increase on the samples. The maximum temperature was reduced to 1300°C but continual cracking of the tubes took place, possibly due to high thermal gradients at the ends and the convective cooling from the nitrogen flow. Preparations were made to utilize the miniature furnace/oven (Applied Test Systems, Inc Miniature Furnace Series 3210 Furnace/Oven (S/N: 02–1302)) (Figure 32) to conduct further testing of the smaller samples to ensure a steady build-up of heat without breaking the samples. TGA-DSC was conducted to help determine the temperature at which the SiC would fully undergo pyrolysis and turn into a ceramic from a preceramic (details will be discussed in TGA-DSC Section).

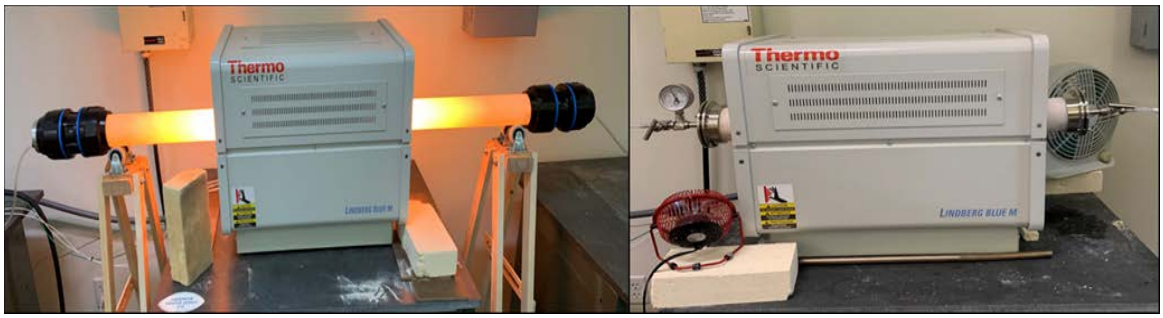

Figure 31. Thermo-Scientific Furnace Before (Left) and After (Right) Photos with Different Alumina Tubes that Cracked After Each Test.

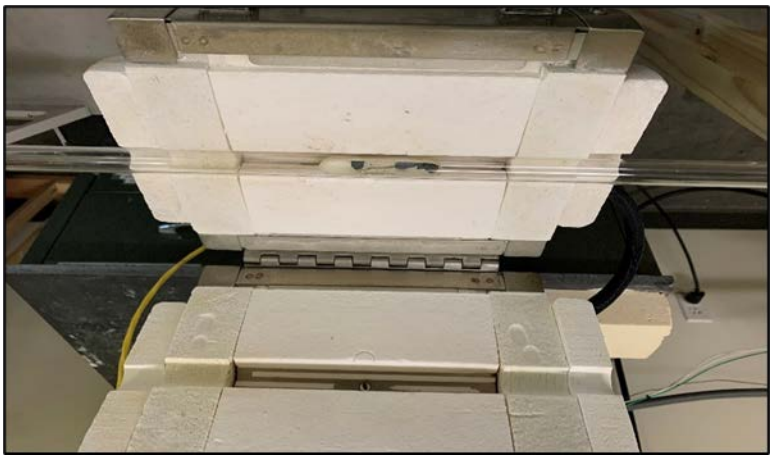

Figure 32. Applied Test Systems, Inc Miniature Furnace Series 3210 Furnace/ Oven (S/N: 02–1302).

After careful and slower progression in the increase in temperature from the miniature furnace, the further testing trials up to 1000℃ resulted in unbroken samples. The rate for the miniature furnace for temperature increases was 2℃/min. Each sample was placed on a crucible to go into the miniature furnace and was able to be observed periodically, if needed, by opening the furnace and seeing if any changes were undergone. Compared to an increase of 5℃/min in the earlier trials of the Thermo-Scientific furnace, the rate of increase seemed to be one of the driving factors for fragmented samples. Once adjusted to 2℃/min, the samples maintained their structure up to our last tested temperature of 1000℃.

4. Characterization of Prepared Samples

a. Particle Size Distribution Analysis

The coarse and fine particle sizes were determined using a particle size distribution analyzer. The particle size distribution analysis can help with determining the appropriate strategy and sizes to consider for mixing to optimize packing density and flow characteristics [46]. The results are plotted in Figure 33 for both the coarse and the fine powders. The fine powders had a lognormal distribution with a mean diameter of 22 µm, a D10 value of 14 µm (10% of the particles are smaller than 14 µm) and a D90 value of 33 µm (90% of the particles are smaller than 33 µm). These are consistent with the powder specification of -400 mesh, which has a sieve mesh opening of 32 µm. The coarse powders had a bimodal distribution with two separate lognormal contributions with mean diameters of 80 µm and 180 µm respectively, with a significant number of particles reaching diameters of 400 µm. The specification for this powder is -200-450 mesh, which corresponds to sieve mesh openings between 75 and 38 µm. It appears that in addition to this size range that was observed as the first peak, another set of large particles have been accidentally mixed in with this powder.

Discovery that the coarse powders containing large fragments caused clogging of printing nozzles that have an opening of 500 to 600 µm geared further work to exclude the use of the coarse-fine ratio. That is when fine powder was used for the remainder of the testing and mixtures. 100% fine SiC powder was used with ratios of 80–84% powder to 16–20% cured SMP-10. Sizes of the mixtures were then approximately 20–25 grams of powder with roughly 5 grams of cured SMP-10. Larger batches of the mixtures were prepared to supply adequate material for testing through printing.

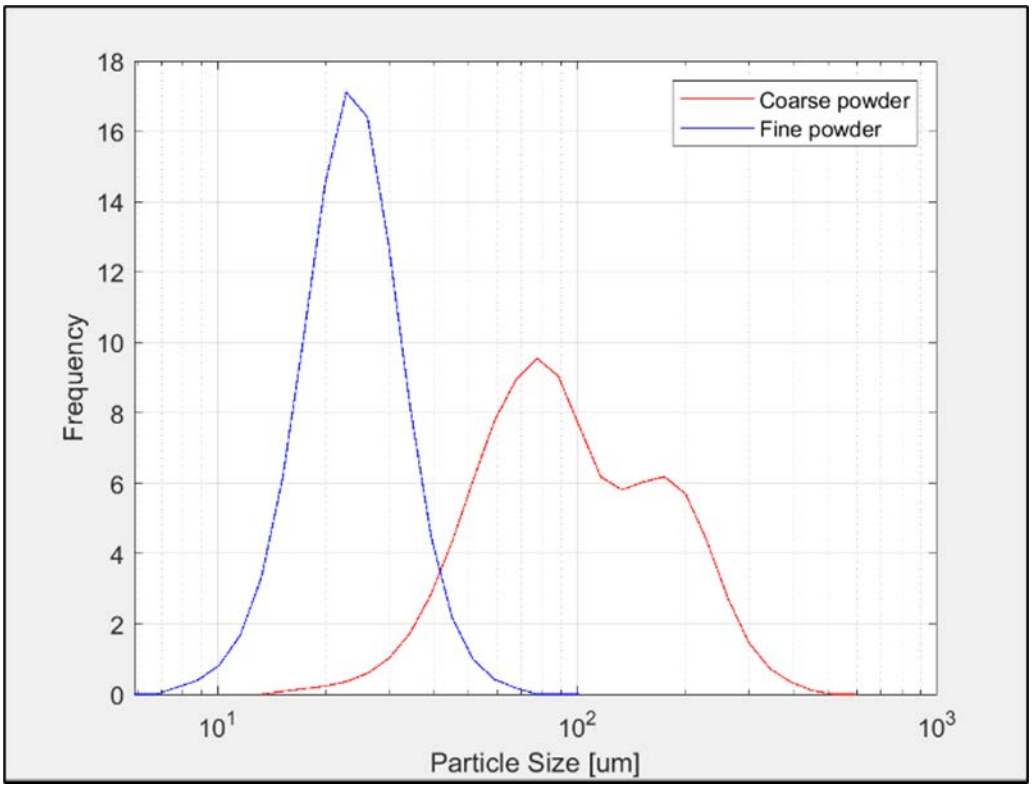

Figure 33. Particle Distribution Frequency versus Particle Size for the Fine and Coarse Powders.

b. XRD

Prior to conducting any curing and testing of mixtures, XRD was done on the two powders (shown in Figures 35 and 36). Based off the XRD PDF card reference number 01-075-8314, the powders were both in the 6H-SiC α phase prior to any curing and/or pyrolysis (Figure 34) [47], [48].

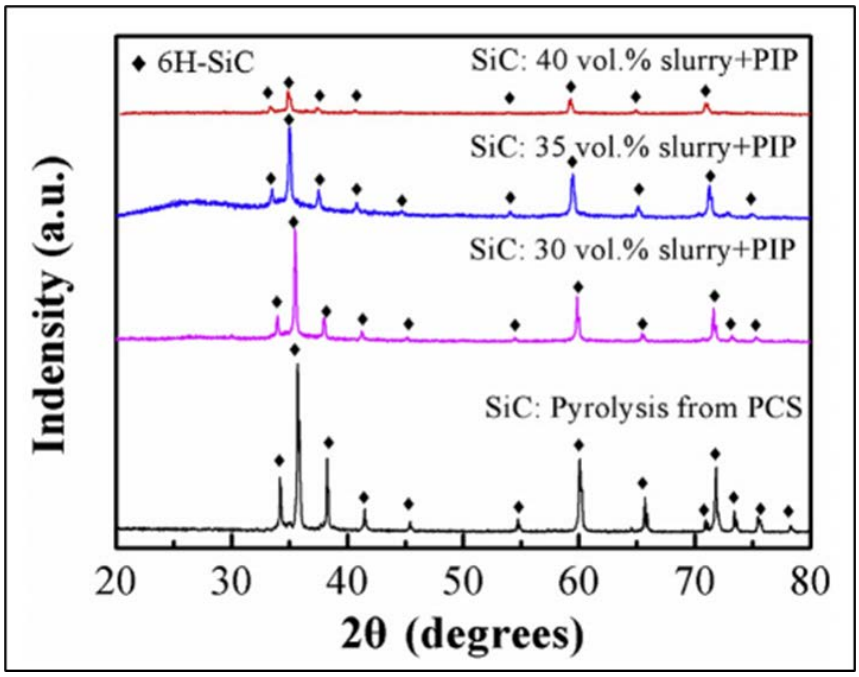

Figure 34. 6H-SiC α Phase Reference. Source: [49].

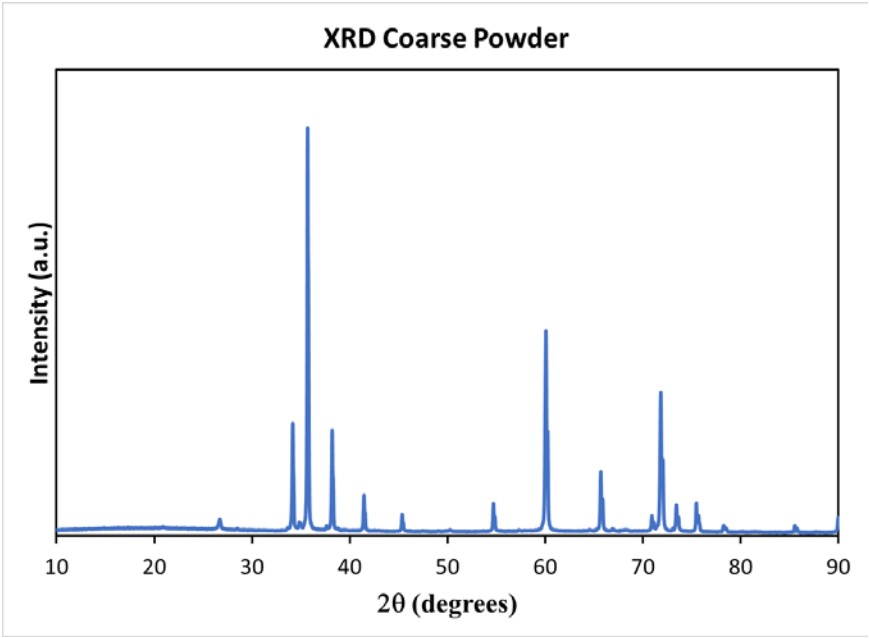

Figure 35. XRD Analyzed Coarse Powder.

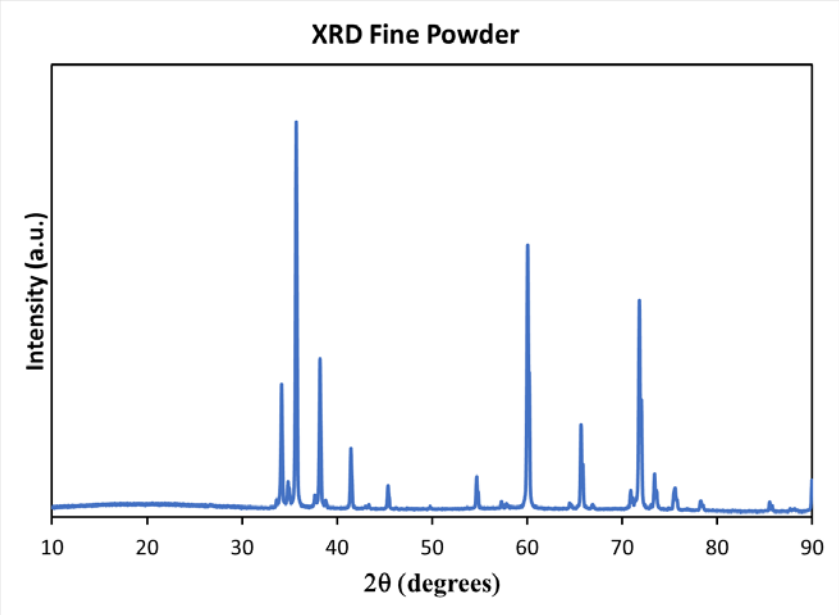

Figure 36. XRD Analyzed Fine Powder.

After the SiC was pyrolyzed at 1600C, only SiC peaks were detected, like the initial powders. (Refer to Figure 37). From XRD and EDS analysis, the corresponding 6H phase correlates to the appropriate SiC percentages present in the samples tested.

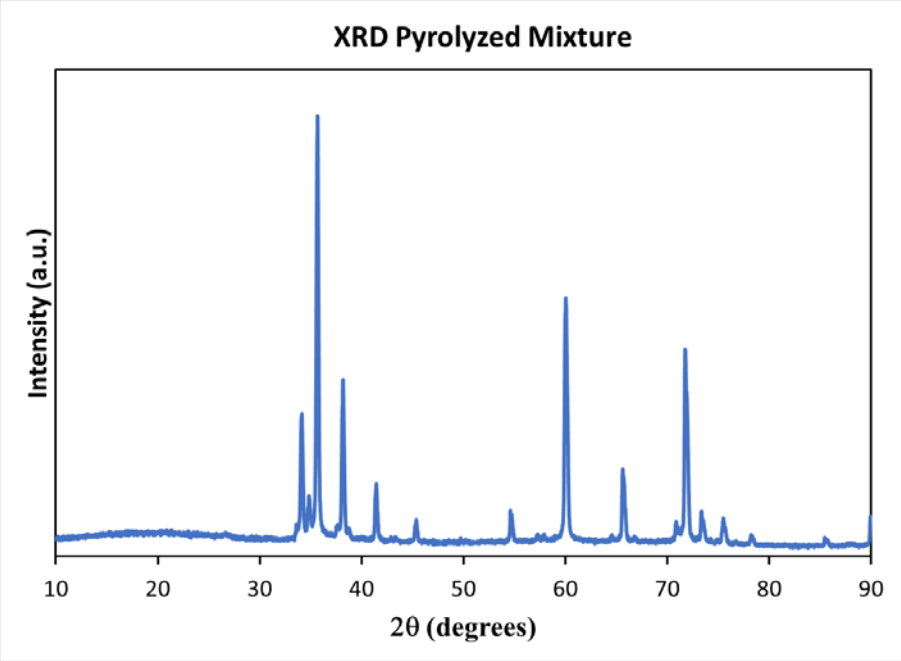

Figure 37. XRD Analyzed Pyrolyzed SiC Powder.

c. SEM

The SiC powders, post-cured mixed samples, and pre- and post- pyrolysis samples were analyzed using the SEM. Analysis of the powders was done to determine the morphology, microstructure, and the dimensions of the particles. The SEM images of the coarse particles at 150x and 250x magnifications are shown in Figure 38.

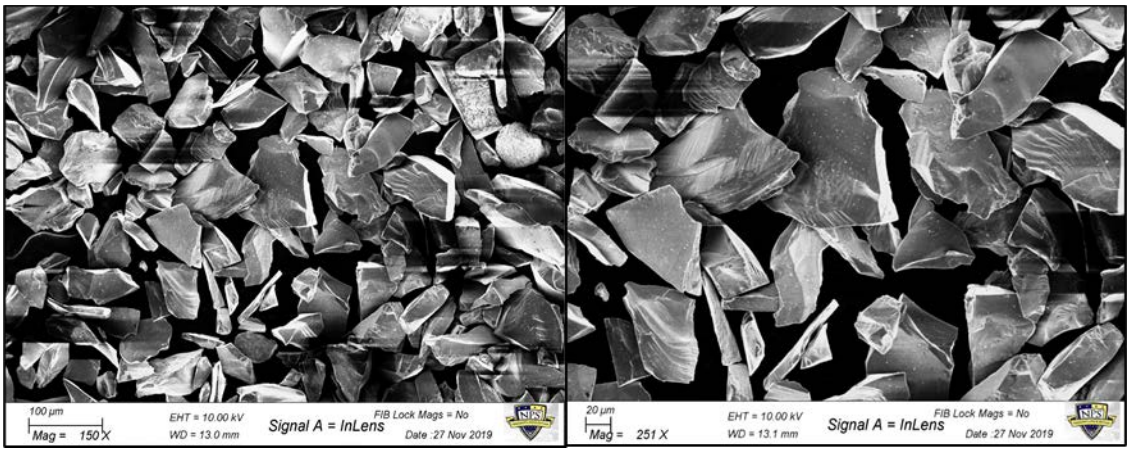

Figure 38. SEM Images of SiC Coarse Powder (Left-150x Magnification, Right-250x Magnification).

For the fine powder, SEM magnifications were 150x and 500x (Figure 39). In general, the particle surfaces appeared smooth with jagged edges, which is typical for ceramics that undergo brittle fracture during powder preparation. The particles had relatively uniform dimensions with a small number of thin or long needle-like particles present. The coarse particles were larger than expected from their specification with some particles having lengths approaching 500 um. This is consistent with the particle size analyzer results. The fine powders appeared similar with smaller overall dimensions.

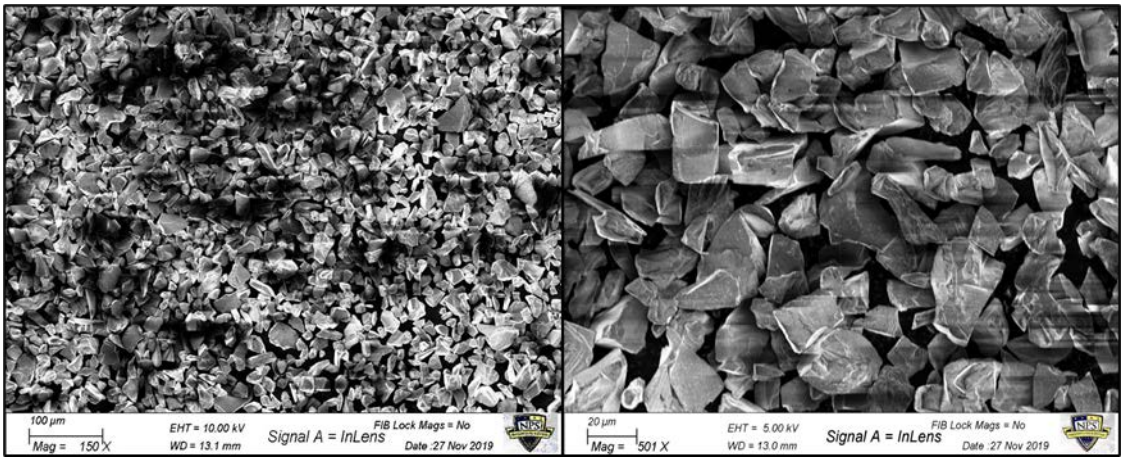

Figure 39. SEM Images of SiC Fine Powder (Left-150x Magnification, Right-500x Magnification).

An 80:20 mixture of 100% fine powder to SMP-10 after curing in a cube mold is shown in Figure 40. Magnifications went from 25x up to 1,000x. At the smaller magnification, the porosity on the surface was evident due to the degassing from the polymer as it cured, which got trapped between the surface and the mold wall. The higher magnification images show a mixture of well-dispersed particles with the cured polymer filling the gaps. The overall, low porosity inside is also clear since the polymer does not undergo significant mass loss at this stage due to the preheating procedure employed.

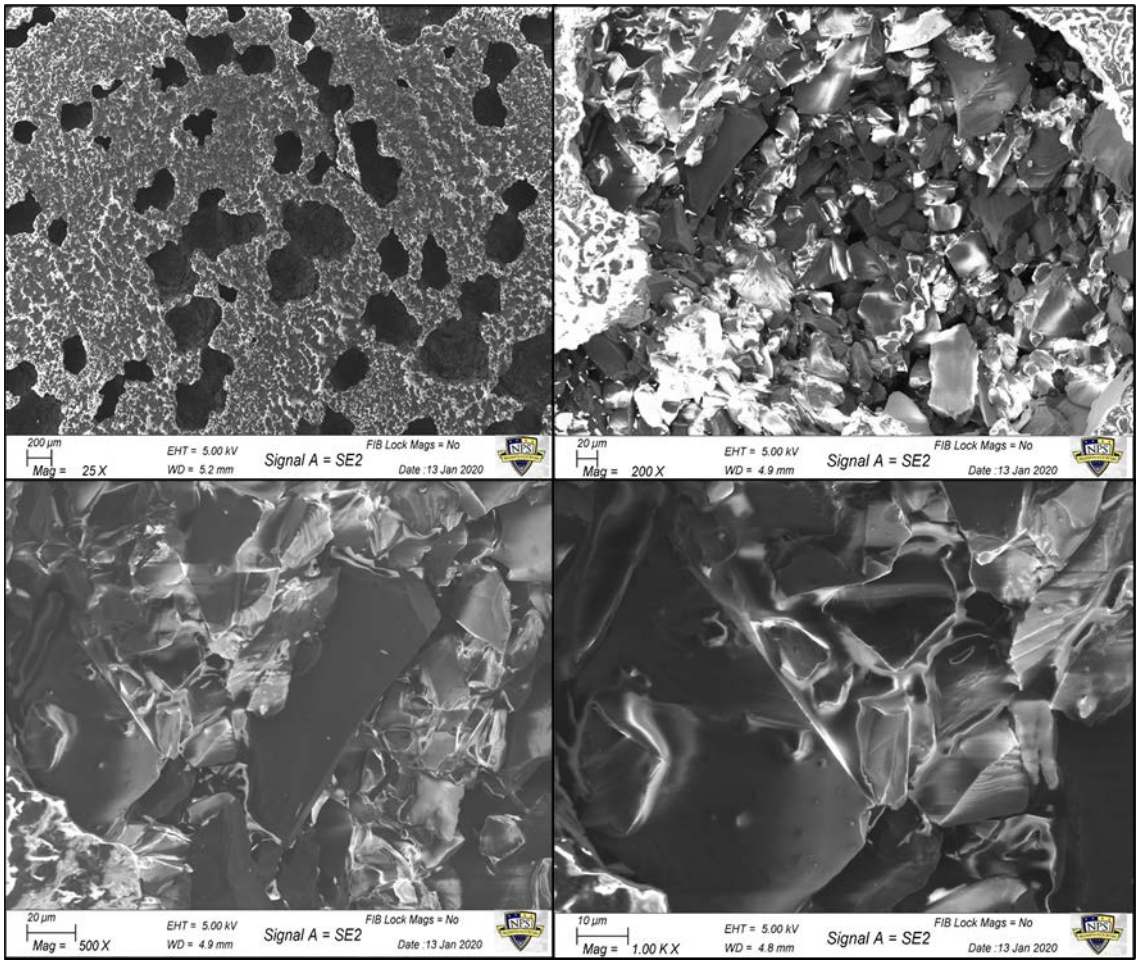

Figure 40. Molded Post-Cured, Non-Vacuumed Mixed (250℃) SiC (25x Magnification-Top Left, 200x Magnification-Top Right, 500x Magnification-Bottom Left, 1Kx Magnification-Bottom Right).

Upon completion of pyrolysis, SEM was done to also analyze the microstructure of the previously analyzed cured samples of 80:20 SiC at 100% fine (Figure 41). Magnifications were 200x up through 2,000x. A larger amount of surface porosity was visible due to the large mass loss experienced by the polymer and the density difference between the polymer (ρ=996 kg/m^3) and SiC (ρ=3210 kg/m^3) that causes polymer shrinking. Molding also inadvertently introduces additional air pockets within the materials. As expected, the structure retained its shape, as the initial powders were in contact while forming voids between them. “Spider-Webs” (represented by the potential nitrogenation on the sample in SEM) were present throughout the microstructure of the sample indicating a separate surface reaction occurring, unlike the rest of the structure. With the pyrolysis stage heating the SiC sample to extremely high temperatures in nitrogen, it is possible that some reaction with the gas had occurred. The “Spider-Webs” required us to further analyze the sample through EDS to determine their chemical composition.

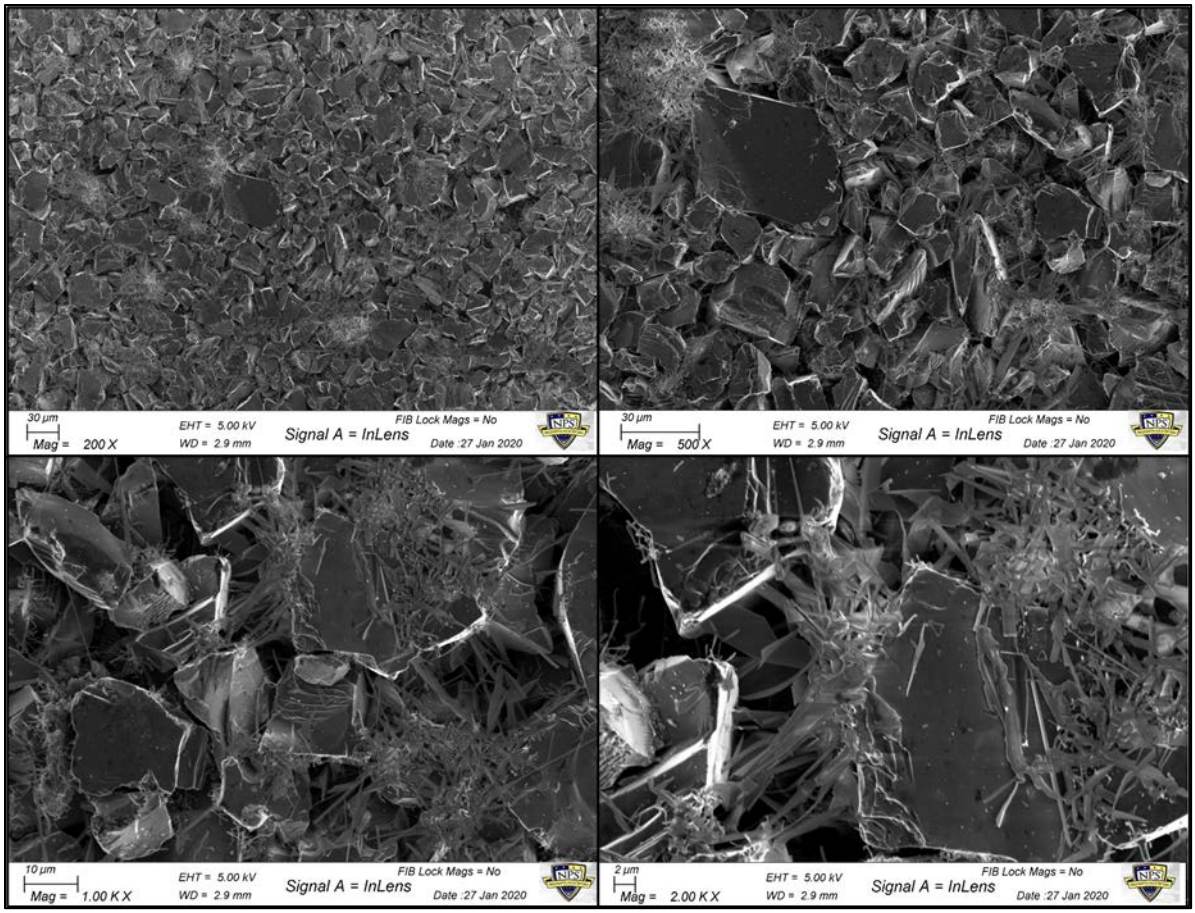

Figure 41. Molded Post-Pyrolysis (After 250℃ Cure) SiC (200x Magnification-Top Left, 500x Magnification-Top Right, 1Kx Magnification-Bottom Left, 2Kx Magnification-Bottom Right).

After analyzing the post-pyrolyzed, molded sample, a post-pyrolyzed, VAP sample was analyzed to determine any significant differences between the two. It was seen that the particles tended to be much closer and more compacted than the hand-molded samples (Fig. 42). It is possible that the vibrations applied during printing aids in removing trapped gases from the initial mixtures forming a better, densified structure. A similar observation was made in the past using the same technique, where VAP (Figure 29) samples have lower porosity compared to molded samples (Figure 30) [4]. Removing the porosity can improve the mechanical strength of the SiC samples and increase the overall thermal conductivity when used for a variety of applications.

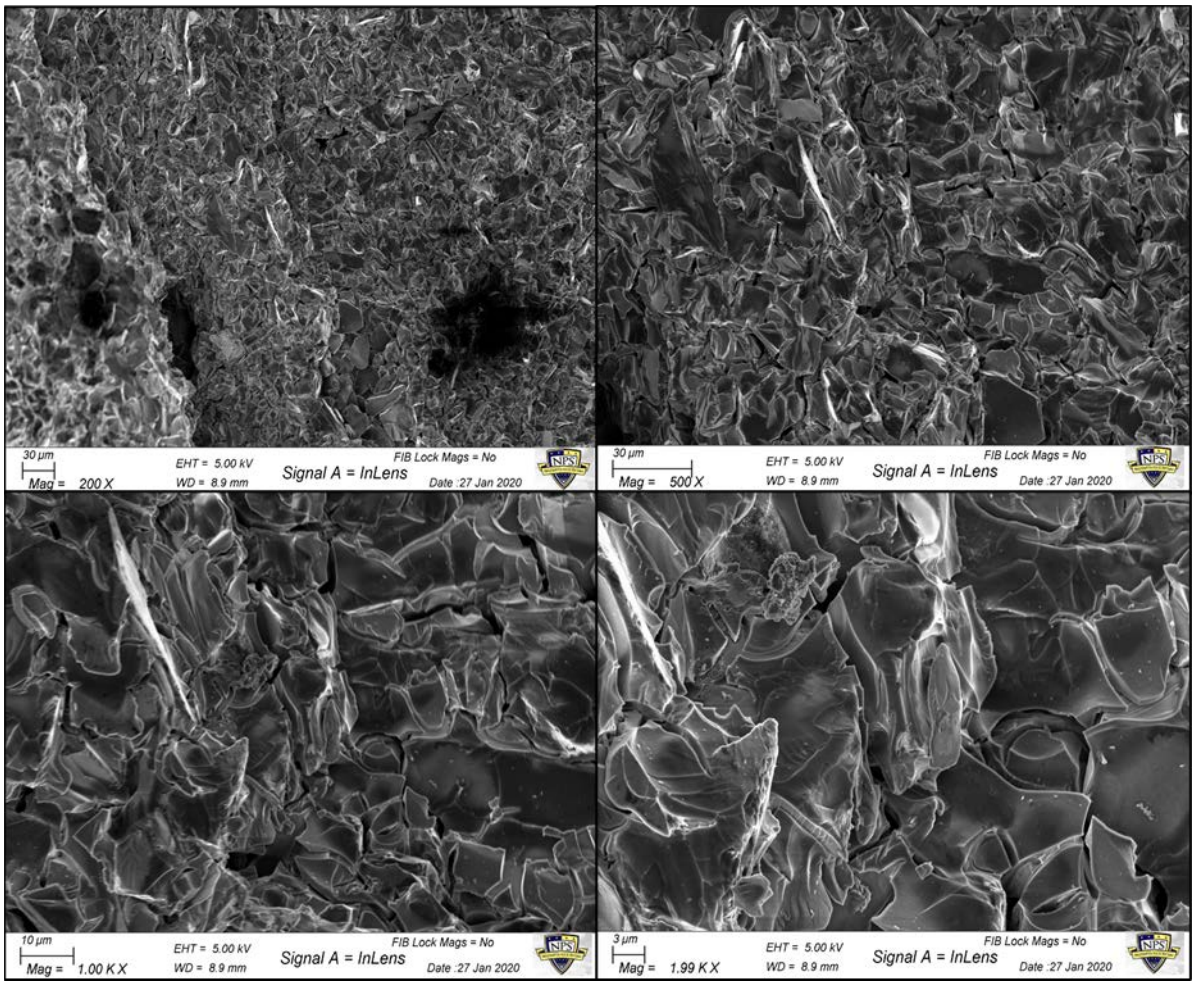

Figure 42. Printed Post-Pyrolysis (After 250℃ Cure) SiC (200x Magnification-Top Left, 500x Magnification-Top Right, 1Kx Magnification-Bottom Left, 2Kx Magnification-Bottom Right).

d. EDS

After conducting SEM, EDS was performed to determine the chemical compositions of the material and to determine if there were impurities within any part of the microstructures of the SiC samples. Initially, the starting powders underwent EDS analysis after SEM to see if there were any impurities present along with determining the percentages of silicon and carbon present within the powders. For most of the coarse powder, the elements or components present were silicon and carbon with one specific area having oxygen where the particles were touching or joined (Figures 43 and 44). In most

cases for the coarse powder, the detected compositions were close to the 1:1 molar ratio with some excess silicon and limited traces of oxygen.

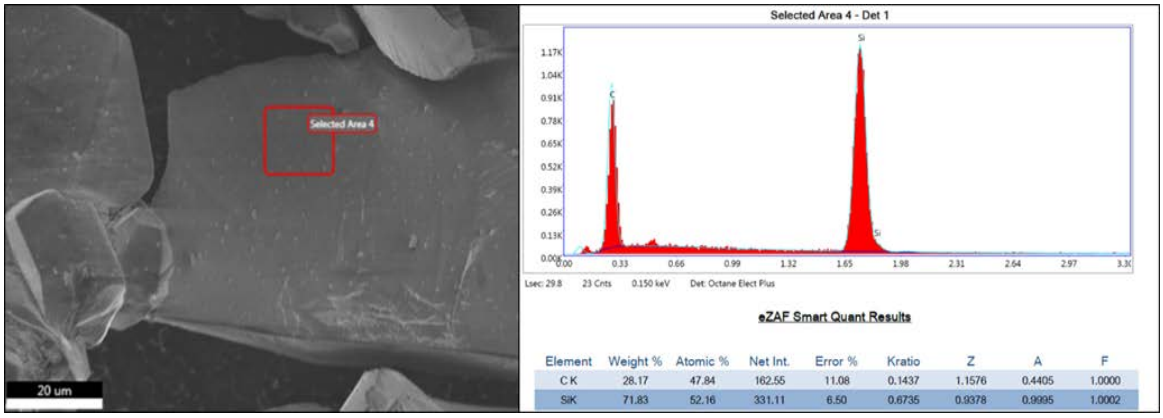

Figure 43. Coarse SiC Powder Area 4 Selected Image and Associated Element Percentages.

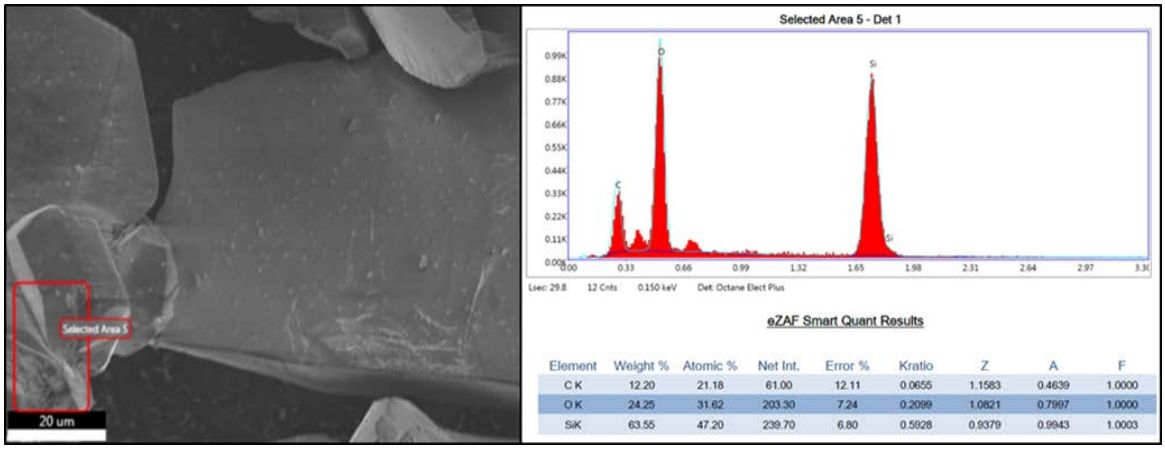

Figure 44. Coarse SiC Powder Area 5 Selected Image and Associated Element Percentages.

When the fine powder was analyzed under EDS, primarily silicon and carbon was present with no traces of oxygen (Figures 45-46). Just like the coarse powder, the silicon had a greater percentage than the carbon regardless of the location or powder particle analyzed. Moving forward, this provided a good baseline on ensuring that there were no impurities present during the initial mixing and combining steps of SMP-10 and the powders (both fine and coarse).

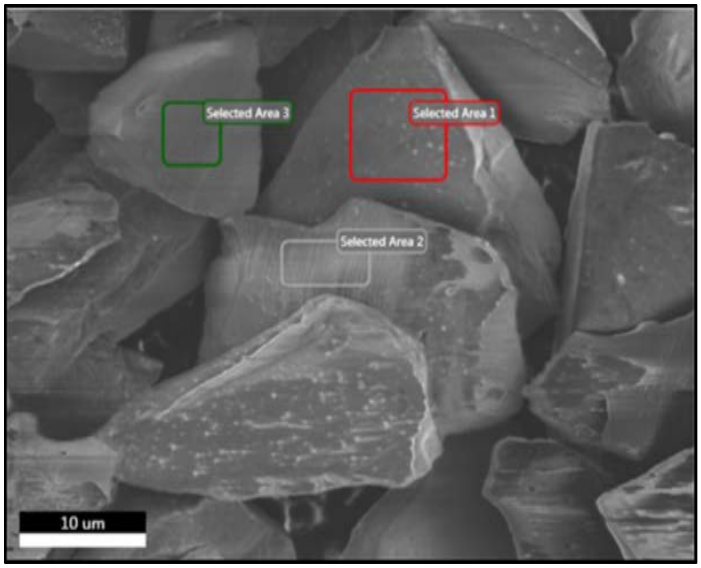

Figure 45. Fine SiC Powder Image.

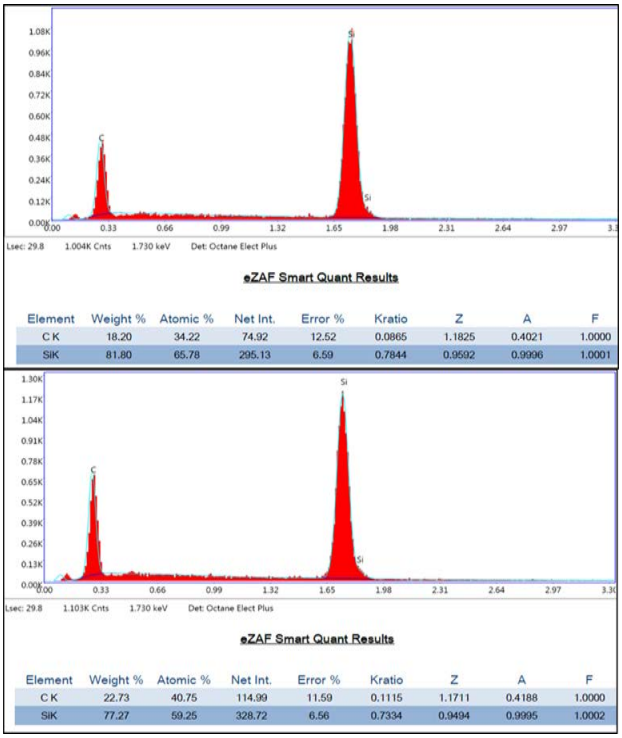

Figure 46. Fine SiC Powder Areas 1 (Top) and 3 (Bottom) Associated Element Percentages.

Upon completion of starting powder analysis, a cured sample was characterized. Note that the polymer surfaces were smooth showing some charging (Figure 47). In the

image, all three selected areas had elemental composition of carbon, oxygen, and silicon with oxygen being the lowest (Figure 48). Neither the initial powders nor polycarbosilane contain oxygen, so its existence can be attributed to oxidation in air. It is possible that SMP-10 tends to oxidize if heated in an oxygen-containing environment. Since the initial stages of curing was performed in air to prevent sample expansion, this might incorporate some oxygen in the mixture. Therefore, it might be beneficial to perform the curing stages in an inert atmosphere.

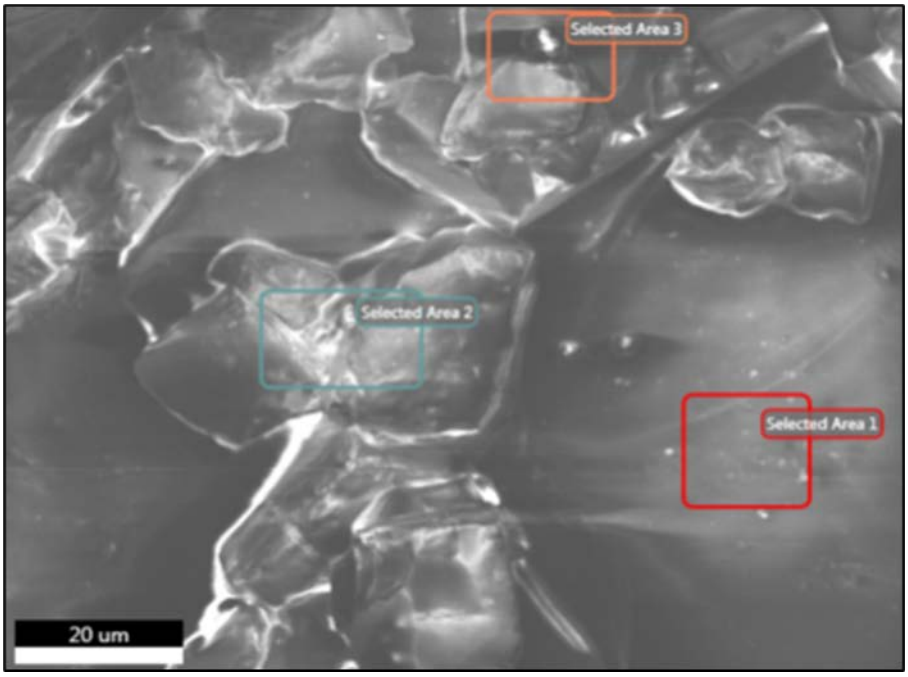

Figure 47. SiC Cured Hand-Molded Sample and Associated EDS Areas Image.

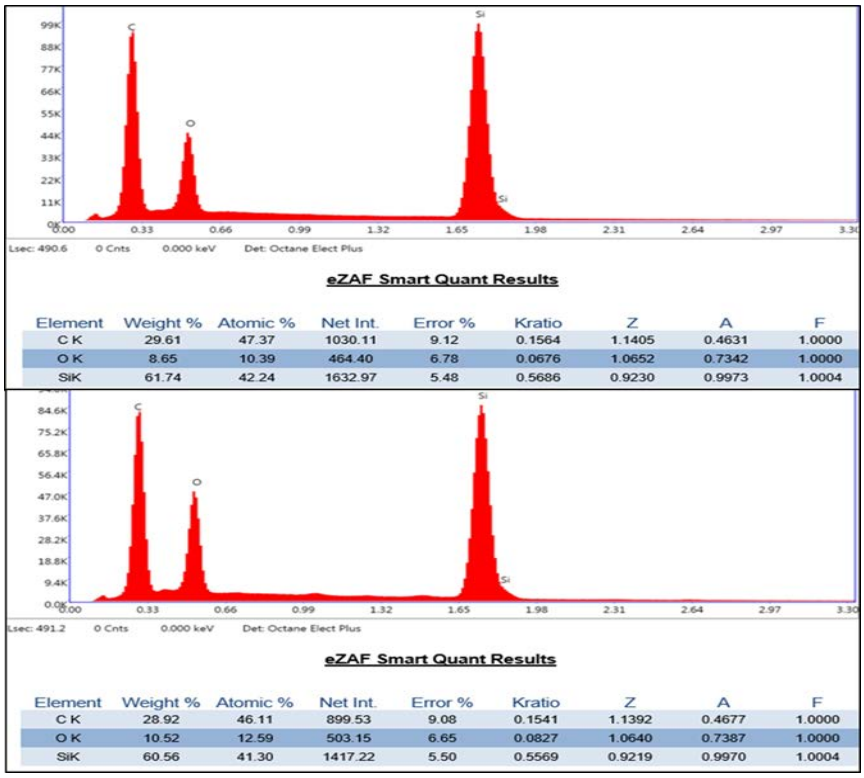

Figure 48. SiC Cured Hand-Mold Sample Areas 1 (Top) and 3 (Bottom) Associated Element Percentages.

After the individual powders and the cured sample, the post-pyrolyzed molded sample was analyzed with EDS conducted specifically to help analyze the composition in between the gaps, on the surfaces, and where the “Spider-Webs” were (as depicted in Figure 49).

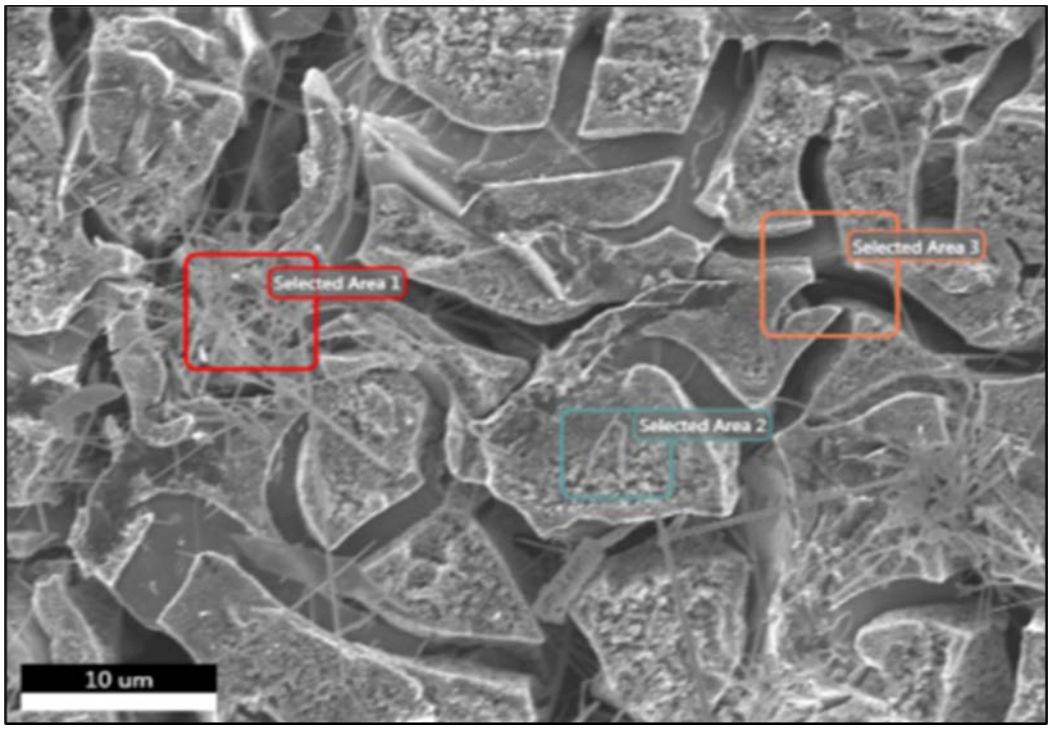

Figure 49. Post-Pyrolysis, Molded Sample and the Associated, Selected Areas for EDS Analysis.

Areas 1 and 3 had the greatest amount of differences in element composition compared to area 2 (Figure 50). Most of area 2 was silicon and carbon, which primarily consists of an initial particle. In area 1 where the "Spider-Webs" were present, nitrogen was a heavy component of the elemental composition. Since the pyrolysis stage used the flow of nitrogen at high temperatures, reactions between SiC and N_2 likely occurred, forming Si_3N_4 (Silicon Nitride) on the surface. For area 3, there was some nitrogen but less than area 1. This area is primarily a surface crack with the actual material surface located at some depth of a few micrometers. Silicon and carbon still maintained most of the elemental composition with some traces of oxygen at lower amounts than the cured polymer. It is possible that this sample is in the form of silicon dioxide, which might have formed from the oxidized SMP-10 polymer. There were some traces of aluminum, possibly originating from the 97.5% purity SiC powder used. In summary, the first post-pyrolyzed molded sample shows that oxidation happened at the surface and nitrogen reactions were present in certain locations.

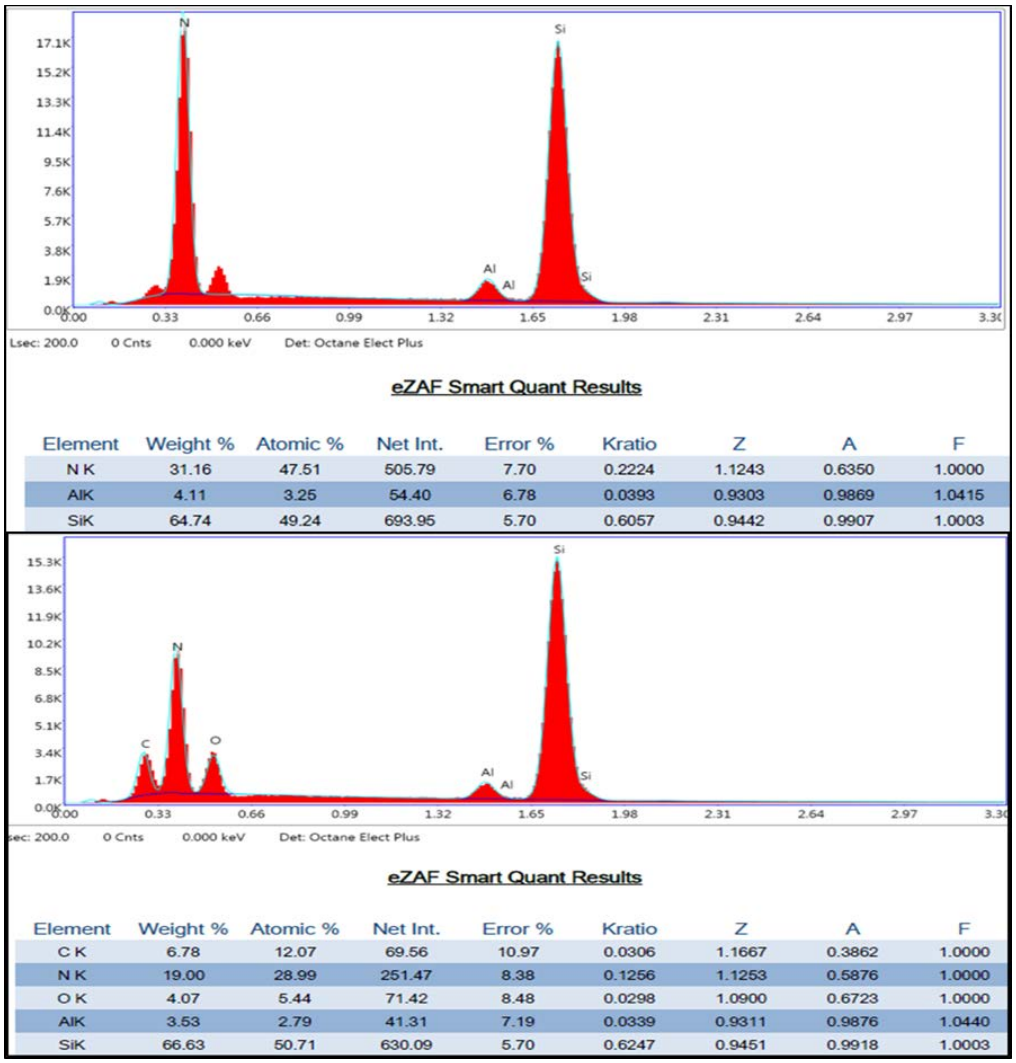

Figure 50. Post Pyrolysis Mold, Areas 1 (Top) and 3 (Bottom) Associated Element Percentages.

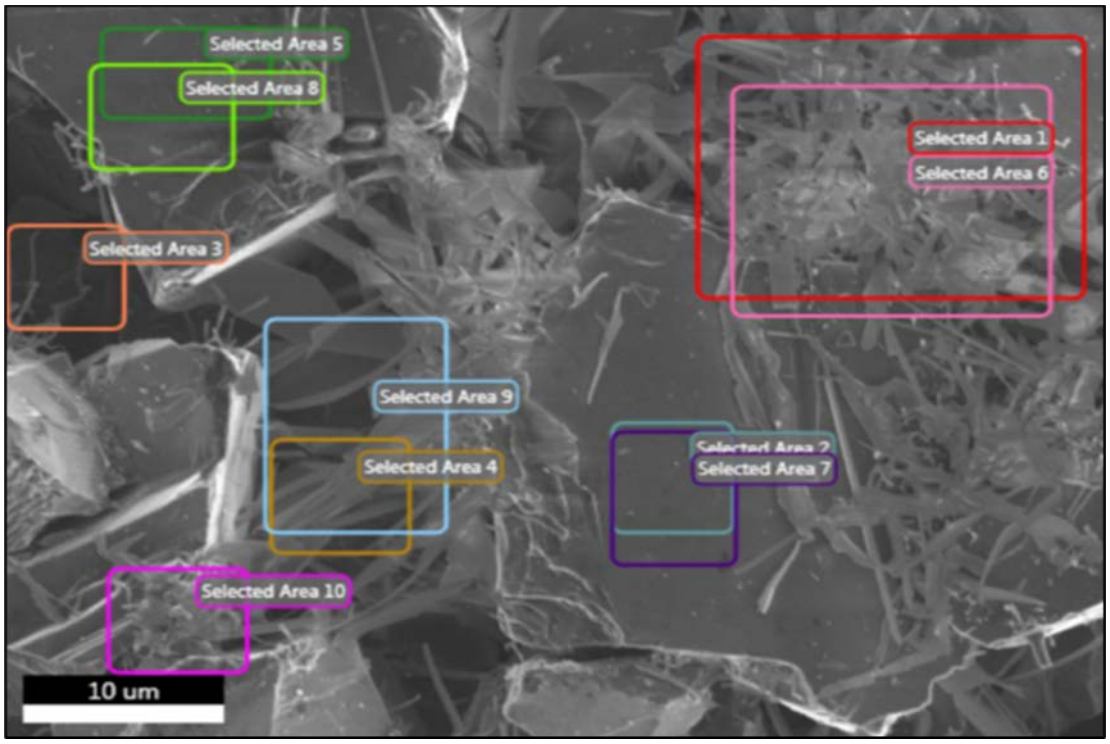

Figure 51. Fine 130℃ Post-Pyrolysis Hand-Mold and Associated EDS Areas Image.

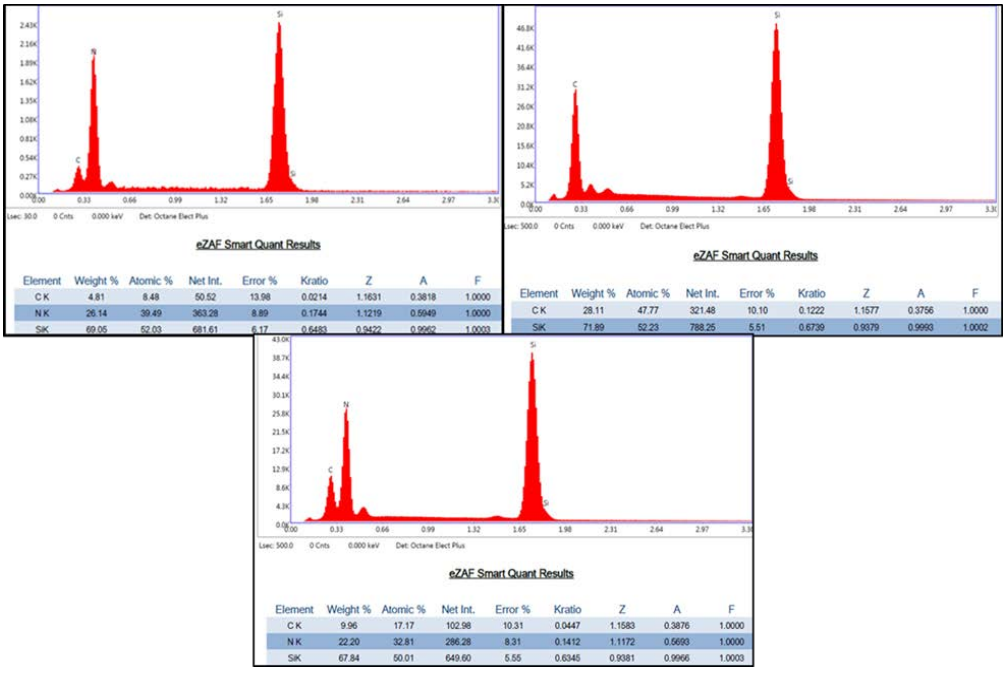

Figure 52. Fine SiC 130℃ Post-Pyrolysis Hand-Mold Areas 1 (Top Left), 8 (Top Right), and 10 (Bottom) Associated Element Percentages.

After analyzing the post-pyrolyzed, molded sample, a VAP sample was also compared that underwent pyrolysis (Figure 53). In this sample, the particles were much more compacted against each other as seen from SEM. The sample also seemed glossier and had greater oxidation occurring on the surfaces compared to the non-printed samples. Through further analysis of other areas, there was no presence of "Spider-Webs" like the hand-molded samples even though it underwent pyrolysis with nitrogen as the inert gas still. The only specific result that was determined from the printed sample after pyrolysis was that the areas where the particles were adjoining was where a greater presence of oxygen was. Oxidation seemed to be more prominent at these areas than compared to the darker colored surfaces of the particles (Figure 54). Porosity was still less present compared to the hand-molded samples. In both cases of samples that underwent SEM and EDS, the samples need to be better mixed and joined prior to crystallization (pyrolysis) to strengthen the microstructure and overall mechanical/chemical properties of the samples to be used for applications or testing.

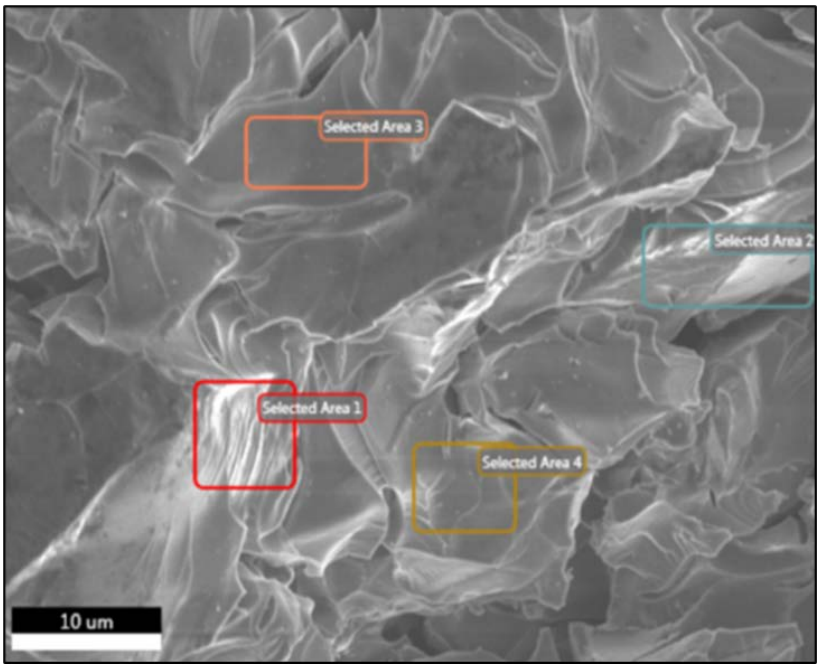

Figure 53. Printed, Post-Pyrolysis SiC 82:18 (100% Fine) and Associated EDS Areas Image.

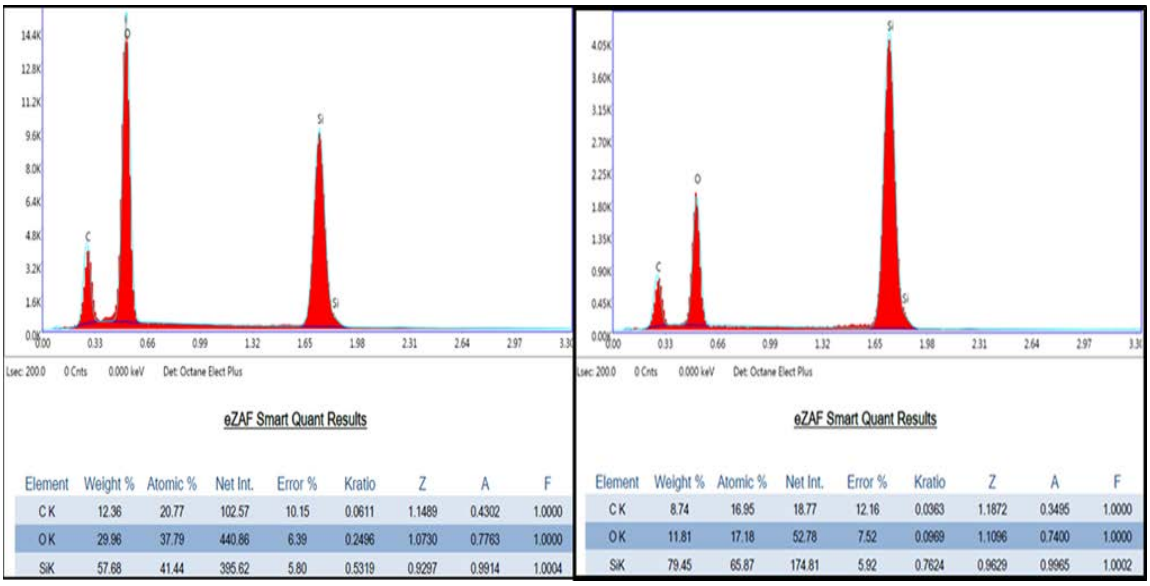

Figure 54. Printed Post-Pyrolysis SiC 82:18 (100% Fine) Areas 1 (Left) and 3 (Right) Associated Element Percentages.

e. DSC/TGA

DSC/TGA was conducted to determine the onset temperature and the amount of mass loss of the SiC/SMP-10 mixtures as the temperature was increased up to 1400°C. Since the SiC samples were initially breaking up during the initial trials of pyrolysis, DSC/TGA was performed to help identify the specific temperatures at where there was substantial mass loss that points to gas formation. Additionally, it can help identify the point at where the SiC samples were completely pyrolyzed. Figure 55 shows the analysis from a sample, where the red trace is the heat flow and the blue curve is the mass percentage. Based off the analysis, the biggest initial drop in mass started around ~350°C and the next big drop started around ~1300°C. From this, pyrolysis should include a dwell before these temperatures to prevent rapid gas formation that can cause a potential explosion of the samples, which was observed in the first pyrolysis experiments with the high-temperature furnace. For example, steady temperature increases employed around 400°C using the smaller (mini) furnace prevented the sample break-up. Due to the limitations of the mini-furnace from going above 1000°C, the testing to determine if SiC would fragment at 1300–1400°C still needs to be determined.

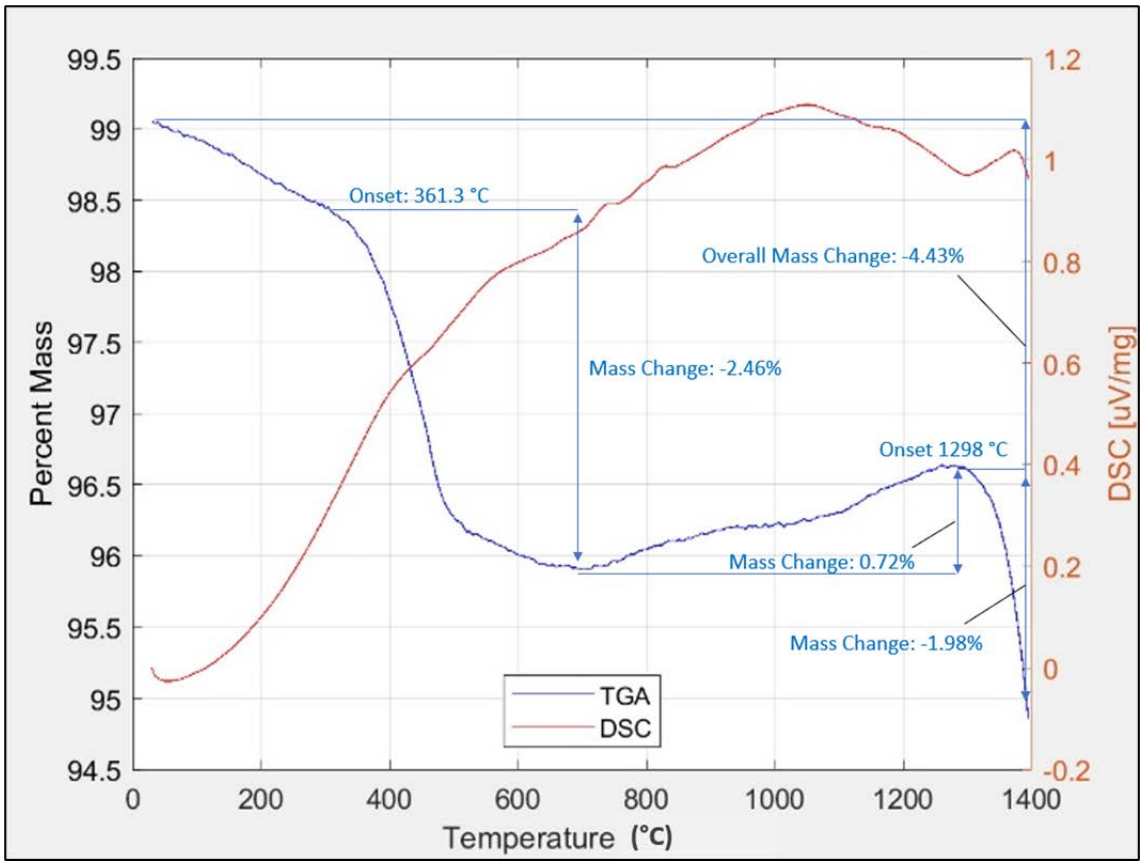

Figure 55. TGA/DSC of SiC Sample Up to 1400℃ Analyzing Mass Loss over Temperature Increase.

B. ROCKET NOZZLE PREPARATION

1. Sample Preparation

After the determination of an adequate ratio for the SiC fine powder to the SMP-10 and a after a few trials for curing and then pyrolysis of one rocket nozzle, two types of fabrication approaches based on 3D printing were considered. One uses polymer molds printed with a commercial printer that are filled with a ceramic-forming mixture and subsequently processed to generate the final ceramic nozzle (Figure 56). The second approach employs dual-extrusion printing, where one print head deposits a thermoplastic polymer on the outer shell, and the inside is filled through VAP of the ceramic precursor. This is essentially 3D printing the mold and the material together in-situ. The latter is a

much more refined printing approach that can generate arbitrary geometries and could reduce the amount of porosity left from filling a mold.

2. Molding

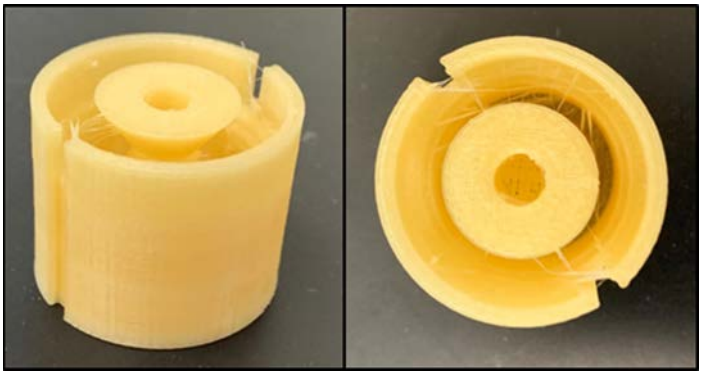

Figure 56. Water-Soluble PVA Rocket Nozzle Mold.

The molds were 3D-printed using two types of polymers, PLA, and polyvinyl alcohol (PVA), a water-soluble support filament. PVA has the advantage of easy removal of the mold by dissolving it in water. PLA must be melted and cleaned from the surface, which tends to stick to the cured mixture and leave some residue.

The printed molds were each filled with the 80:20 SiC fine powder/SMP-10 mixture after it had been prepared using the previously described processes. Since the material was difficult to manually fill the mold due to its highly viscous consistency, it was post-processed using the speedmixer to settle the material all the way down in the mold. For example, the first mold that was filled manually was discovered to have some gaps at the bottom after pyrolysis. The mold was first hand-filled and then compacted as much as possible. The filled mold was then put into one of the large containers for the speedmixer and packed with paper tissues and centered to secure it in the mixing container (Figure 57). Paper tissues were then placed on top of the mold to fully fill the container and then capped. These tissues were used to prevent the mold from spinning inside the container. The container was then processed with:

1 cycle at 1200 RPM for 1 min and

4 cycles at 3000 RPM for 5 secs

In between each cycle, more material would be packed until it was deemed that no more material could be packed. Each of the samples prepped prior to curing followed this same speedmixer process to compact the material further into the mold.

Figure 57. Semi-Packed, SiC Rocket Nozzle, Preceramic Mixture in PLA Mold Prepping for the Speedmixer.

The PLA molds typically had a much sturdier frame compared to PVA, so the material could be compacted easier. For the water-soluble mold, the center mold piece for the nozzle funnel was not as stiff and moved slightly during packing causing a disproportionate amount of SiC to be packed surrounding the nozzle funnel part of the mold. After conducting the speedmixer packing process, the filled rocket nozzle molds were ready for curing and pyrolysis (see Figures 58 and 59).

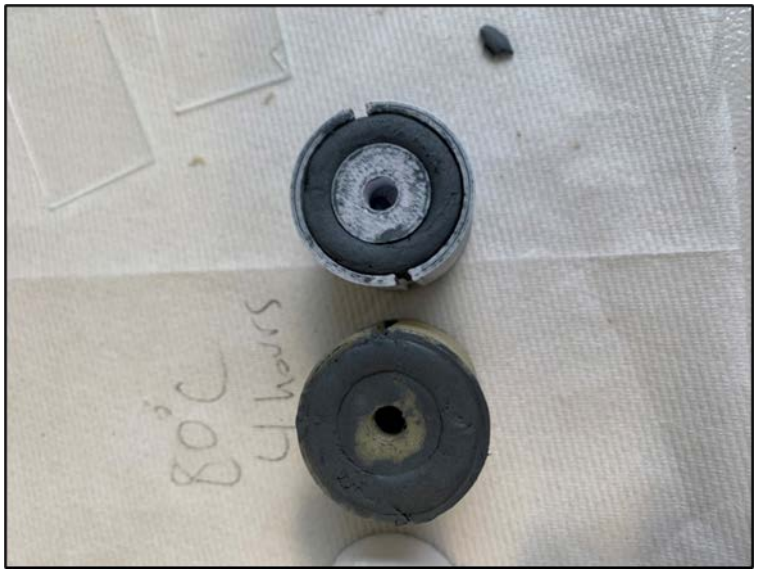

Figure 58. Molded, SiC Rocket Nozzle (One PLA Mold-Top and One Water-Soluble Mold-Bottom) Top View.

Figure 59. Molded, SiC Rocket Nozzle (One Water-Soluble Mold-Left and One PLA Mold-Right) Side View.

3. Curing and Pyrolysis

A similar approach to the previous samples was employed to cure and pyrolyze the molded samples. The curing went through the three stages of curing moving up to 248.8°C for 4 hours for the first PLA sample and 10 hours for the subsequent samples (Figure 60). Upon completion, the PLA melted around the cured parts with some PLA residue left, which could be cleaned while the sample was still hot to a limited extent using tweezers

(Figure 61). For the PVA mold, the sample was first cured through the first two stages (80℃ and 100℃) to harden the SiC mixture without melting the PVA mold. Afterwards, the PVA mold was dissolved completely by placing the semi-cured assembly for two days in water (Figure 62). Upon completion of the curing, the PLA-molded sample was pyrolyzed (Figure 63). It underwent the same cycle as the miniature SiC samples tested previously. As the temperatures reached up to about 1600℃, it was predicted that the PLA residue would completely melt off.

Figure 60. Molten PLA During Curing in Thermovac.

Figure 61. Post-Cured Rocket Nozzle with Remnants of PLA Mold Melted on SiC.

Figure 62. Post-Cured, Rocket Nozzle Mold that was from Water-Soluble Mold.

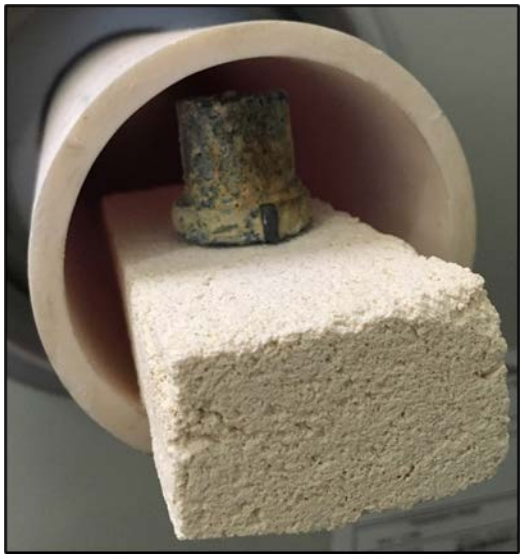

Figure 63. Post-Cured Rocket Nozzle (from Figure 61) Being Placed in Furnace for Setup of Pyrolysis.

Upon completion of the pyrolysis process for the first PLA sample, the material acquired a dark color, which has also been observed in other studies [41]. The rocket nozzle came out partially intact with just a few parts of it broken off during pyrolysis (Figure 64). Based off the DSC/TGA analysis, the likely temperature where the SiC would have cracked is either around 400℃ or around 1300℃. It is also possible that the curing time of 4 hours for each step (12 hours total) might not have been enough to fully cure the polymer, since these samples are larger than the initial smaller samples. The remaining uncured material

could produce more gas that could crack the parts. Following this, the curing time was increased to 10 hours for each step (30 hours total) for the two samples, one with PLA mold and one with PVA mold. The heating schedule for pyrolysis was also modified with dwell times of 1 hour at 300, 350, 400, 500 and 1000℃, which was the maximum temperature. This was done to prevent sample break-up. The samples are shown in Figure 65. The PLA molded sample was completely intact, whereas the PVA molded sample was cracked into two pieces. The samples were nearly identical with approximately 0.5% decrease in length. The sample mass losses were around 5 wt.%, which is the expected value based on the cumulative mass loss from SMP-10 and the polymer mass fraction. These results show that this printable formulation can generate net-shape parts with no appreciable mass loss or dimensional changes.

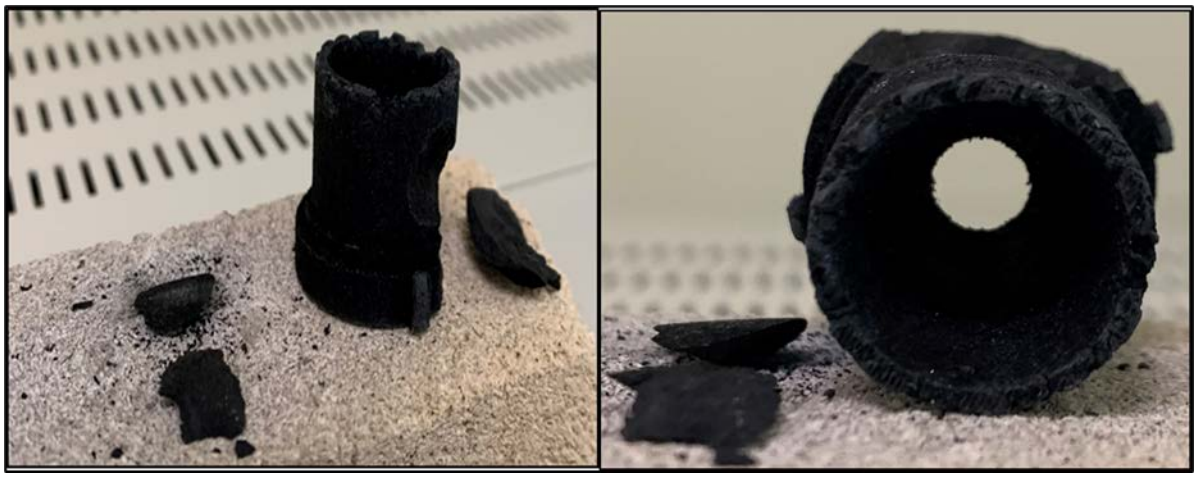

Figure 64. Post-Pyrolyzed Molded Rocket Nozzle from Figure 63.

Figure 65. PVA (Top) vs. PLA (Bottom) Rocket Nozzle Pre-Pyrolysis (Left) vs. Post-Pyrolysis (Right) Trial.

4. Microstructural Characterization of the Molded Pyrolyzed Rocket Nozzle

After pyrolyzing the molded rocket nozzle from the PLA, a flat piece of the rocket nozzle was cut off to be put into SEM. It was then analyzed under 200x, 500x, and 1000x magnification revealing a dense structure and one with various areas of micro-porosity throughout the nozzle (Figure 66). This shows that a better packing process of the material can improve porosity. Additionally, the adhesion between the particles of the SiC appears better than those of the previously, SEM-analyzed, non-rocket nozzle samples.

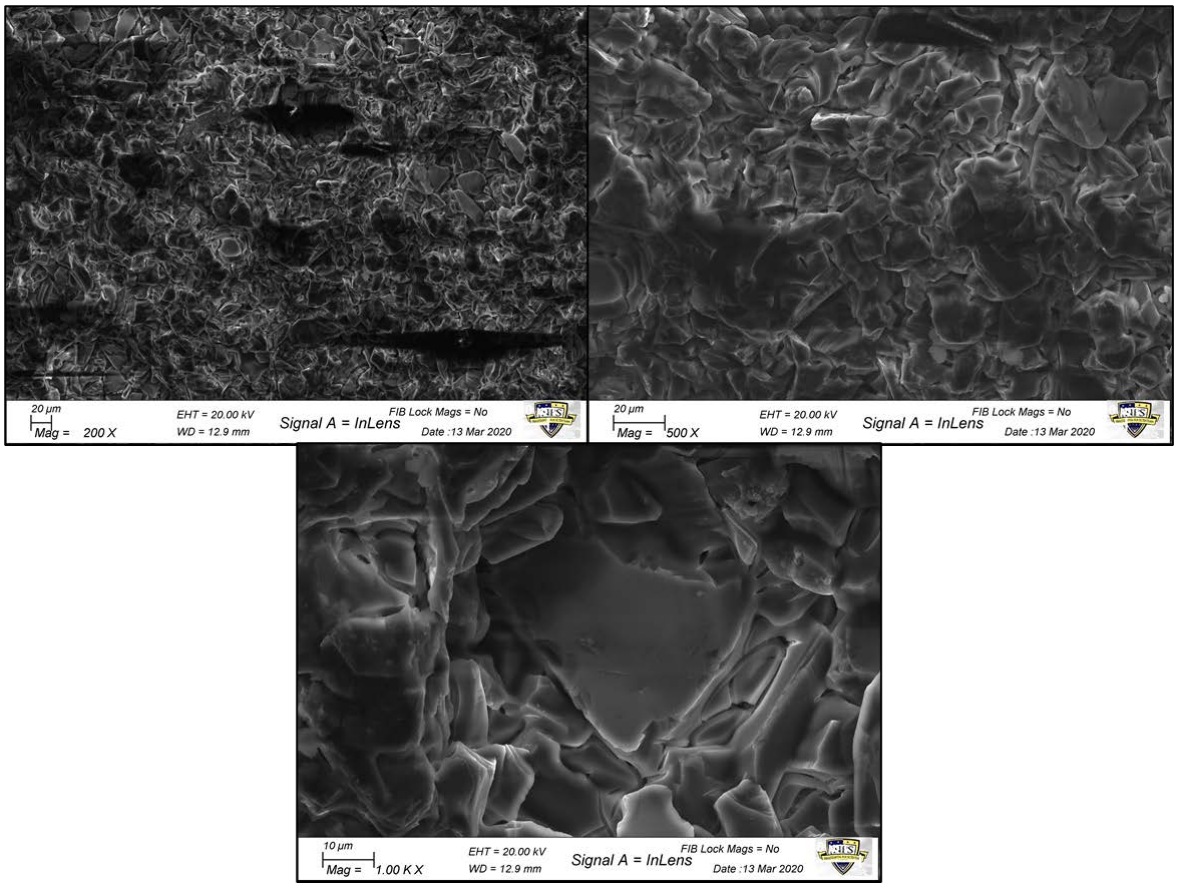

Figure 66. Post-Pyrolyzed Molded Rocket (Figure 64) Nozzle under SEM.

5. Dual-Head Printing of Rocket Nozzles

The dual-extruder approach required modifications of a commercial polymer printer by replacing one of the heads with a VAP head (Figure 67). This enables the printing of each layer with two different components. Since the polymer solidifies rapidly after decomposition, it can provide enough support to prevent the sagging of the SiC mixtures that was observed with the other samples. To accomplish this, the slicing settings in Simplify3D were modified to account for the different tool-head offsets, print rates and combination of separate models.

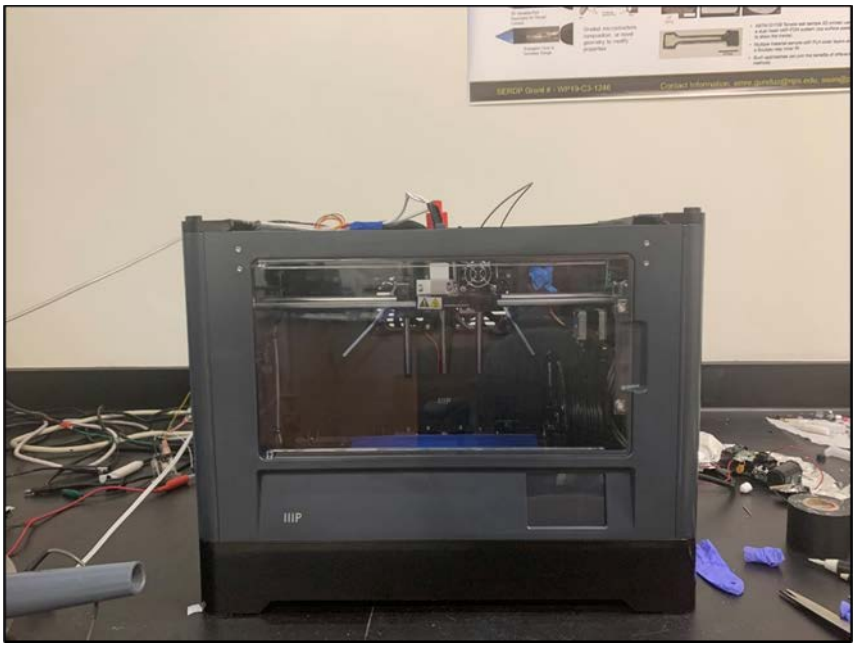

Figure 67. Dual Extruder Vibration-Assisted Printer (VAP) Used for Rocket Nozzle printing.

Since a rocket nozzle model takes approximately 14 g of mixed material, which nearly fills the whole syringe, most of the printing was done on partial models using a polymer clay instead. A final, printed sample using SiC infill was tested after a few trials of the polymer clay. The VAP settings used were identical to those in the single-head section. One of the samples is shown in Figure 68, which is the bottom 2 mm of the rocket nozzle model. In Figure 69, it shows the SiC being used as the infill. Although initially there was concern over the effects of the hot deposited polymer on the clay material, the tests showed that there was no noticeable effect. Overall, the results showed that it is feasible to co-print these materials without any significant interaction.

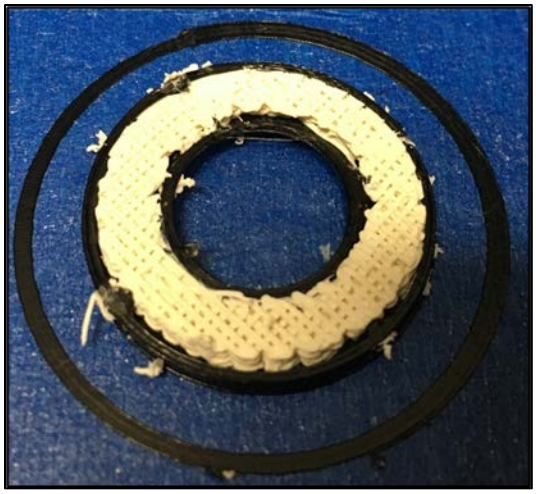

Figure 68. Dual-Extrusion, VAP, Partial Rocket Nozzle Trial with a Polymer Clay Infill.

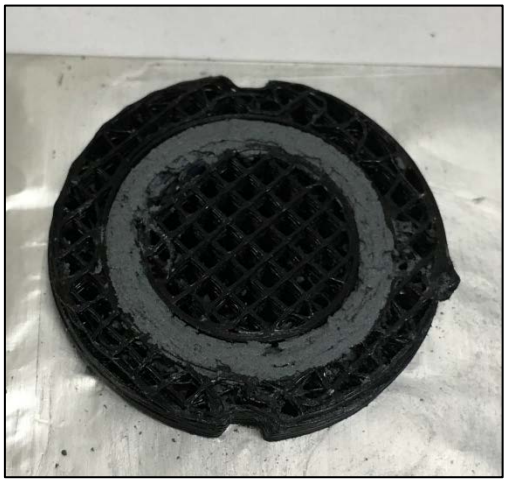

Figure 69. Dual-Extrusion, VAP, Partial Rocket Nozzle Trial with SiC Polymer Infill.

IV. CONCLUSIONS

AM promises advancements for many aerospace applications in the foreseeable future. The development and implementation of different approaches for fabricating parts can allow for the evaluation of the full potential of AM. Being able to use any material to fabricate any part with arbitrary geometries can significantly benefit the performance of parts related to aerospace applications.

For this study, adequate mixing, curing, sintering, and characterization of formulations was achieved and further mechanical and thermal testing is necessary for 3D-printed parts based on this mixture. Additional VAP needs to be done to help distinguish the more subtle differences between the non-printed and printed parts. Differences in dimensions, porosity, density, and adhesion of both non-printed and printed SiC powders with SiC polymers was determined. Additional rocket nozzle testing is needed on actual printed nozzles as well as heating under steady sources of heat such as gas flames.

This specialized work of AM of rocket nozzles utilizing higher, solids-loading SiC to achieve minimal porosity that withstands higher temperatures is the first of its kind, specifically through VAP technology. The ability to use VAP depends on material formulation and optimization, and most of this work is focused on accomplishing this goal. The primary approach described in this thesis uses a mixture of SiC powders and a SiC forming polymer, SMP-10, to form a thick, clay-like paste that is then extruded through the VAP nozzle to print the parts layer by layer. The parts are cured and pyrolyzed to transform the polymer into a solid SiC binder that holds the SiC powders together.

The as-received SMP-10 loses significant amounts of mass up to 35 wt.% during curing and pyrolysis. To minimize the mass loss at later stages, the initial stages focused on removing the highest amount of volatiles possible without significantly curing and thickening the polymer, since that could increase porosity and warp the AM parts. It was determined that for samples in 1 g and 10 g batches, mass losses of up to 12 wt.% and 8 wt.% can be achieved, respectively, when they are heated up to approximately 90°C for 24 hours under vacuum. The difference is due to the higher surface area to volume ratio for

the smaller batches that allows more volatiles to be removed. The polymer tends to oxidize if this heating is performed in air. It was also discovered that SMP-10 ages and gels rather quickly, 3-4 months after opening the container, at ambient conditions. Therefore, it should be stored in a refrigerator, if possible, to prevent aging.

The most suitable SiC powders investigated were the fine -400 mesh powders, which formed smooth clay-like mixtures with SMP-10 that flowed consistently through the 3D printing nozzles. Based on the results from the Particle Distribution Analyzer and the printing trials with VAP, the coarse powder (-200+450 mesh) was larger in size than its specifications and was clumpier after being printed. The fine powder allowed for a better ability to print and produced a more uniform micro-structure. The coarse and fine powder mixtures tended to reduce the viscosity for the same amount of solids loading (powder to polymer ratio) as the particle packing was improved. However, coarse powder contained some large, off-specification particles that were close to the size of the printer nozzle, which regularly got clogged by these particles.

The optimal solids-loading range was approximately between 80-84 wt.% SiC powder and 16-20 wt.% heat-treated SMP-10. The ratio that was used for the final 3D printing was 80 wt.% fine SiC powder and 20 wt.% SMP-10. This provided a better fill-in of smaller gaps within the finalized mix along with helping reinforce the CMC after pyrolysis [50]. Too much SMP-10 made the mixture too soft whereas too little (<16 wt.%) made the mixture too stiff and difficult to print. The 80:20 ratio along with the other configurations for VAP contributed to the overall successful printing of samples. The mixing of the samples in a centrifugal mixer at high speeds posed some challenges due to the samples heating up and partially curing during the process. This required interruptions during the mixing to allow for cooling and shortened mixing cycles. The final satisfactory cycle settings were 1200 RPM for 2 minutes and 3000 RPM for only 5 seconds. These were repeated until the material was uniformly mixed, with air cooling in between. The samples were mixed in a special container that could be evacuated to remove trapped air, which causes break-up of samples during pyrolysis.

For the curing of the samples, three temperature stages at 80, 100, and 248.8°C provided the smallest part expansion. An initially high temperature (>100°C) caused the

still-soft samples to expand and produce gas pockets. This potentially contributed to the overall break-up of some of the samples as they underwent pyrolysis. With the three stages, the material hardened sufficiently at 80℃ before any gases were generated, allowing it to retain its shape at the higher temperature stages. Upon the final stage at the maximum temperature of 248.8℃, the samples were fully cured and ready for pyrolysis. The most appropriate durations to ensure full curing were 4 hours per 6.35 mm depth of sample from each surface for each stage. For example, a 12.7 mm size cube requires 4 hours of curing for each three stages.

The pyrolysis process involved slow heating up to 1600℃ of the samples in an alumina tube under nitrogen gas flow in a high-temperature tube furnace. The SMP-10 reportedly pyrolyzes to form amorphous SiC at a temperature of 1000℃, which starts crystallization at a temperature of 1300℃. The many trials of modifying heating rates, dwell times, and gas flow rates to prevent sample and alumina tube cracking pointed out a requirement of very low heating rates at approximately 2℃/min and gas flow rates of 100 mL/min. The DSC/TGA results showed large mass losses with onset temperatures of 350℃ and 1300℃. These provided suitable values for dwell temperatures for the pyrolysis process to prevent sample cracking. Later trials in a smaller furnace showed that the samples can be pyrolyzed without breaking up, if the temperature is ramped up at ~5℃/min starting at 300℃ up to 1000℃ with 100℃ increments having a 30 min dwell time each. Additionally, the earlier fragmented samples potentially had a large amount of trapped air, which prompted the use of vacuum mixing.

The sample microstructures, elemental composition, and phase content showed well-sintered, crystalline structures. The samples did not change their shape after pyrolysis due to the powders already being in contact with each other at these high, solids loadings. As a comparison, parts prepared with just the initial SMP-10 would shrink approximately to a third of its original size. The phases detected were mostly SiC but some oxidation and nitridation was detected on the surface, possibly due to exposure to air and to nitrogen gas during pyrolysis.

The prepared mixtures were used to 3D print 6 mm cubes using the single head VAP system with a nozzle size of 0.5 mm, layer heights of 0.2, 0.3 and 0.5 mm, a print rate

of 10 mm/s and a back-pressure range of 20-100 psi depending on the material composition. The print rate was primarily limited by the printed track that dragged the rest of the sample at high speeds. The bottom of the cubes tended to deform as more layers were printed due to the nozzle pushing on the sample as it squished the extruded part from a diameter of 0.5 mm down to the layer height of 0.2 mm. This is typically not a problem with polymer printers as the bottom layer is already solidified but it becomes an issue when the printed material is not hardened. Increasing the layer height to 0.3 mm and above helped this issue. For example, if the layer height was increased to the diameter of the nozzle, the sagging did not occur. However, such a large, layer height leaves large gaps between the printed tracks, which is not desirable. To help with the deformation issue, some initial, small samples were prepared using a dual-head VAP system, which 3D printed the outer walls with either PLA or PVA and produced the infill with the preceramic mixture. This approach, 3D prints the mold at the same time with the material of interest. This showed promise for directly printing the nozzle as the deformation issues that were observed with the single head could be eliminated.

The curing and pyrolysis of the rocket nozzles was mostly successful following the procedures described above. The parts were prepared by 3D-printed molds consisting of PLA or PVA that were filled with the ceramic-forming mixture. The molds were initially filled and only packed by hand, but that left some voids towards the bottom of the molds. To improve packing, the hand-filled molds were placed in the centrifugal mixer. This was very effective in increasing packing and removing the voids. Upon curing, PLA molds were melted and could be removed to a degree, leaving some residue that was well adhered to the cured mixture. This can possibly be an issue during pyrolysis if the PLA that contains oxygen reacts with the preceramic polymer. PVA molds, on the other hand, could be dissolved in water over two days to completely remove them from the samples, leaving pristine parts. However, PVA molds were not as stiff as PLA and tended to move slightly at thin cross-sections during packing. Final nozzle samples pyrolyzed up to 1000°C with additional dwell times at 300, 350, 400, and 500°C remained intact. These samples showed no shrinkage and had a mass loss of 5 wt.% as predicted.

With the VAP AM being a newer approach to fabricating SiC parts for use in aerospace applications, there is still much that could be done or improved upon. Testing of variable mixtures of the SMP-10 and SiC powders required much research time since there were many different aspects at play that contributed to successful AM of a sample. The material must be supportive and strong enough to allow for layers to be built on each other during printing. Without strong adhesion between each layer and a large resistance to creep based off the mixture ratio, the samples would not be printed precisely. The reported formulations, preparation procedures, and initial 3D printing of samples in this study supports the feasibility of the VAP approach. The VAP approach also forms a solid basis for further work in mechanical, thermal, and performance characterization of the printed SiC parts and composites that have good high-temperature properties and oxidation resistance.

THIS PAGE INTENTIONALLY LEFT BLANK

V. FUTURE WORK

With the base, SiC-material formulation established, the follow-up work should focus on optimizing pyrolysis and sintering conditions that yield strong parts. Potentially, fillers can be introduced to accomplish both, desired oxidation resistance and higher thermal conductivity properties, or even just act as a reactive binder. These fillers can also provide additional mechanical strength.

3D printing using the dual-extrusions, VAP approach using water-soluble, PVA filaments appears to be the most promising method to fabricate larger samples for future studies. These can generate more complex, multi-material models with channels and other embedded features.

Potential tensile testing and compression testing needs to be done on SiC products (both printed and molded) that could provide greater merit on why VAP is better for fabricating composite parts than regular fabrication approaches, especially for rocket testing aspects.

An additional promising future work consists of using ultra-high temperature ceramics (UHTCs). With these ceramics being able to provide better ablation, higher melting points, hardness, retained strengths, thermal shock resistance, and the ability to operate in extreme environments, it seems the most likely aspect to be tested and incorporated with VAP AM parts of SiC. For rocket nozzles, UHTCs are promising future incorporations with SiC mixtures. Using Zirconia-based PDC or other similar composites could improve the overall oxidation resistance and stability whereas Hafnium could improve the thermo-conductivity and resistance up to greater than 1600°C when mixed with SiC. Further mixing of different elements and parts could provide limitless potential for varying structural properties of aerospace parts, especially for rocket nozzles.

THIS PAGE INTENTIONALLY LEFT BLANK

LIST OF REFERENCES

[1] K. Krnel, Z. Stadler, and T. Kosmač, "Preparation and properties of C/C–SiC nano-composites," *J. of the Eur. Ceramic Soc.*, vol. 27, no. 2, pp. 1211–1216, January 2007.

[2] M. S. McClain, I. E. Gunduz, and S. F. Son, "Additive manufacturing of carbon fiber reinforced silicon carbide solid rocket nozzles," presented at the AIAA Scitech 2019 Forum, San Diego, CA, Jan. 7–11, 2019.

[3] B. Lu, D. Li, and X. Tian, "Development trends in additive manufacturing and 3d printing," *Engineering*, vol. 1, no. 1, pp. 85–89, Mar. 2015.

[4] M. S. McClain, I. E. Gunduz, and S. F. Son, "Additive manufacturing of ammonium perchlorate composite propellant with high solids loadings," *Proc. of the Combustion Inst.*, vol. 37, no. 3, pp. 3135–3142, 2019.

[5] I. E. Gunduz, M. S. McClain, P. Cattani, G. T.-C. Chiu, J. F. Rhoads, and S. F. Son, "3D printing of extremely viscous materials using ultrasonic vibrations," *Additive Manufacturing*, vol. 22, pp. 98–103, Aug. 2018.

[6] P. Thakre and V. Yang, "Effect of surface roughness and radiation on graphite nozzle erosion in solid rocket motors," *J. of Propulsion and Power*, vol. 28, no. 2, pp. 448–451, Mar. 2012.

[7] A. Schrand, "Additive manufacturing in the DoD," DSIAC, 2019. [Online]. Available: https://www.dsiac.org/resources/journals/dsiac/fall-2018-volume-5-number-4/additive-manufacturing-dod, 2019

[8] L. Boccaletto and J.-P. Dussauge, "High-performance rocket nozzle concept," *J. of Propulsion and Power*, vol. 26, no. 5, pp. 969–979, Sep. 2010.

[9] G. Hagemann, H. Immich, T. V. Nguyen, and G. E. Dumnov, "Advanced rocket nozzles," *J. of Propulsion and Power*, vol. 14, no. 5, pp. 620–634, 1998.

[10] S. C. Joshi and A. Sheikh, "3D printing in aerospace and its long-term sustainability," *Virtual and Physical Prototyping*, vol. 10, no. 4, pp. 1–11, Nov. 2015.

[11] J. Roesler, H. Harders, and M. Baeker, *Mechanical Behaviour of Eng. Materials: Metals, Ceramics, Polymers, and Composites*. Berlin, Germany: Springer Science & Business Media, 2007.

[12] J. Stanfield, "NASA Marshall advances 3-D printed rocket engine nozzle technology," *Space Daily*, Mar. 2018.

[13] P. Colombo, G. Mera, R. Riedel, and G. D. Sorarù, "Polymer-derived ceramics: 40 years of research and innovation in advanced ceramics," *J. of the Amer. Ceramic Soc.*, vol. 93, no. 7, pp. 1805–1837, 2010.

[14] M. S. McClain, I. E. Gunduz, and S. F. Son, *Additive Manufacturing of Carbon Fiber Reinforced Silicon Carbide Solid Rocket Nozzles-Figure 6 Image*, in *AIAA Scitech 2019 Forum*, AIAA.

[15] P. Greil, "Polymer derived engineering ceramics," *Adv. Eng. Materials*, vol. 2, no. 6, Jun. 14, 2000.

[16] P. Colombo, G. Mera, R. Riedel, and G. D. Sorarù, *Polymer-Derived Ceramics: 40 Years of Research and Innovation in Adv. Ceramics-Polymer to Ceramic Transformation and Processing of Polymers Image*, 2010.

[17] J.-H. Eom, Y.-W. Kim, and S. Raju, "Processing and properties of macroporous silicon carbide ceramics: A review," *J. of Asian Ceramic Societies*, vol. 1, no. 3, pp. 220–242, Sep. 2013.

[18] E. V. Bongio, S. L. Lewis, D. R. Welson, and W. J. Sherwood, "Polymer derived ceramic matrix composites for friction applications," *Advances in Applied Ceramics*, vol. 108, no. 8, pp. 483–487, Nov. 2009.

[19] Y. Wang, Z. Chen, and S. Yu, "Ablation behavior and mechanism analysis of C/ SiC composites," *J. of Materials Research and Tech.*, vol. 5, no. 2, .pp. 170–182, Apr.–Jun. 2016.

[20] S. Cox, "Processing and characterization of continuous basalt fiber reinforced ceramic matrix composites using polymer derived ceramics," Master's thesis, Dept. Mat. Sci and Eng., Univ. of Cent. Fla., Orlando, FL, USA, 2014.

[21] K. Young-Wook, K. Shin Han, S. In-Hyuck, and K. Hai-Doo, "Fabrication of open-cell, microcellular silicon carbide ceramics by carbothermal reduction," *Jour. Of the Amer. Cer., Soc.*, vol. 88, no. 10, Jun. 2005, pp. 2949–2951.

[22] H. Y. Ryu, Q. Wang, and R. Raj, "Ultrahigh-temperature semiconductors made from polymer-derived ceramics," *J. of the Amer. Ceramic Soc.*, vol. 93, no. 6, pp. 1668–1676, 2010.

[23] B. Lee et al., "American ceramic society bulletin: April 2017," *Amer. Ceramic Soc.*, Apr. 2017. [Online]. Available: http://ceramics.org/wp-content/bulletin/ 2017/pdf/April2017.pdf

[24] J. Koo, H. Stretz, J. Weispfenning, Z. Luo, and W. Wootan, "Nanocomposite rocket ablative materials: processing, microstructure, and performance," in *45th AIAA/ASME/ASCE/AHS/ASC Structures, Structural Dynamics & Materials Conference*, Palm Springs, CA, 2004.

[25] S. Kumar et al., “Fabrication and erosion studies of C–SiC composite Jet Vanes in solid rocket motor exhaust,” *J. of the Eur. Ceramic Soc.*, vol. 31, no. 13, pp. 2425–2431, Nov. 2011.

[26] G. P. Sutton and O. Biblarz, *Rocket Propulsion Elements*, 9th ed. New York, NY, USA: John Wiley & Sons, 2017.

[27] L. Mohan Kumar, K. M. Usha, E. N. Anandapadmanabhan, and P. Chakravarthy, “Effect of fibre orientation on the properties and functional performance of ablative materials for solid rocket Motors,” *Trans Indian Inst Met*, vol. 70, no. 9, pp. 2407–2413, Nov. 2017.

[28] S. Nambu and M. Enoki, *Strength and Toughness of Graphite Materials for Solid Rocket Motor*, 449–452 vols. Trans Tech Publications, 2004.

[29] H. F. R. Schoyer, “Comparison of methods for the calculation of rocket nozzle wall temperatures,” *AIAA Journal*, vol. 18, no. 7, pp. 841–842, Jul. 1980.

[30] American Society for Testing and Materials (ASTM) Int.. “Physical testing standards and mechanical testing standards.” Accessed Jun. 22, 2019. [Online]. Available: https://www.astm.org/Standards/physical-and-mechanical-testing-standards.html

[31] A. Steckl. “Scanning electron microscopy (SEM),” Jove. Accessed Jun. 20, 2019. [Online]. Available: https://www.jove.com/science-education/5656/scanning-electron-microscopy-sem.

[32] R. Ketcham. “X-ray computed tomography (CT),” Montana State University. Accessed Jun. 21, 2019. [Online]. Available: https://serc.carleton.edu/msu_nanotech/methods/CT.html

[33] “Computer Tomography-Principle of X-Ray Tomography: X-Ray Tomography,” *Werth, Inc*, 30-May-2017. [Online]. Available: https://www.werthinc.com/computer-tomography-principle-x-ray-tomography/. [Accessed: 23-Nov-2019].

[34] NTS. “SEM/EDS analysis.” Accessed Jun. 24, 2019. [Online]. Available: https://www.nts.com/services/testing/electrical/sem-eds-analysis/.

[35] “Energy Dispersive Analysis,” *Metallurgical Engineering Services*, 2020. [Online]. Available: https://www.metengr.com/testing-services/chemical-analysis/energy-dispersive-x-ray-eds. [Accessed: 25-Apr-2020].

[36] B. L. Dutrow and C. M. Clark. “X-ray powder diffraction (XRD),” Geochemical Instrumentation and Analysis. Accessed Jun. 24, 2019. [Online]. Available: https://serc.carleton.edu/research_education/geochemsheets/techniques/XRD.html

[37] Rigaku Corporation. X-ray diffraction—sample.raw material. 2019. [Online]. Available: https://www.rigaku.com/en/techniques/xrd.

[38] Starfire Systems. “StarPCS SMP-10: Silicon carbide matrix precursor.” 2019. [Online]. Available: https://www.starfiresystems.com/wp-content/uploads/2018/03/SMP-10.pdf

[39] Sigma Aldrich. “Silicon Carbide.” Accessed Jul, 17, 2019. [Online]. Available: https://www.sigmaaldrich.com/catalog/substance/siliconcarbide401040921211?lang=en&region=US

[40] S. Kaur, R. Riedel, and E. Ionescu, “Structure of SMP-10,” *J. of the Eur. Ceramic Soc.*, vol. 34, no. 15, pp. 3571–3578, Dec. 2014.

[41] S. A. Potticary, “Chemical and behavioral study of commercial polycarbosilanes for the processing of SiC fibers,” M.S. thesis, Dept. of Mech. And Mat. Eng., University of Cincinnati, Cincinnati, OH, USA, 2017.

[42] D. S. King, Z. D. Apostolov, T. S. Key, C. M. Carney and M. K. Cinibulk, “Novel processing approach to polymer-derived ceramic matrix composites,” *Int. J. of Applied Ceramic Tech.*, in press.

[43] Horiba, “Partica LA-950V2 laser scattering particle size distribution analyzer.” [Online]. Available: https://www.horiba.com/fileadmin/uploads/Scientific/Documents/PSA/LA950_V2_bro.pdf. [Accessed: 22-Dec-2019].

[44] RTP, “Modeling and Processing Guidelines for PLA (Polylactic Acid) Compounds.” Accessed Feb. 28, 2020. [Online]. Available: https://www.rtpcompany.com/technical-info/molding-guidelines/pla-compounds/

[45] B. Yao, B. Lu, Q. Huang, Z.-R. Huang, and Q. Yuan, “The preparation of SiC ultrafine fibers containing low amount of oxygen by the electrospinning and pyrolysis of vinyl-modified polycarbosilane,” *Ceramics Int.*, vol. 46, no. 7, pp. 9894–9900, Dec. 2019.

[46] Horiba, “Particle characterization – how to select a particle size analyzer.” [Online]. Available: https://www.horiba.com/scientific/products/particle-characterization/particle-size-analysis/select-a-particle-size-analyzer/. [Accessed: 14-Mar-2020].

[47] G. C. Capitani, S. D. Pierro, and G. Tepesta, “The 6H-SiC structure model: Further refinement from SCXRD data from a terrestrial moissanite,” *American Mineralogist*, vol. 92, no. 2-3, pp. 403-407, 2007.

[48] R. He, G. Ding, K. Zhang, and Y. Li. “Fabrication of SiC ceramic architectures using stereolithography combined with precursor infiltration and pyrolysis” *Ceramics Int.*, vol. 45, pp. 14006-14014, April 2019.

[49] R. He, G. Ding, K. Zhang, and Y. Li. “6H-SiC α phase XRD Image Reference” *Ceramics Int.*, vol. 45, pp. 14006-14014, April 2019

[50] W. Krenkel, “Carbon fiber reinforced CMC for high-performance structures,” *Int. J. of Applied Ceramic Tech.*, vol. 1, no. 2, pp. 188–200, Jan. 2005.

THIS PAGE INTENTIONALLY LEFT BLANK

INITIAL DISTRIBUTION LIST

1. Defense Technical Information Center
   Ft. Belvoir, Virginia

2. Dudley Knox Library
   Naval Postgraduate School
   Monterey, California